Novel tacrine-tryptophan hybrids: Multi-target directed ligands as potential treatment for Alzheimer's disease / Chalupova K.; Korabecny J.; Bartolini M.; Monti B.; Lamba D.; Caliandro R.; Pesaresi A.; Brazzolotto X.; Gastellier A.-J.; Nachon F.; Peichal J.; Jarosova M.; Hepnarova V.; Jun D.; Hrabinova M.; Dolezal R.; Zdarova Karasova J.; Mzik M.; Kristofikova Z.; Misik J.; Muckova L.; Jost P.; Soukup O.; Benkova M.; Setnicka V.; Habartova L.; Chvojkova M.; Kleteckova L.; Vales K.; Mezeiova E.; Uliassi E.; Valis M.; Nepovimova E.; Bolognesi M.L.; Kuca K.. - In: EUROPEAN JOURNAL OF MEDICINAL CHEMISTRY. - ISSN 0223-5234. - ELETTRONICO. - 168 (2019) : pp. 491-514. [10.1016/j.ejmech.2019.02.021]

ARCHIVIO ISTITUZIONALE DELLA RICERCA

Alma Mater Studiorum Università di Bologna
Archivio istituzionale della ricerca

Novel tacrine-tryptophan hybrids: Multi-target directed ligands as potential treatment for Alzheimer's disease

This is the final peer-reviewed author's accepted manuscript (postprint) of the following publication:

Published Version:

Availability:
This version is available at: https://hdl.handle.net/11585/700033 since: 2020-02-20

Published:

DOI: http://doi.org/10.1016/j.ejmech.2019.02.021

Terms of use:

Some rights reserved. The terms and conditions for the reuse of this version of the manuscript are specified in the publishing policy. For all terms of use and more information see the publisher's website.

This item was downloaded from IRIS Università di Bologna (https://cris.unibo.it/).
When citing, please refer to the published version.

07 May 2024

(Article begins on next page)

Accepted Manuscript

Novel tacrine-tryptophan hybrids: Multi-target directed ligands as potential treatment for Alzheimer's disease

Katarina Chalupova, Jan Korabecny, Manuela Bartolini, Barbara Monti, Doriano Lamba, Rosanna Caliandro, Alessandro Pesaresi, Xavier Brazzolotto, Anne-Julie Gastellier, Florian Nachon, Jaroslav Pejchal, Michaela Jarosova, Vendula Hepnarova, Daniel Jun, Martina Hrabinova, Rafael Dolezal, Jana Zdarova Karasova, Martin Mzik, Zdena Kristofikova, Jan Misik, Lubica Muckova, Petr Jost, Ondrej Soukup, Marketa Benkova, Vladimir Setnicka, Lucie Habartova, Marketa Chvojkova, Lenka Kleteckova, Karel Vales, Eva Mezeiova, Elisa Uliassi, Martin Valis, Eugenie Nepovimova, Maria Laura Bolognesi, Kamil Kuca

PII: S0223-5234(19)30135-7

DOI: https://doi.org/10.1016/j.ejmech.2019.02.021

Reference: EJMECH 11113

To appear in: *European Journal of Medicinal Chemistry*

Received Date: 16 December 2018

Revised Date: 7 February 2019

Accepted Date: 7 February 2019

Please cite this article as: K. Chalupova, J. Korabecny, M. Bartolini, B. Monti, D. Lamba, R. Caliandro, A. Pesaresi, X. Brazzolotto, A.-J. Gastellier, F. Nachon, J. Pejchal, M. Jarosova, V. Hepnarova, D. Jun, M. Hrabinova, R. Dolezal, J. Zdarova Karasova, M. Mzik, Z. Kristofikova, J. Misik, L. Muckova, P. Jost, O. Soukup, M. Benkova, V. Setnicka, L. Habartova, M. Chvojkova, L. Kleteckova, K. Vales, E. Mezeiova, E. Uliassi, M. Valis, E. Nepovimova, M.L. Bolognesi, K. Kuca, Novel tacrine-tryptophan hybrids: Multi-target directed ligands as potential treatment for Alzheimer's disease, *European Journal of Medicinal Chemistry* (2019), doi: https://doi.org/10.1016/j.ejmech.2019.02.021.

This is a PDF file of an unedited manuscript that has been accepted for publication. As a service to our customers we are providing this early version of the manuscript. The manuscript will undergo copyediting, typesetting, and review of the resulting proof before it is published in its final form. Please note that during the production process errors may be discovered which could affect the content, and all legal disclaimers that apply to the journal pertain.

Graphical abstract

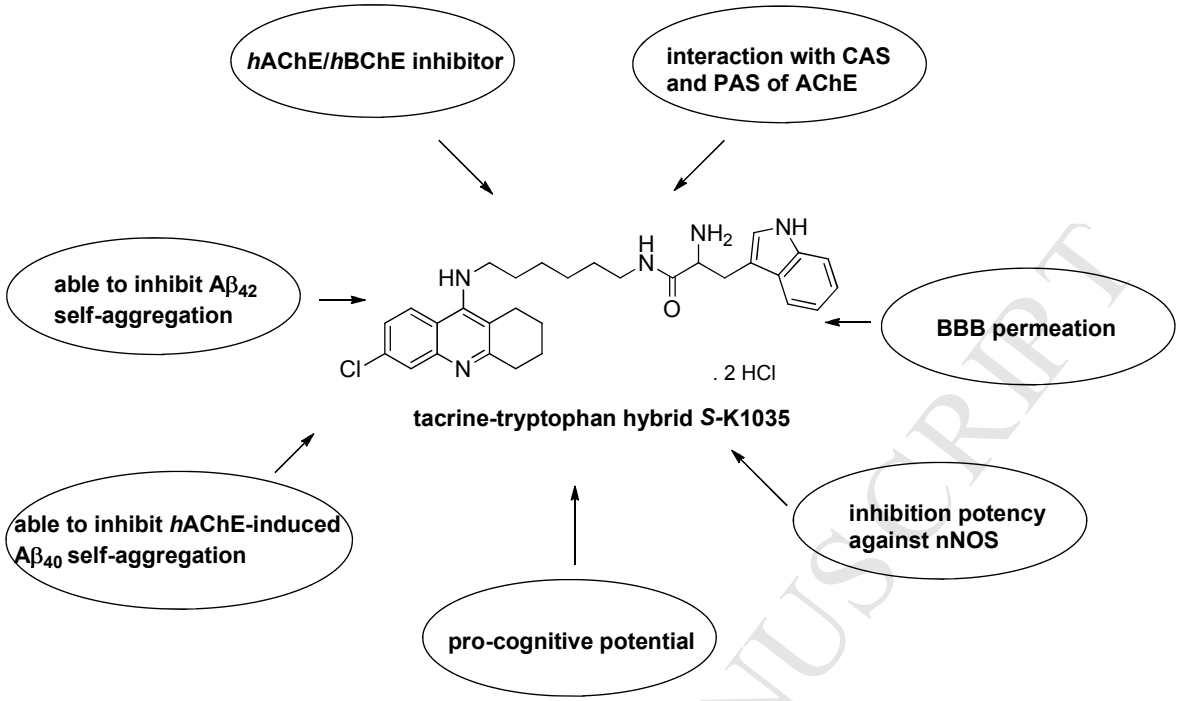

ACCEPTED MANUSCRIPT

Novel tacrine-tryptophan hybrids: multi-target directed ligands as potential treatment for Alzheimer's disease

ACCEPTED MANUSCRIPT

Katarina Chalupova[1,2,‡], Jan Korabecny[1,3,4,‡], Manuela Bartolini[5], Barbara Monti[5], Doriano Lamba[6], Rosanna Caliandro[6], Alessandro Pesaresi[6], Xavier Brazzolotto[7], Anne-Julie Gastellier[7], Florian Nachon[7], Jaroslav Pejchal[3], Michaela Jarosova[8], Vendula Hepnarova[3,4], Daniel Jun[3,4], Martina Hrabinova[3,4], Rafael Dolezal[2,4], Jana Zdarova Karasova[3,4], Martin Mzik[9], Zdena Kristofikova[1], Jan Misik[3,4], Lubica Muckova[3], Petr Jost[3,4], Ondrej Soukup[1,3,4], Marketa Benkova[4], Vladimir Setnicka[10], Lucie Habartova[10], Marketa Chvojkova[1,11], Lenka Kleteckova[1,11], Karel Vales[1,11], Eva Mezeiova[1,4], Elisa Uliassi[5], Martin Valis[12], Eugenie Nepovimova[2], Maria Laura Bolognesi[5,*] and Kamil Kuca[2,4*]

[1] *National Institute of Mental Health, Topolova 748, 250 67 Klecany, Czech Republic*

[2] *Department of Chemistry, University of Hradec Kralove, Rokitanskeho 62, 500 03 Hradec Kralove, Czech Republic*

[3] *Department of Toxicology and Military Pharmacy, Faculty of Military Health Sciences, Trebesska 1575, 500 01 Hradec Kralove, Czech Republic*

[4] *Biomedical Research Centre, University Hospital Hradec Kralove, Sokolska 581, 500 05 Hradec Kralove, Czech Republic*

[5] *Department of Pharmacy and Biotechnology, Alma Mater Studiorum-University of Bologna, Via Belmeloro 6, I-40126 Bologna, Italy*

[6] *Istituto di Cristallografia, Consiglio Nazionale delle Ricerche, Area Science Park - Basovizza, S.S. n° 14-Km 163.5, I-34149 Trieste, Italy*

[7] *Institut de Recherche Biomédicale des Armées, Département de Toxicologie et Risques Chimiques, 1 Place Général Valérie André, 91220, Brétigny-sur-Orge, France*

[8] *Department of Pharmaceutical Chemistry and Drug Control, Faculty of Pharmacy in Hradec Kralove, Charles University in Prague, Heyrovskeho 1203, 500 05 Hradec Kralove, Czech Republic*

[9] *Institute of Clinical Biochemistry and Diagnosis, University Hospital, Sokolska 581, 500 05 Hradec Kralove, Czech Republic*

[10] *Department of Analytical Chemistry, University of Chemistry and Technology Prague, Technicka 5, 166 28 Prague, Czech Republic*

[11] *Institute of Physiology, Czech Academy of Sciences, Videnska 1083, 142 20 Prague, Czech Republic*

[12] *Department of Neurology, Charles University in Prague, Faculty of Medicine in Hradec Kralove and University Hospital, Simkova 870, 500 03 Hradec Kralove, Czech Republic*

Abstract: A combination of tacrine and tryptophan led to the development of a new family of heterodimers as multi-target agents with potential to treat Alzheimer's disease. Based on the *in vitro* biological profile, compound ***S*-K1035** was found to be the most potent inhibitor of human acetylcholinesterase (*h*AChE) and human butyrylcholinesterase (*h*BChE), demonstrating balanced IC_{50} values of 6.3 and 9.1 nM, respectively. For all the tacrine-tryptophan heterodimers, favorable inhibitory effect on *h*AChE as well as on *h*BChE was coined to the optimal spacer length ranging from five to eight carbon atoms between these two pharmacophores. ***S*-K1035** also showed good ability to inhibit Aβ_{42} self-aggregation (58.6 ± 5.1% at 50 μM) as well as *h*AChE-induced Aβ_{40} aggregation (48.3 ± 6.3% at 100 μM). The X-ray crystallographic analysis of *Tc*AChE in complex with ***S*-K1035** pinpointed the utility of the hybridization strategy applied and the structures determined with the two **K1035** enantiomers in complex with *h*BChE could explain the higher inhibition potency of ***S*-K1035**. Other *in vitro* evaluations predicted the ability of ***S*-K1035** to the cross blood-brain barrier and revealed a moderate inhibition potency against neuronal nitric oxide synthase. Based on the initial promising biochemical data and a safer *in vivo* toxicity compared to tacrine, ***S*-K1035** was administered to scopolamine-treated rats and it was able to dose-dependently revert amnesia.

ACCEPTED MANUSCRIPT

Introduction

Alzheimer's disease (AD) is an age-related neurodegenerative disease and the most common cause of dementia associated with selective loss of cognitive ability and behavioral disturbances ultimately leading to death [1]. The progressive impairment of neurological conditions of patients with AD produces devastating problems on the patients themselves and very high economic burden for their families and society [2]. Unfortunately, the etiology of AD is still not fully understood. To date, several factors have been demonstrated to be responsible for AD development and progression, thus playing an eminent role in the pathogenesis of AD [3,4]. These distinct neuropathological hallmarks include depositions of extracellular β-amyloid (Aβ) into plaques and intracellular neurofibrillary tangles composed of hyper-phosphorylated tau protein. Both of them are suspected to be involved in the pathophisology of AD, however, their exact mechanism rather remains unclear. The difference between the plaques and tangles lies in their structure and effect on the nerve cells in the brain tissues [5]. Besides, the most pronounced hypothesis for AD development stems from low levels of acetylcholine (ACh), oxidative stress and bio-metal dyshomeostasis [6–8]. Low levels of ACh resulting from neuronal death are associated with cognitive and memory deterioration. Based on these observations, enhancement of cholinergic neurotransmission and recovery of ACh levels may alleviate AD symptoms [9]. The administration of cholinesterase inhibitors (ChEIs) builds upon the cholinergic hypothesis, and represent the most prominent agents exerting beneficial therapeutic option in AD therapy [10]. Acetylcholinesterase (AChE, E.C. 3.1.1.7) and butyrylcholinesterase (BChE, E.C. 3.1.1.8) represent two types of cholinesterase (ChE) enzymes which are able to hydrolyze ACh. On the other hand BChE is also able to hydrolyze bulkier substrates like butyrylcholine (BCh). AChE has a nearly 20 Å deep and narrow gorge with two major binding sites. At the bottom of the gorge, catalytic anionic site (CAS) resides whereas peripheral anionic site (PAS) is located near the cavity entrance. Experimental

ACCEPTED MANUSCRIPT

evidence showed that AChE inhibitors (AChEIs) able to simultaneously bind CAS and PAS may have a higher beneficial effect in AD therapy by their indirect anti-aggregating action [11]. Indeed, affinity of AChEIs for PAS confers ability against Aβ aggregation by preventing assembly of Aβ monomers into fibrils and other highly toxic complexes with Aβ [12,13].

Increasing evidence on the role of the two types of ChE in the AD brain pointed out a gradual switch of the hydrolyzing activity, from AChE to BChE, along with the disease progression. In fact, AChE levels were reported to gradually decrease, while BChE levels remain unaltered or significantly increase in the hippocampus and temporal cortex [14,15]. Furthermore, cortical BChE accumulation has been shown to be associated with the formation of neuritic plaques and neurofibrillary tangles [16]. Considering all of the above mentioned observations, AChE/BChE inhibitors may provide beneficial therapeutic effects in AD treatment.

In line with the multifactorial nature of this pathology, it is now recognized that several pathological features coexist in AD and play a role in a still undefined cause-effect circle. In this scenario, even if several factors have been hypothesized to contribute to AD pathogenesis, Aβ dyshomeostasis is one of the most studied therapeutic targets. The pathological processes related to AD correlate well with the misfolded Aβ peptide, which leads to the formation of amyloid oligomers and aggregates [17]. Aβ of variable length (from 39 to 43 residues) is generated by a sequential cleavage of the amyloid precursor protein (APP) by the subsequent action of β- and γ-secretases. Aβ_{42} tends to aggregate more rapidly than Aβ_{40} and displays higher neurotoxicity [18,19]. Aβ aggregates trigger a cascade of biochemical processes, which ultimately lead to neuronal dysfunction [20]. Many efforts are being made to develop appropriate treatment strategies either to decrease the Aβ production or enhance the Aβ clearance [21].

Current therapy of AD is mainly limited to administration of three AChEIs, namely donepezil, rivastigmine and galantamine, and one *N*-methyl-D-aspartate (NMDA) receptor antagonist, memantine. Unfortunately, these drugs do not effectively address the multifactorial nature of AD, exerting only a palliative effect [22,23].

Tacrine (**3**, THA, Figure 2) was the first ChEI approved in 1992 by the Food and Drug Administration (FDA) for the AD therapy and withdrawn from clinical use in 2003 because of the hepatotoxic and gastrointestinal side effects [24,25]. The ongoing research aiming at finding novel and presumably more potent THA analogues with suppressed toxicity led to the discovery of 7-methoxytacrine (**1**, 7-MEOTA, Figure 2), a centrally active AChEI endowed with a limited toxicity compared to THA, due to a distinct metabolic fate [26]. Furthermore, the THA derivative 6-chlorotacrine (**2**, 6-Cl-THA, Figure 2) showed better AChE inhibitory profile and selectivity than THA [27,28]. Thanks to the easy accessibility and the low molecular weight, THA and 6-Cl-THA are still widely used as starting fragments for the development of hybrid molecules with additional pharmacological properties beyond ChE inhibition [29].

ACCEPTED MANUSCRIPT

Over the last decades, the field of tacrine-based multi-target directed ligands (MTDLs) has grown enormously [30–33]. Early encouraging results were obtained when THA dimer bis(7)-tacrine (**4**, Figure 1), was rationally designed to contact both AChE central and peripheral site, thus acting as a dual binding site AChEI. Indeed, **4** showed improved AChE inhibition, as well as a large array of anti-AD activities, including neuroprotection against glutamate-mediated excitotoxicity [34,35]. The latter is presumably associated to **4** inhibition potency of neuronal nitric oxide synthase (nNOS) [36]. Indeed, excessive nitric oxide generated by nNOS mediates the downstream signal transduction of the NMDA receptors thus leading to excitotoxic neuronal cell death [37]. Thus, **4** has spurred the development of several MTDLs featuring either homo- and hetero-dimeric structures and targeting different pathological pathways intertwined to oxidative stress, mitochondrial dysfunction, metal dyshomeostasis, amyloid aggregation and tau protein hyper-phosphorylation [3,38–40].

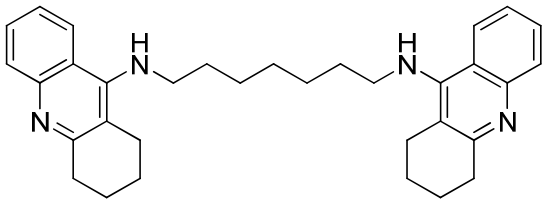

Figure 1. Chemical Structure of bis(7)-tacrine (**4**), First Dual Binding Site AChEI.

Design of novel tacrine-tryptophan heterodimers

As part of our efforts in identifying MTDLs as drug candidates for AD, we became interested in hybrids obtained by linking THA and tryptophan (Trp) fragments. Our starting point was the biological profile of THA-based [41–45], melatonin-based [46,47] and Trp-based [48–50] hybrids, which are endowed with a wide spectrum of potential disease-modifying activities against AD.

Recently, we have reported on a series of tacrine-naphthoquinone (THA-NQ) hybrids possessing a multifunctional character, which included cholinesterase inhibition related to the THA scaffold, anti-amyloid properties conveyed by the NQ moiety, antioxidant properties, the ability to cross blood-brain barrier (BBB) and, more importantly, lower hepatotoxicity if compared to THA. The most prominent THA-NQ hybrid, in terms of the most balanced and multipotent activity towards all the selected targets, was **5** (Figure 2) [51].

L-Tryptophan (L-Trp, Figure 2) is an essential amino acid acting as serotonin (5-HT) precursor. Studies on patients with AD have shown that an acute reduction of L-Trp intake impairs learning and memory [52,53] and that an increased L-Trp intake decreases intraneuronal accumulation of Aβ in the hippocampus in a transgenic mice model of AD [54]. Additionally, thanks to the key involvement of Trp residues of amyloidogenic proteins in the misfolding process [55], L-Trp possesses strong potential as a fragment for the development of targeted anti-amyloid agents [48]. On this basis, Segal's and Gazit's groups

ACCEPTED MANUSCRIPT

synthesized and investigated 1,4-naphthoquinon-2-yl-L-tryptophan (**6**, L-NQ-Trp, Figure 2) as a promising inhibitor of Aβ aggregation [56]. **6** was able to inhibit Aβ aggregation, decrease Aβ cytotoxicity, reduce the amount of amyloid brain burden in a transgenic Drosophila model for AD, thereby prolonging lifespan and completely abolishing the defective locomotion [56]. Studies from the same group also showed that the L-NQ-Trp analogue, Cl-1,4-naphthoquinone-2-yl-L-tryptophan (**7**, Cl-L-NQ-Trp, Figure 2), can inhibit tau aggregation *in vitro* and *in vivo* [49]. Computer simulations investigations have provided further insights into Aβ_{42}/L-NQ-Trp interaction mode [57]. Another reason for linking THA with Trp stems from the structural similarity of the designed molecules **8** and **9** with the THA-melatonin hybrids developed by Rodrigues-Franco *et al.* as MTDLs against AD. Hybrid **8** showed a multifaceted profile combining cholinergic and antioxidant properties together with low toxicity (Figure 2) [46]. In 2009, the same group developed 6-Cl-THA-melatonin hybrids [47]. The best-in-class compound **9** (Figure 2) exhibited good cholinergic inhibitory activity, antioxidant and anti-amyloid properties and excellent neuroprotective effects against Aβ and oxidative stress. Thus, it is feasible that **8** and **9** could similarly span AChE gorge, inhibit amyloid self-aggregation and exert similar beneficial properties.

Based on all aforementioned considerations, herein, we describe the synthesis and biological profile investigation of a novel multi-target hybrids family combining a Trp moiety with a THA scaffold tethered by aliphatic linkers of varying length. The characterization of the biological profile of the synthesized THA-Trp heterodimers includes an *in vitro* evaluation of (i) the inhibitory activity against human AChE (*h*AChE) and human BChE (*h*BChE), (ii) crystallographic analysis of the most promising compound in complex with *Torpedo californica* AChE (*Tc*AChE), (iii) anti-amyloid properties (inhibition of Aβ_{42} self-aggregation and of AChE-induced Aβ_{40} aggregation), (iv) prediction of BBB penetration using parallel artificial membrane permeation assay (PAMPA) , (v) *in vitro* effect on the cell viability, (vi) inhibitory activity against neuronal nitric oxide synthase (nNOS), and (vii) *in vivo* behavioral studies using a scopolamine-induced cognitive deficit rat model.

ACCEPTED MANUSCRIPT

ACCEPTED MANUSCRIPT

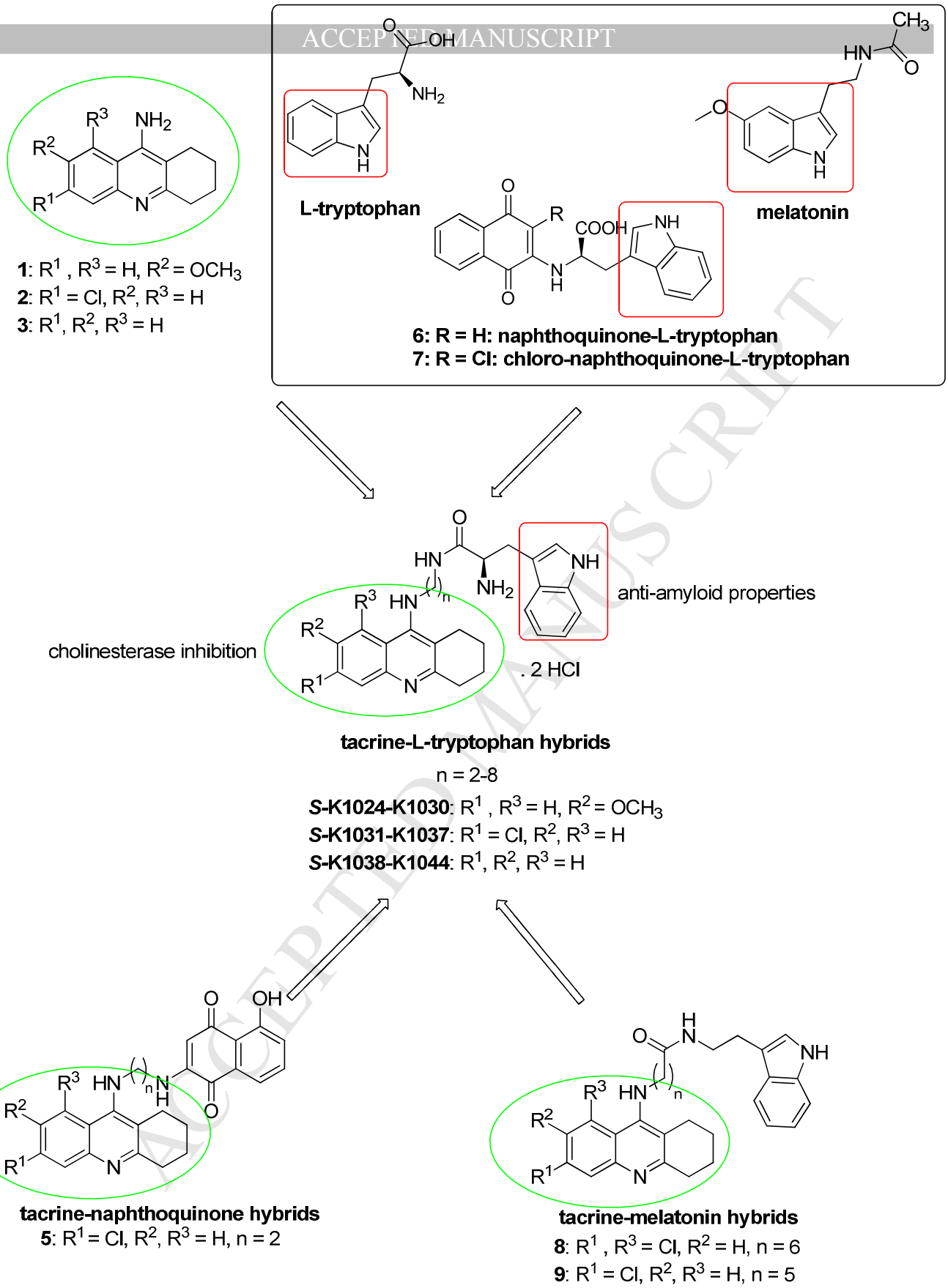

Figure 2. Design Strategy for Novel THA-Trp Hybrids

Results and discussion

ACCEPTED MANUSCRIPT

Chemistry. The general synthetic procedure for tacrine-tryptophan hybrids ***S*-K1024-K1044** is shown in Scheme 1. The starting 9-chlorotacrines **10-12** were prepared according to the previous reports and the spectral data were in good agreement with literature reports [58,59]. The treatment of **10-12** with appropriate 1,ω-diaminalkanes in the presence of phenol yielded the desired intermediates **19-39** (70-90%) [60]. *N*-[(*tert*-Butoxy)carbonyl]-L-tryptophan (**16**) was prepared in high yield (87%) from commercially available L-tryptophan (**13**) via protection of the amino group using triethylamine (TEA) and di-*tert*-butyl dicarbonate. Spectral data were in good agreement with literature reports [61]. Finally, the intermediates **19-39** with different linker sizes were coupled with Boc-protected L-tryptophan **16** in the presence of TEA and benzotriazol-1-yloxytris(dimethylamino)phosphonium hexafluorophosphate (BOP) to afford Boc-protected tacrine-tryptophan heterodimers **40-62** in low-to-excellent yields (15-91%). The deprotection and the final conversion into dihydrochloride salts took place in one pot to obtain the desired tacrine-tryptophan hybrids ***S*-K1024-K1044** in moderate-to-excellent yields (38-99%). Moreover, 6-Cl-THA-containing derivatives bearing an *R*-isomer (***R*-K1035**) and a racemic mixture (**rac-K1035**) from D-tryptophan and DL-tryptophan, respectively, were synthesized for comparative purposes following an analogous procedure. Structural determination and signal assignments of the final compounds were accomplished by the application of standard NMR experiments (^{1}H, ^{13}C, ^{1}H-^{1}H COSY, ^{1}H-^{13}C HSQC, HMBC, DEPT). The structural characterization also involved melting point assessment and liquid chromatography-high-resolution mass spectrometry (LC-HRMS). The absolute configuration of ***S*-K1035,** as the most promising compound in the series, has been validated via electronic circular dichroism (Supporting information).

ACCEPTED MANUSCRIPT

ACCEPTED MANUSCRIPT

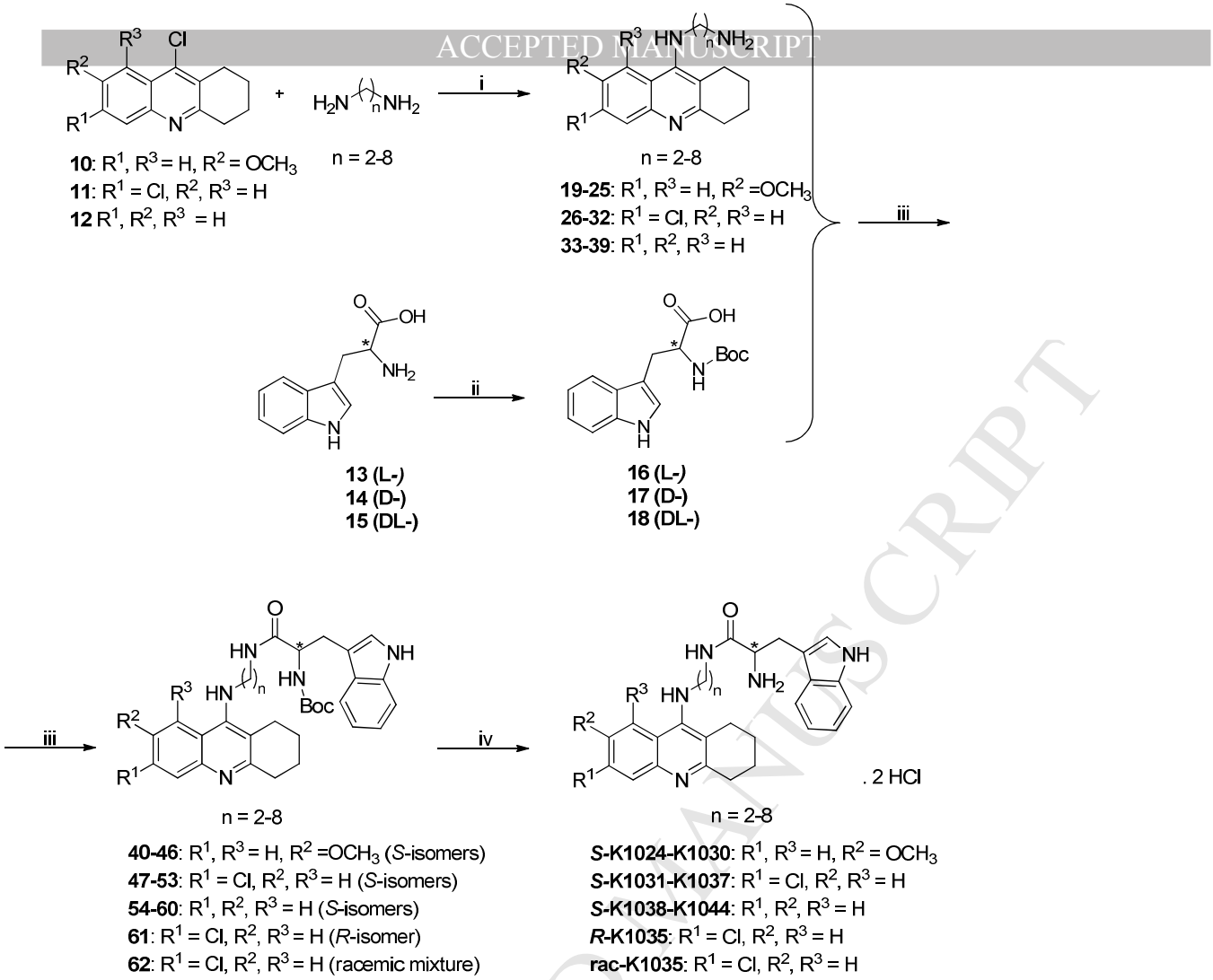

Reagents and conditions: (i) phenol, 130 °C, 4 h; (ii) TEA, MeOH, Boc_2O, RT, 24 h; (iii) TEA, BOP, DMF, RT, 24 h; (iv) 4 M HCl, MeOH, RT, 24 h.

Scheme 1. General Procedure for the Synthesis of Tacrine-Tryptophan Hybrids ***S*-K1024-K1044**, ***R*-K1035** and **rac-K1035**

Cholinesterase inhibitory activity

Three series of THA-Trp conjugates underwent initial biological screening for their inhibitory potential against *h*AChE and *h*BChE (Table 1). All data for 7-MEOTA-tryptophan hybrids ***S*-K1024-K1030**, 6-Cl-THA-tryptophan heterodimers ***S*-K1031-K1037** and THA-tryptophan derivatives ***S*-K1038-K1044** were determined using the spectrophotometric method by Ellman *et al.*, using 7-MEOTA, 6-Cl-THA, and THA as reference compounds (Table 1) [62,63].

In each series, the pharmacophores were combined via alkyl chains of different length (n = 2-8). The length of the chain is considered a crucial factor affecting the inhibitory activity against both ChEs as shown for many previously reported THA hybrids previously reported [29,41,42,51,59,60,64–66]. This characteristic feature stems from the optimal anchoring of each moiety (THA and Trp) to specific enzyme binding sites, which are located in a spatially defined area of ChE. It has been previously shown that AChE shares 54% homology of BChE [67]. However, some distinct differences between these two α/β hydrolases are present,

ACCEPTED MANUSCRIPT

such as in the gorge dimension; indeed, the bulkier BChE active gorge grants a lower substrate specificity compared to AChE [68]. Hence, it is expected that an optimal chain-length and activity may differ between each THA-containing subset for AChE and BChE. In general, the presence of longer methylene tethers was associated with a favorable inhibitory effect on *h*AChE as well as on *h*BChE, and the optimal length of the spacer was found to lie between five to eight carbon atoms for both ChEs in all the families bearing either THA, 6-Cl-THA or 7-MEOTA scaffolds.

All novel hybrids (except for derivative ***S*-K1026**) turned out to be potent inhibitors of *h*AChE with IC_{50} values ranging from micromoles to nanomoles. Derivative ***S*-K1035** (IC_{50} = 6.3 nM) bearing 6-Cl-THA moiety and a six-methylene spacer showed single digit nanomolar inhibitory potency against *h*AChE. ***S*-K1035** was 1585-, 51- and 3-times a more potent *h*AChE inhibitor than 7-MEOTA, THA and 6-Cl-THA, respectively. Among hybrids bearing the 7-methoxytacrine fragment, the most promising derivative was ***S*-K1027** (IC_{50} = 620 nM), which exhibited a 16.2-fold increased inhibitory activity against *h*AChE with respect to the single fragment 7-MEOTA. All hybrids carrying the 6-Cl-THA (except for hybrid ***S*-K1031**) displayed inhibitory potency towards *h*AChE in the same order of magnitude of the parent compound 6-Cl-THA. These findings are congruent with previous report, unveiling that the hydrogen replacement by chlorine at position 6 of the THA scaffold leads to an enhancement of the binding affinity towards AChE [69]. Similarly to the observations for 6-Cl-THA derivatives, hybrids containing THA (***S*-K1038-K1043**) showed inhibitory activities toward *h*AChE comparable to that of the reference compound THA. The only exception to this trend was hybrid ***S*-K1044,** which exhibited a 4.2-fold higher inhibitory potency compared to that exerted by THA.

Concerning the inhibition of *h*BChE, all 23 hybrids were potent inhibitors with IC_{50} values ranging from the micromoles to nanomoles. All hybrids carrying the 7-methoxytacrine template were better *h*BChE inhibitors than 7-MEOTA with inhibitory activities in the sub-micromolar range. All 6-Cl-THA heterodimers displayed higher inhibitory potency towards *h*BChE than the parent compound 6-Cl-THA. Among hybrids from the THA family, the most potent derivative was ***S*-K1042** (IC_{50} = 3.9 nM), which exhibited a 20.3-fold increased inhibitory activity compared to THA. Considering all series, the most pronounced inhibitors were the heterodimers bearing a six-methylene linker, namely ***S*-K1035** (bearing a 6-Cl-THA fragment) and ***S*-K1042** (bearing a THA fragment), which were endowed with nanomolar BChE inhibitory potency (IC_{50} = 9.1 and 3.9 nM, respectively).

Table 1. *In vitro* anticholinesterase activity, inhibition of Aβ_{42} self-aggregation and prediction of BBB crossing for THA-Trp derivatives and reference compounds

Cmpd	n	R^1	R^2	R^3	*h*AChE IC_{50} ± SEM (nM)[a]	*h*BChE IC_{50} ± SEM (nM)[a]	SI for *h*AChE[b]	Inhibition Aβ_{42} self-aggregation % ± SD[c]	BBB assay[e]

ACCEPTED MANUSCRIPT

***S*-K1024**	2	H	OCH_3	H	5700 ± 370	480 ± 15	0.08	54.7 ± 0.7	CNS-
***S*-K1025**	3	H	OCH_3	H	1300 ± 50	1800 ± 70	1.40	51.6 ± 1.5	CNS-
***S*-K1026**	4	H	OCH_3	H	12000 ± 770	520 ± 22	0.04	47.0 ± 7.0	CNS-
***S*-K1027**	5	H	OCH_3	H	620 ± 21	190 ± 6.7	0.3	51.9 ± 1.4	CNS-
***S*-K1028**	6	H	OCH_3	H	940 ± 61	55 ± 1.2	0.06	58.0 ± 5.7	CNS±
***S*-K1029**	7	H	OCH_3	H	980 ± 47	78 ± 2.7	0.08	57.9 ± 2.3	CNS±
***S*-K1030**	8	H	OCH_3	H	1300 ± 80	130 ± 4	0.10	54.5 ± 6.2	CNS+
***S*-K1031**	2	Cl	H	H	160 ± 8	340 ± 17	2.09	18.7 ± 7.0	CNS±
***S*-K1032**	3	Cl	H	H	70 ± 4	140 ± 6.2	1.99	19.9 ± 2.1	CNS±
***S*-K1033**	4	Cl	H	H	62 ± 2.2	120 ± 3.9	1.95	28.9 ± 1.4	CNS±
***S*-K1034**	5	Cl	H	H	76 ± 1.8	74 ± 1	0.97	50.6 ± 6.6	CNS±
***S*-K1035**	6	Cl	H	H	6.3 ± 0.2	9.1 ± 0.3	1.43	58.6 ± 5.1	CNS+
***R*-K1035**	6	Cl	H	H	6.9 ± 0.3	140 ± 5	19.7	60.7 ± 2.5	CNS+
rac-K1035	6	Cl	H	H	7.4 ± 0.4	13 ± 0.6	1.77	57.2 ± 1.5	CNS+
***S*-K1036**	7	Cl	H	H	19 ± 0.5	52 ± 1.1	2.76	59.0 ± 3.8	CNS+
***S*-K1037**	8	Cl	H	H	50 ± 1.3	140 ± 2.8	2.89	59.4 ± 6.2	CNS+
***S*-K1038**	2	H	H	H	730 ± 32	56 ± 2.1	0.08	44.0 ± 5.3	CNS-
***S*-K1039**	3	H	H	H	580 ± 33	40 ± 1.0	0.07	46.4 ± 6.2	CNS-
***S*-K1040**	4	H	H	H	1300 ± 93	123 ± 2.4	0.10	59.1 ± 2.6	CNS+
***S*-K1041**	5	H	H	H	320 ± 16	23 ± 0.7	0.07	54.3 ± 5.5	CNS-
***S*-K1042**	6	H	H	H	120 ± 3.8	3.9 ± 0.1	0.03	55.5 ± 5.2	CNS-
***S*-K1043**	7	H	H	H	120 ± 3.5	25 ± 1.0	0.22	60.9 ± 4.4	CNS-
***S*-K1044**	8	H	H	H	76 ± 1.1	64 ± 1.7	0.84	63.6 ± 2.1	CNS±
1		H	OCH3	H	10000 ± 97	18000 ± 80	1.76	<5	CNS+
2		Cl	H	H	20 ± 1.0	1800 ± 97	89	<5	CNS+
3		H	H	H	320 ± 13	80 ± 1.0	0.25	<5	CNS+
5 (tacrine-naphthoquinone)[51]	2	Cl	H	H	0.72 ± 0.06	540 ± 16	752.7	37.5 ± 4.9[d]	nd
8 (tacrine-melatonine)[46]	6	Cl	H	Cl	0.008 ± 0.0004	7.8 ± 0.4	975	nd	nd
9 (tacrine-melatonine)[47]	5	Cl	H	H	0.730 ± 0.03	180 ± 5	241	nd	CNS+
D,L-NQ-TRP	-	-	-	-	nd	nd	nd	25.4 ± 3.2	nd
6	-	-	-	-	nd	nd	nd	28.5 ± 3.6	nd

[a] Results are expressed as the mean of at least three experiments; [b] Selectivity for *h*AChE is determined as a ratio of *h*BChE IC_{50}/*h*AChE IC_{50}; [c] % Inhibition of Aβ_{42} self-aggregation at [I] = 50 μM. The [Aβ_{42}]/[I] ratio was equal to 1/1. Values are the mean from two to four independent experiments each performed in duplicate ± SD; [d] Inhibition of Aβ_{42} self-aggregation at [I] = 10 μM [e]Prediction of BBB penetration by the PAMPA-BBB assay. "nd" stands for not determined, CNS stands for central nervous.

ACCEPTED MANUSCRIPT

The selectivity index (SI) was calculated for all compounds within the study by comparing the IC_{50} value for *h*BChE inhibition with that achieved for *h*AChE inhibition. Most 7-MEOTA and THA hybrids were *h*BChE-selective (SI $\leq$ 1.0) or non-selective (SI $\cong$ 1.0) ChE inhibitors, while 6-Cl-THA hybrids showed a weak preference for AChE. This is in agreement with the selectivity profile of the implemented tacrine core. Hence, whereas all the tacrine hybrids were BChE selective in agreement with the higher affinity for BChE of THA, higher preference for *h*AChE was exhibited by hybrids bearing the 6-Cl-THA fragment. However, if compared with the selectivity profile of 6-Cl-THA (SI = 100.7), all 6-Cl-THA hybrids showed a much smaller SI with values ranging from 0.97 (non-selective) to 2.90 (slightly selective for *h*AChE).

Due to the increasing interest for dual AChE/BChE inhibition [70], this finding makes these hybrids particularly appealing. Indeed, it has been observed that levels of BChE in the brain increase with aging, while those of AChE decrease. This points out the importance of BChE inhibition in moderate to severe stages of AD [71]. The correctness of this idea has already been proved with the development of bisnorcymserine, a BChE-selective inhibitor, which is currently under evaluation in a Phase 1 clinical trial (ClinicalTrials.gov identifier: NCT01747213).

On the basis of anticholinesterase activity results, the best ChE inhibitor ***S*-K1035** was chosen as a prototype for investigating of the importance of the stereochemistry in ChE inhibition. For this purpose, the *R*-isomer (***R*-K1035**) and the racemic mixture (**rac-K1035**) were synthesized. In this regard, we have preserved the 6-Cl-THA scaffold and six-methylene tether and used either D-Trp to yield the *R*-isomer ***R*-K1035**, or the racemic Trp to afford the optically inactive **rac-K1035**. The stereochemistry of the Trp fragment does not seem to have any significant influence on the inhibition of *h*AChE as demonstrated by similar inhibitory activities of ***R*-K1035**, **rac-K1035** and ***S*-K1035**. However, and very surprisingly, a stereoselective interaction was highlighted for *h*BChE, with *S*-enantiomer being 15-fold more potent than the *R*-isomer (9.1 nM *vs.* 140 nM).

In comparison with the previously reported THA-NQ and THA-melatonin derivatives, the THA-Trp hybrids reported herein retained excellent *h*AChE inhibitory potency and showed increased activity towards *h*BChE. This makes them balanced dual AChE/BChE inhibitors, with potentially greater clinical efficacy and fewer side-effects.

Propidium displacement studies

The presence of a 6-methylene-tether chain in ***S*-K1035** makes this hybrid in principle able to span the gorge and likely reach the enzyme's PAS. Hence, to confirm this hypothesis and get deeper understanding of the mechanism of inhibition and to investigate the ability of ***S*-K1035** to interact with PAS, displacement studies using propidium were carried out [72,73]. Propidium, chemically 3,8-diamino-5-{3-[diethyl(methyl)ammonio]propyl}-6-phenylphenanthridinium diiodide, selectively associates with the PAS of AChE exhibiting an eight-fold enhancement of fluorescence [72,74]. Back-titration experiments with an

ACCEPTED MANUSCRIPT

increasing concentration of ***S*-K1035** showed a concentration-dependent decrease in the fluorescence intensity associated with the propidium–AChE complex. Following the method of Taylor and Lappi [73] a dissociation constant of 4.82 μM (Figure 3, SI) was calculated. This value shows that the interaction of ***S*-K1035** with PAS is about 6.9-fold weaker than that of propidium [74].

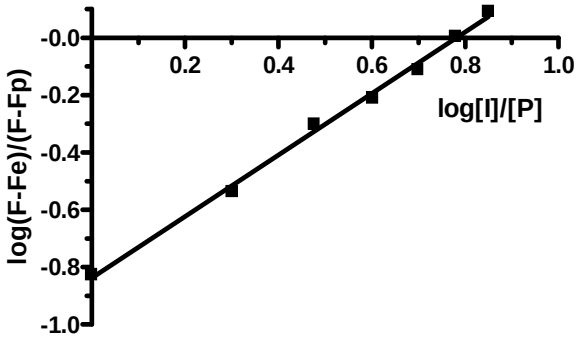

Figure 3: Determination of K_D value at the PAS for the most active derivative ***S*-K1035** by displacement studies. K_D value is calculated from the antilog of the Y-intercept value. P stands for propidium iodide and I stands for the tested inhibitor; Fe is the initial fluorescence intensity when enzyme sites are saturated with P, F_P is the fluorescence intensity when propidium is completely displaced from the enzyme, and F denotes the fluorescence intensity after adding a determined amount of the displacing agent during the titration experiment.

X-ray Crystallography of *Tc*AChE – *S*-K1035 Complex

In order to gain insights into the molecular determinants responsible for the high AChE inhibitory activity of ***S*-K1035**, the crystal structure of the inhibitor-bound *Tc*AChE (Figure 4) was determined by X-ray crystallography at a 2.50 Å resolution (summary of Crystallographic Data of the *Tc*AChE − ***S*-K1035** complex in Supporting Information, Table S2).

The position and orientation of ***S*-K1035** with respect to the key residues in the *Tc*AChE active-site gorge confirmed the critical role of the 6-Cl-THA fragment, which binds at the CAS.

The conformation of Phe330 in the *Tc*AChE − ***S*-K1035** complex (χ_1 = 145.4°, χ_2 = 63.1°) was found to be significantly different than those observed in the apo *Tc*AChE structure [75] – PDB ID 1EA5 (χ_1 = -126.6°, χ_2 = -48.9°), in the *Tc*AChE− tacrine-benzofuran hybrid complex [76] – PDB ID 4W63 (χ_1 = 92.6°, χ_2 = 110.3°), and in either of the two alternative conformations observed in the *Tc*AChE − NF595 [(N-(1,2,3,4-tetrahydroacridin-9-yl)-8-[(1,2,3,4-tetrahydroacridin-9-yl)thio]octan-1-amine)] [77] − PDB ID 2CEK complex (χ_1 = 76.1°, χ_2 = 83.1°; χ_1 = 96.9°, χ_2 = 80.4°)

In the *Tc*AChE− ***S*-K1035** complex, the swinging gate residue Phe330 closely matches the conformations observed in the *Tc*AChE – tacrine [78] – PDB ID 1ACJ (χ_1 = 157.1°, χ_2 = 61.8°), *Tc*AChE − bis(5)-tacrine [79] – PDB ID 2CMF (χ_1 = 160.6°, χ_2 = 67.1°) and *Tc*AChE – **4**,[79] – PDB ID 2CKM (χ_1 = 143.9°, χ_2 = 66.1°) and *Tc*AChE – **5**,[51] – PDB ID 4TVK (χ_1 = 141.5°, χ_2 = 62.5°) complexes, respectively.

ACCEPTED MANUSCRIPT

The 6-chloroquinoline substructure of ***S*-K1035** is embedded in a pocket lined with several aromatic residues (Trp233, Phe288, Phe330, Phe331, and Trp84). The central aromatic ring of the 6-Cl-THA is facing Trp84 while the lateral aromatic ring is facing Phe330.

The endocyclic nitrogen is hydrogen bonded to the main-chain carbonyl oxygen of the catalytic residue His440 (2.89 Å). It can be inferred, from this distance and from the pK_a = 9.8 of tacrine [80], that the 6-chloroquinoline moiety of ***S*-K1035** is protonated.

The contribution of the electron withdrawing effect by the chlorine atom to the AChE inhibitory activity of ***S*-K1035** (*h*AChE IC_{50} = 6.3 nM) with respect to the un-substituted ligand ***S*-K1042** (*h*AChE IC_{50} = 120 nM) may stem from non-specific close spatial contacts with neighboring amino acid residues. Indeed, the chlorine atom of ***S*-K1035** is nested in a hydrophobic pocket delimited by Phe330, Trp432, Met436, Ile439, and Tyr442.

The chlorine atom exhibits the strongest interaction with Trp432 (min. and max. distances of 3.4 Å and 4.3 Å, respectively). Hence, it is plausible that short-range dispersion forces are responsible for the optimal fit of the 6-chloroquinoline fragment in the binding pocket. In principle, the observed increase in affinity conferred by the chlorine atom may be due either to direct interactions with neighboring amino acids, or the modulation of the π−π stacking interaction of the tetrahydroacridine rings of ***S*-K1035**.

Conversely, the presence of the electron donating methoxy group at position 7 of the quinoline fragment in ***S*-K1028**, very significantly reduce the inhibitory activity toward AChE (IC_{50} = 940 nM) with respect to the un-substituted ligand ***S*-K1042** (IC_{50} = 120 nM). The observed significant drop of the AChE inhibitory activity can likely be attributed to a steric hindrance effect occurring between the methoxy group of ***S*-K1042** and (**1**) and the hydroxyl group of Tyr334. This segment includes *Tc*AChE Asp72, an important residue in the catalytic pathway that is positioned near a constriction, at the boundary between the peripheral and anionic binding sites, and that is primarily engaged in hydrogen bonding with Tyr334 [81].

Interestingly, in the *Tc*AChE−***S*-K1035** complex, the NH_2 group of ***S*-K1035** is not involved in hydrogen bonding with otherwise structurally conserved water molecules belonging to the active site water network. The orientation of the L-Trp moiety is stabilized by a weak hydrogen bonding interaction of 4.4 Å between the indole NH of the L-tryptophan moiety and the CO of Asn280. The likely protonated NH_2 moiety of the L-tryptophan fragment (pK_a = 9.4) is, in turn, engaged in a cation-π interaction with Trp279 (distances ranging between 3.2 Å and 4.3 Å) and in a weak hydrogen bonding interaction (4.1 Å) with the OH of Tyr70.

In addition, the positions of the backbone atoms of Trp279 do not significantly differ from their native positions (PDB ID 1EA5), the C_α atom being departed by 0.2 Å.

Likewise, in the structure of the *Tc*AChE−***S*-K1035** complex the side chain of Trp279 adopts a close orientation (χ_1 = -64.5°, χ_2 = 87.8°) with respect to that observed in the native *Tc*AChE structure (PDB ID 1EA5) (χ1 = -62.3°, χ2 = 96.7°). Conversely, a dramatic re-orientation of the Trp279 side chain was

ACCEPTED MANUSCRIPT

observed in the crystal structures of *Tc*AChE−tacrine (PDB ID 1 ACJ) (χ_1 = -53.6°, χ_2 = 31.2°), *Tc*AChE−NF595 (PDB ID 2CEK) (χ_1 = -118.2°, χ_2 = -131.9°), *Tc*AChE−bis(5)-tacrine (PDB ID 2CFM) (χ_1 = -76.3°, χ_2 = 95.2°), *Tc*AChE−**4** (PDB ID 2CKM) (χ_1 = -121.4°, χ_2 = -132.8°), *Tc*AChE−tacrine-benzofuran hybrid (PDB ID 4W63) (χ_1 = 51.3°, χ_2 = -82.0°), and *Tc*AChE−**5** (PDB ID 4TVK) (χ_1 = -71.4°, χ_2 = 100.7°), respectively.

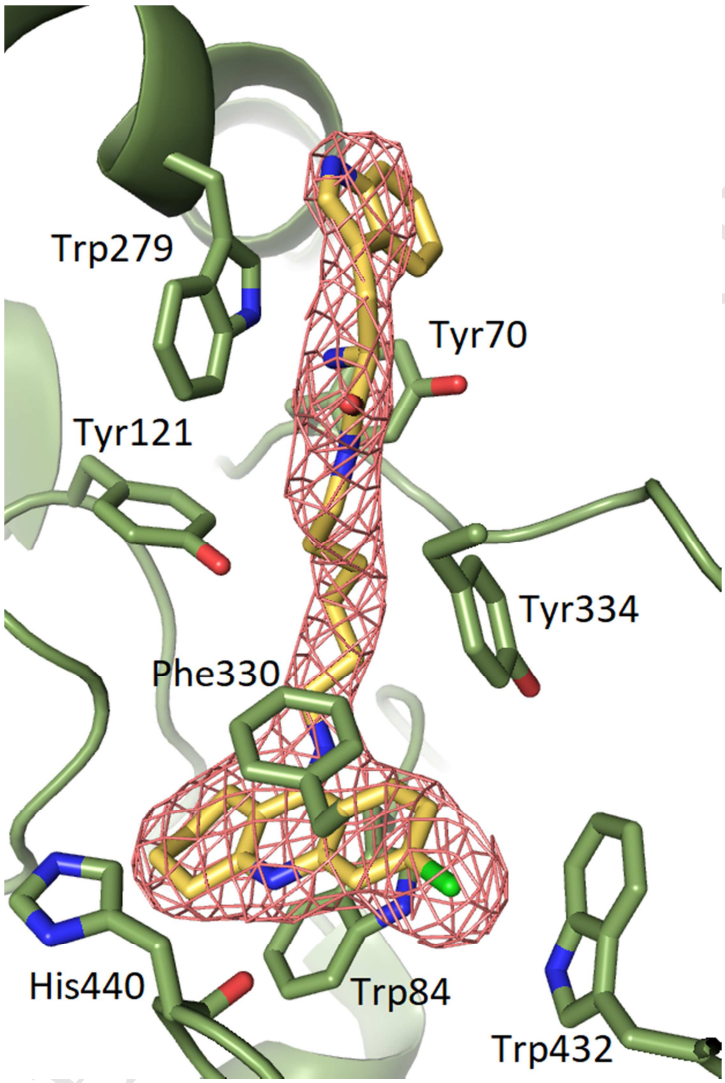

Figure 4. Close-up view of the active site of *Tc*AChE in complex with ***S*-K1035**. The final $2F_o$ - F_c σ_A-weighted electron density map, carved around ***S*-K1035**, is contoured at 1.0σ. The ***S*-K1035** inhibitor is rendered as a stick model with carbon, oxygen, and nitrogen atoms colored yellow-orange, red, and blue, respectively. Selected key protein residues (with carbon atoms colored in green) in the vicinity of ***S*-K1035** are rendered in stick format and labeled appropriately. The figure was created using PyMOL (http://www.pymol.org).

X-ray Crystallography of *h*BChE – *S*-K1035 and *h*BChE – *R*-K1035 complexes

Positions of both ***S***- and ***R*-K1035** are almost similar in human BChE, mainly stabilized by hydrophobic interactions (Figure 5 and S4). The chlorotacrine moiety of ***S***- and ***R*-K1035** interacts through π-π interactions with Trp82, their centroids being respectively at 3.7 Å and 3.8 Å distances. This interaction is similar to that observed in the structure of human BChE in complex with THA (PDB entry 4BDS). Their

ACCEPTED MANUSCRIPT

endocyclic nitrogen of THA scaffold is hydrogen bonded to the backbone carbonyl oxygen of His438, respectively at 2.8 Å and 2.9 Å distances, for ***S*-** and ***R*-K1035**. The chlorine atom is accommodated in a pocket formed by residues Ala328, Trp430, Met434, Met437 and Tyr440. Surprisingly and contrarily to *Tc*AChE, the tryptophan moiety of both ***S*-** and ***R*-K1035** folds back toward the chlorotacrine moiety in human BChE. This behavior can be explained by the larger active site gorge of BChE compared to AChE (500 vs 300 $Å^3$) and the lack of aromatic residues able to stabilize the indole moiety at the gorge entrance. For example, Trp279 in *Tc*AChE which interacts with the indole moiety (see above) is replaced by the aliphatic residue Ala277 in human BChE. The primary amine of ***S*-K1035** forms a hydrogen-bond with the backbone carbonyl oxygen of Ser287 (2.9 Å), while for the ***R*-** enantiomer it forms a similar hydrogen-bond with the backbone carbonyl oxygen of Pro285 (2.4 Å). Additionally, the amide nitrogen of ***S*-K1035** forms a hydrogen bond with the backbone carbonyl oxygen of Pro285 (2.7 Å). More interestingly, the orientation of the indole rings of the tryptophan moiety is the most significant difference between ***S*-** and ***R*-K1035** *h*BChE structures. In the ***R*-** conformation, the indole group does not make any specific interaction apart from hydrophobic ones with the surrounding residues. On the contrary, in the ***S*-** conformation, in addition to similar hydrophobic interactions, the nitrogen atom of the indole group is engaged in a hydrogen bond with a water molecule of the structural water network (3.4 Å), the latter being bridged to Oγ of Thr120 (2.5 Å) and a second water molecule (3.0 Å). These differences and additional interactions specific to the ***S*-** enantiomer plausibly account for the lower IC_{50} measured compared to the ***R*-** enantiomer.

ACCEPTED MANUSCRIPT

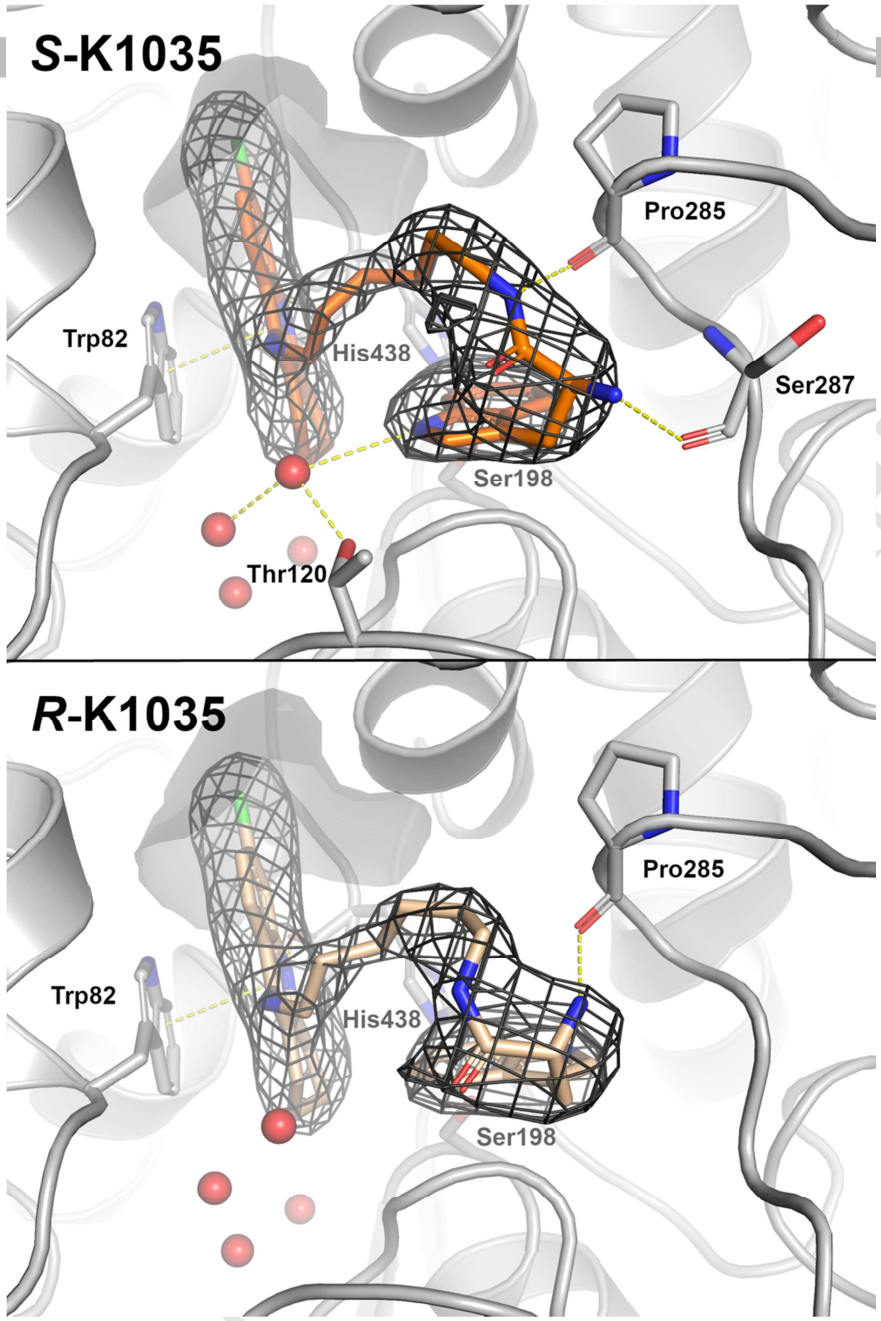

Figure 5. Comparative binding of the different enantiomers of **K1035** in human BChE. Cartoon representations of human BChE in complex with ***S*-K1035** (top, PDB entry 6I0B) or ***R*-K1035** (bottom, PDB entry 6I0C). Key residues are represented as sticks with carbon atoms in grey. Ligands are represented as stick models with carbon atoms represented in orange for ***S*-K1035** or beige for ***R*-K1035**. Nitrogen, oxygen and chlorine atoms are represented in blue, red and green, respectively. The pocket accommodating the chlorine atom is represented as a grey surface. Water molecules are shown as red spheres. The specific interactions such as hydrogen bonds or π-π interactions are represented as yellow dashed lines. The dark grey meshes represent omit polder maps of each **K1035** ligand contoured at 5 sigmas. The figure was created using PyMOL (http://www.pymol.org).

Inhibition of Aβ aggregation

ACCEPTED MANUSCRIPT

Despite the ongoing debate about the role of Aβ in the onset and progression of AD, new lines of evidence support the concept that accumulation of Aβ and its oligomerization may act as a triggering factor in AD. Therefore, there is a high interest in understanding and inhibiting this process. Amyloid is a nucleation-dependent phenomenon which, is triggered by peptide conformational change [82]. Aromatic residues, including tryptophan, seem to play a role in the self-aggregation process by favoring the stabilization of amyloid structures through the formation of π-stacking interactions [83–86]. Based on this observation, inhibitors bearing aromatic residues capable to target these aromatic recognition residues might reduce amyloid aggregation and act as disease modifying agents. In 2009, the D-tryptophan-α-aminoisobutyric acid dipeptide was shown to be able to interact with low-molecular-weight soluble Aβ oligomers and inhibit their toxicity [87]. Furthermore, D. Segal and E. Gazit research groups have recently shown that **6** was able to strongly reduce both amyloid oligomerization and amyloid fibril formation [56].

Based on these findings, in order to define the structural elements important for amyloid inhibition, all tacrine-tryptophan hybrids were assayed (at an inhibitor/Aβ ratio of 1/1) for their ability to inhibit the spontaneous aggregation of the most amyloidogenic isoform of Aβ, namely Aβ_{42}, by using a ThT-based fluorescence assay, which allows the monitoring of amyloid fibril formation [88,89]. Since amyloid aggregation is a very delicate process during which several different oligomeric isoforms are in equilibrium and the *in vitro* inhibitory activity may be strongly influenced by the assay conditions, **6** and its racemate 1,4-naphthoquinon-2-yl-DL-tryptophan (D,L-NQ-Trp) were synthesized and assayed for comparative reasons as reference compounds under the same assay conditions. To the best of our knowledge, the effect of chirality of Trp heterodimers on amyloid recognition has never been studied before.

An analysis of the results listed in Table 1 reveals that all hybrids were able to significantly inhibit Aβ_{42}-self-aggregation and that most of them, excluding ***S*-K1031**, ***S*-K1032** and ***S*-K1033**, were endowed with inhibitory potencies in a narrow range, i.e. from 44.0% (***S*-K1038**) to 63.6% (***S*-K1044**). The presence of higher molecular complexity given by the presence of the Trp moiety and the spacer chain seems to be important for the inhibitory activity, since THA and its analogues 7-MEOTA and 6-Cl-THA were not able to significantly inhibit amyloid aggregation.

The length of the spacer chain plays a different role for the three series of hybrids. Indeed, the similar inhibition percentage provided by all of the 7-MEOTA and THA hybrids points to the conclusion that the length of the spacer is not relevant for the inhibitory activity towards Aβ_{42} self-aggregation. Conversely, it seems to influence the inhibitory activity in the case of the 6-Cl-THA derivatives, since an increase in potency was observed when the length between the 6-Cl-THA and Trp fragments was increased from two to six methylene units (from 18.7 to 58.6%). The inhibitory potency remained almost unchanged for a further increase of the spacer length from six (***S*-K1035**) to eight methylene units (***S*-K1037**). Thus, for the 6-Cl-THA-Trp hybrids six/eight methylenes represent the optimal spacer length. This behavior may suggest a possible different mode of interaction for the 6-Cl-THA hybrids compared to the other two series of hybrids

ACCEPTED MANUSCRIPT

and may be beneficial to further investigation. Comparing the inhibitory potencies of hybrids from the three series bearing a space chain with six/eight methylenes, only slight differences can be observed. In the case that the chain length is optimal, the maximum inhibitory activity can be achieved independently from the type of the THA fragment. It might also be further reasoned that the methoxy substituent in position 7 and the chlorine in position 6 do not significantly influence the inhibitory activity towards amyloid self-aggregation. Finally, the stereocenter of the Trp fragment does not play any critical role (compare inhibition by ***S*-K1035**, ***R*-K1035** and **rac-K1035**).

Weaker inhibition was observed for **6** and its racemate assayed under the same experimental conditions with inhibition percentages (25.4% and 28.5%, respectively) considerably lower than those expected on the basis of the published data (IC_{50} = 50 nM) [56]. This difference might be ascribed to the different peptide used for the assay ($A\beta_{42}$ in our study and $A\beta_{40}$ in the study of Scherzer-Attali *et al.* [56]). Alternatively, since quenching phenomena were excluded and concentration dependence was confirmed, inhibition by **6** might be strongly affected by the type of oligomeric species and kinetics of their formation, which are different under different assay conditions. In the assay conditions used in this work, the newly synthesized tryptophan-tacrine hybrids performed significantly better than **6** and its racemate.

Besides self-aggregation, Aβ aggregation can be also triggered by molecular chaperones. AChE is listed among the „Aβ pathological chaperones“ due to its ability to promote the conformational changes in amyloid monomers and to trigger Aβ oligomerization [13,90]. Furthermore, *in vitro* study showed that AChE was able to form stable complexes with Aβ that were more toxic than Aβ aggregates alone [91]. Due to this non-classical role, AChE has gained much attention in the last decades. The chaperone activity of AChE towards Aβ is thought to be mediated by the PAS, through electrostatic interactions with the cationic area of Aβ [92].

Therefore, as ***S*-K1035** is able to interact with the AChE PAS (shown by X-ray studies on the ***S*-K1035**-AChE complex), we assayed the inhibitory activity of ***S*-K1035**, in comparison with that of ***R*-K1035** and **rac-K1035,** using a previously developed and validated protocol to verify whether the ability of ***S*-K1035** to interact with PAS translates into an inhibition of the molecular chaperone activity of AChE towards Aβ [90] Because of high costs of the assay, only the most promising derivative and its enantiomer were evaluated. The results were compared with those of the known AChEIs THA, donepezil, galantamine, rivastigmine, which were previously tested using the same experimental conditions [90,93]. The achieved data are listed in Table 2. THA was re-assayed as a negative control. It is well known that THA, galantamine, and rivastigmine are not able to significantly inhibit AChE-induced Aβ aggregation, while donepezil acts as a quite weak inhibitor [90] Due to structural similarity and known activity towards AChE-induced amyloid aggregation, **4** was selected as a positive reference compound. Inhibition percentage concurs with previous data [94].

ACCEPTED MANUSCRIPT

The inhibitory activity of novel compounds at the screening concentration was weaker than that of **4** but significantly higher than reference drugs and **6**. The weaker activity, compared to **4**, is in agreement with results from the crystal structure analysis [79]. The more and the less energetically favored π–π "sandwich" and "T shaped" stacking configurations between either the outer THA moiety of **4** or the indole ring of ***S*-K1035** and the Trp279 indole ring have been observed in the *Tc*AChE- **4** (PDB ID 2CKM) and *Tc*AChE- ***S*-K1035** complexes, respectively. The average distances and the tilting angles between the planes of the above-mentioned rings are of 4.0 Å and 1.0 ° in the *Tc*AChE- **4** complex and of 4.9 Å and -49.2 ° in the *Tc*AChE- ***S*-K1035** complex. These represent key molecular determinants that nicely support the observed lower percentage of *in vitro* inhibition of *h*AChE-induced Aβ_{40} aggregation of 48 ± 6.3% by ***S*-K1035** *vs.* 66.7 ± 4.3% by **4** (Table 2).

Interestingly, the stereochemistry seems to play a role, although to a very limited extent. Indeed, the compounds bearing the L-Trp unit, i.e. ***S*-K1035** and **6**, are slightly more active than those bearing the D-Trp (48.3% *vs*. 36.7% for the *S*- and *R*-enantiomer of the 6-Cl-THA derivative, respectively).

This inhibitory activity toward AChE-induced amyloid aggregation, together with the direct action on amyloid self-aggregation, may have a synergic role in the reduction of the neurotoxic effects of amyloid aggregates in the brain of AD patients.

Table 2. *In vitro* inhibition of Aβ_{40} aggregation induced by *h*AChE

Cmpd	Inhibition *h*AChE-induced Aβ_{40} aggregation (% ± SEM)[a]
***S*-K1035**	48.3 ± 6.3
***R*-K1035**	36.7 ± 4.7
rac-K1035	45.3 ± 4.0
D,L-NQ-Trp	34.2 ± 3.4
6	29.4 ± 0.6
THA	8.1 ± 2.1
4	66.7 ± 4.3
Donepezil	22[b]
Galantamine	17.9 ± 0.1[c]
Rivastigmine	<5[c]

[a] % inhibition of *h*AChE-induced Aβ_{40} aggregation at [I] = 100 μM. The Aβ_{40}/*h*AChE ratio was equal to 100/1. Values are the mean of two experiments each performed in duplicate ± SEM. [b] Data from reference[90] [c] Data from reference[93]

In vitro blood-brain barrier permeation assay

Penetration across the blood-brain barrier (BBB) is an essential property for compounds targeting the central nervous system (CNS). The brain permeability via passive diffusion of the novel THA-Trp hybrids has been predicted through a parallel artificial membrane permeation assay of the BBB (PAMPA-BBB) described by

ACCEPTED MANUSCRIPT

Di *et al*. [95,96]. The analysis allowed us to obtain preliminary data prior to the administration of the compounds to animals. The permeability is expressed as P_e ($P_e \times 10^{-6}$ cm·s^{-1}) with the following limits: P_e > 4.0 for compounds with high prediction of BBB permeation (CNS +), P_e < 2.0 for compounds with low BBB permeation (CNS -), and 4.0 > P_e > 2.0 for compounds with uncertain BBB permeation (CNS ±). Based on the results (Table 1), seven tested THA-Trp hybrids exhibited the potential to cross the BBB via passive diffusion. Two basic patterns for BBB permeation can be found. In detail, i) BBB permeability is inferred by tacrine scaffolds with more to less permeable hybrids as follows 6-Cl-THA > 7-MEOTA > THA; ii) chain elongation leads to increased BBB permeability with the exception of the THA subset. It is generally accepted that Log*P* as well as log*D* are important factors for the prediction of passive diffusion. However, it has been reported that donor/acceptor systems better predict the permeability than Log*P* and log*D* values as other factors, such as ionization state, hydrogen bonding, and molecular size influence the permeability. This might explain why analogues with longer alkyl chain, i.e. with higher lipophilicity represented by higher Log D value showed lower penetration potential than their analogues having shorter alkyl chain in THA subset [97].

***In vitro* cell viability**

Safety of novel tacrine-tryptophan derivatives and their parent compounds (THA, 7-MEOTA, 6-Cl-THA, L-Trp) was assessed on the Chinese hamster ovary (CHO-K1) and human liver carcinoma (HepG2) cell lines using the standard 3-(4,5-dimethylthiazol-2-yl)-2,5-diphenyltetrazolium bromide (MTT) cell viability assay [98]. HepG2 cell line were purposely selected to investigate the preliminary hepatotoxicity profile. Indeed, it is well-known that hepatotoxicity is a critical issue that needs to be addressed when dealing with THA derivatives. In this regard, while all derivatives were assayed for cytotoxicity on CHO-K1 cells, the hybrids tested on HepG2 cells were selected on the basis of the anticholinesterase inhibitory activities. Eight hybrids, i.e. ***S*-K1028**, ***S*-K1029**, ***S*-K1035**, ***S*-K1036**, ***S*-K1042**, ***S*-K1044**, ***R*-K1035**, ***rac*-K1035** (two hybrids from each family), were inspected and the results are summarized in Table 3. Using CHO-K1 cell line, THA ranked as the compound with the lowest cytotoxic effect. Only one compound from the novel series, ***S*-K1043** also showed similar cytotoxicity in the same order of magnitude as THA towards the CHO-K1 cell line. However, these data reflect only the direct effect on isolated cell lines omitting the drug metabolism. Accordingly, it has been shown that the metabolism of **3** plays a crucial role on its hepatotoxicity [99]. In a similar way, 7-MEOTA can be considered as a relatively non-hepatotoxic tacrine derivative because of a different metabolic pathway, which further ensures its straight elimination from the organism [26].

Concerning each subset of tacrine-Trp hybrids, some conclusions can be drawn based on the obtained data. The order of toxicity is as follows: THA derivatives < 7-MEOTA analogues < 6-Cl-THA derivatives. 6-Cl-THA hybrids are presumably the most toxic because of the highest lipophilicity and thus easiest cell permeation disturbing cell viability. Furthermore, increasing the number of methylene units in the linker

ACCEPTED MANUSCRIPT

chain exacerbates the cytotoxicity. This feature also correlates well with compound lipophilicity [65]. Reference compounds 7-MEOTA, and 6-Cl-THA were found the least toxic on HepG2 cells, while all novel hybrids were more hepatotoxic than Trp, THA, 7-MEOTA and 6-Cl-THA with the Trp precursor being the least toxic. Interestingly, ***R*-K1035** and **rac-K1035** showed IC_{50} values comparable to that of ***S*-K1035** that allowed us to conclude that chirality is not the key factor for hepatotoxicity.

Table 3. Cell viability evaluation of tacrine-tryptophan hybrids and reference compounds

Cmpd	CHO-K1 cytotoxicity IC_{50} (μM) ± SEM[a]	HepG2 cytotoxicity IC_{50} (μM) ± SEM[a]
***S*-K1024**	131 ± 3	nd
***S*-K1025**	95 ± 11	nd
***S*-K1026**	73 ± 18	nd
***S*-K1027**	46 ± 3	nd
***S*-K1028**	23 ± 3	16 ± 0.5
***S*-K1029**	14 ± 1	5.6 ± 0.5
***S*-K1030**	43 ± 12	nd
***S*-K1031**	26 ± 6	nd
***S*-K1032**	29 ± 5	nd
***S*-K1033**	16 ± 1	nd
***S*-K1034**	21 ± 3	nd
***S*-K1035**	21 ± 2	4.9 ± 0.4
***S*-K1036**	24 ± 5	6.0 ± 0.5
***S*-K1037**	65 ± 10	nd
***S*-K1038**	200 ± 20	nd
***S*-K1039**	116 ± 4	nd
***S*-K1040**	34 ± 3	nd
***S*-K1041**	83 ± 1	nd
***S*-K1042**	90 ± 4	26 ± 1.1
***S*-K1043**	248 ± 6	nd
***S*-K1044**	47 ± 3	9.3 ± 1.2
***R*-K1035**	15 ± 2	4.2 ± 0.6
rac-K1035	21 ± 3	5.1 ± 0.3
1	63 ± 4	120 ± 3
2	71 ± 2	71 ± 1.1
3	248 ± 11	190 ± 7.5
13	nd	17000 ± 900

ACCEPTED MANUSCRIPT

[a] Values are the mean ± SEM of three independent measurements. "nd" stands for not determined.

ACCEPTED MANUSCRIPT

***In vitro* effects of compounds on the activity on neuronal nitric oxide synthase**

NMDA receptors are associated with particular NOS isoforms through a postsynaptic density protein. The excessive stimulation of the receptors activates synthesis of nitric oxide (NO) especially via nNOS isoform - NO pathway is involved in the neuropathology of many neurodegenerative diseases, including AD [100]. In addition to NMDA receptor antagonists, such as memantine, the reduction of excessive NO generation by inhibiting the activity of nNOS could be the viable therapeutic approach for AD [101]. Particular attention in this field has been turned to dimeric compound **4** (Figure 1) acting synergistically *via* the blockade of NMDA receptors and inhibition of nNOS. Besides **4**, other well-known nNOS inhibitors with potential implication in AD treatment, such as N^G-monomethyl-L-arginine (L-NMMA) and 7-nitroindazole (7-NI) (Figure 5) showed inhibition potency in the same order of magnitude with IC_{50} values in the micromolar concentration [102]. In the *in vitro* experiment, we evaluated all THA-Trp hybrids ***S*-K1024-K1044**, ***R*-K1035** and **rac-K1035** showing moderate inhibition ability against nNOS with IC_{50} values in the range of 18-45 μM (Table 4). Note that all of the reference compound, *i.e*. THA, 6-Cl-THA, 7-MEOTA and **13** were ineffective proposing that nNOS inhibition potency is an unique feature delivered by a combination of different tacrine scaffolds with L-Trp. Our data indicates that the length of aliphatic linkers or chirality (comparison of effects of ***S*-K1035**, ***R*-K1035** and **rac-K1035**) do not play a significant role in the nNOS inhibition. To conclude, all of the new heterodimers resulted to be only slightly less effective inhibitors of nNOS in comparison with bis(7)tacrine, L-NMMA.

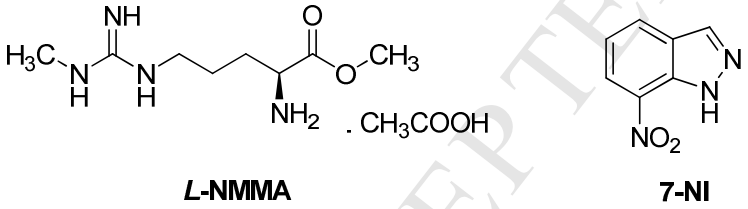

***L*-NMMA** **7-NI**

Figure 5. Structures of NOS inhibitors N^G-monomethyl-*L*-arginine (*L*-NMMA) and 7-nitroindazole (7-NI).

Table 4. Effect of the compounds on the nNOS activity

Cmpd	nNOS IC_{50} (μM) ± SEM)[a]
***S*-K1024**	19 ± 1
***S*-K1025**	30 ± 7
***S*-K1026**	27 ± 3
***S*-K1027**	26 ± 9
***S*-K1028**	27 ± 7
***S*-K1029**	26 ± 9

ACCEPTED MANUSCRIPT

***S*-K1030**	45 ± 10
***S*-K1031**	39 ± 10
***S*-K1032**	31 ± 12
***S*-K1033**	26 ± 8
***S*-K1034**	27 ± 10
***S*-K1035**	26 ± 11
***S*-K1036**	27 ± 4
***S*-K1037**	43 ± 11
***S*-K1038**	33 ± 4
***S*-K1039**	32 ± 10
***S*-K1040**	18 ± 1
***S*-K1041**	26 ± 12
***S*-K1042**	33 ± 2
***S*-K1043**	32 ± 8
***S*-K1044**	37 ± 8
***R*-K1035**	26 ± 4
***rac*-K1035**	33 ± 9
4[b]	2.9 ± 0.21
L-NMMA[b]	4.1 ± 0.17
7-NI[b]	0.7 ± 0.19

[a] Values are the mean ± SEM of three independent measurements. [b] Data from reference[102].

In vivo toxicity and behavioral studies

In order to predict the *in vivo* toxic effect of ***S*-K1035**, the assessment of acute toxicity upon intraperitoneal (i.p.) administration (fixed dose procedure) was performed in adult Wistar rats. The maximum tolerated dose (MTD) of ***S*-K1035** was determined to be 70 $mg \cdot kg^{-1}$. At this dose, only mild to moderate signs of intoxication occurred, including partial piloerection, persistent oculonasal discharge, intermittent abnormal breathing pattern, intermittent tremors and prostration, diminishing spontaneously within approximately 2 h. No weight loss was observed in rats administered with the dose corresponding to MTD within 24 and 48 h. For comparative purposes but using intramuscular (i.m.) administration, THA revealed a toxicity expressed at the MTD of 34 $mg \cdot kg^{-1}$ [103].

Knowing the tolerated dose, the therapeutic efficacy of tested drugs was assessed in the animal models of the disease. Namely, the effect of ***S*-K1035** in scopolamine-induced model of cognitive deficit in adult Wistar rats was investigated. Scopolamine, a competitive muscarinic ACh receptor antagonist, causes deficits in multiple cognitive domains and it is considered as an appropriate model for assessing the efficacy

ACCEPTED MANUSCRIPT

of various procognitive compounds [104]. Different AChEIs including THA [105], donepezil [104] and phenserine [106], were found to have therapeutic effect in modifications of scopolamine model in rats.

The effect of ***S*-K1035** on cognition was tested in the Morris water maze (MWM; long-term memory version), which represents one of the most common tests of spatial cognition of laboratory rodents. The MWM task designed by Jackson and Soliman was modified and used [105]. The rats underwent 3 days of intact training and on the 4th day before MWM, drugs were applied. The effect of drugs was assessed by comparing the performance of the group on MWM day 3 (group baseline, without drugs) with the performance of the same group on day 4 (with drugs). ***S*-K1035** was applied intracerebroventricularly (i.c.v.; at two concentrations:10 nM and 100 nM), scopolamine (SCOP) was applied intraperitoneally (i.p.; 5 $mg \cdot kg^{-1}$), saline (SAL) was applied i.c.v and i.p.. There were five treatment groups: (1) SAL i.c.v. + SAL i.p.; (2) SAL i.c.v. + SCOP i.p.; (3) ***S*-K1035** 100 nM i.c.v. + SAL i.p.; (4) ***S*-K1035** 10 nM i.c.v. + SCOP i.p.; (5) ***S*-K1035** 100 nM i.c.v. + SCOP i.p. (Figure 6).

In our experiment, ***S*-K1035** was applied i.c.v. and its effect was observed in modified MWM. The MWM design containing only one application of the tested drug and scopolamine was chosen, because it is suitable for the i.c.v. application (in comparison with repeated i.c.v. applications, which can represent an increased risk of the head implant damage by repeated manipulations). This MWM design involving the application of scopolamine after intact training in MWM requires a relatively high dose of scopolamine (5 $mg \cdot kg^{-1}$, used in our study and in the work of Jackson and Soliman [105]).

It should be also mentioned that the lower concentration of ***S*-K1035** administered (10 nM) mimics the administration of ***S*-K1035** at a concentration close to its IC_{50} values towards cholinesterase enzyme, i.e. 6.3 nM for *h*AChE. The higher dose of ***S*-K1035** administered (100 nM) is more than ten-times higher. The need of this high dose is related to the rather high dose of scopolamine used in the experimental set up (as mentioned above). Indeed, it is worth mentioning that in the study of Jackson and Soliman who studied the effect of THA upon scopolamine-induced cognitive impairment in a similar modification of MWM (application of 5 $mg \cdot kg^{-1}$ of scopolamine preceded by intact training in MWM), also a high dose of THA (8 $mg \cdot kg^{-1}$) was used to overcome the effect of this dose of scopolamine.

The results showed that there was no significant difference between groups on day 3 (baseline, before the treatment) in any of the four studied parameters (distance moved, escape latency, average distance from platform, time in target sector). In saline-treated animals (SAL i.c.v. + SAL i.p.), no significant difference between day 3 and day 4 performance in any of parameters measured was found, showing that the manipulations during the injections alone had no effect on rat performance.

Administration of scopolamine (SAL i.c.v. + SCOP i.p.) caused a significant increase of distance moved ($p = 0.0043$), escape latency ($p = 0.0194$), average distance from platform ($p = 0.0152$), and a considerable

ACCEPTED MANUSCRIPT

decrease in time spent in the target sector (p = 0.0411). These findings indicate cognitive deficit and therefore confirm the validity of the modification of the model used.

In control group of ***S*-K1035** (higher dose) treated animals (***S*-K1035** 100 nM i.c.v. + SAL i.p.) only, no significant change in any of parameters measured was found. The i.c.v. application of ***S*-K1035** alone thus did not have any detrimental effect on rat performance. In addition, in the ***S*-K1035** treated animals, we did not observe any evident cholinergic effects like salivation or tremors.

In the group treated with the lower dose of ***S*-K1035** and with scopolamine (***S*-K1035** 10 nM i.c.v. + SCOP i.p.), there was a significant increase between the distance moved on day 3 and day 4 (p= 0.0411), showing that the lower dose of ***S*-K1035** was not sufficient to alleviate the increase of distance moved caused by scopolamine. On the other hand, concerning escape latency, average distance from platform, time in target sector, there were no differences between day 3 and day 4, indicating ***S*-K1035** was able to ameliorate these parameters even at a lower dose. Therefore, the therapeutic effect of the lower dose of ***S*-K1035** was only partial. Most importantly, in the ***S*-K1035** (higher dose) and scopolamine-treated rats (***S*-K1035** 100 nM i.c.v. + SCOP i.p.), we did not find any significant difference between day 3 and day 4 performance in any parameter studied, demonstrating the beneficial effect of ***S*-K1035** in the scopolamine-induced cognitive deficit rat model.

In summary, we proved a dose-dependent beneficial effect of ***S*-K1035** in scopolamine-induced cognitive deficit rat model. This favorable result is consistent with the AChE inhibiting action of ***S*-K1035**, as some other AChEIs were found to be effective in modifications of the scopolamine model in MWM in rats. THA was effective in a similar modification of MWM, in which it completely alleviated escape latency impairment caused by scopolamine. Similar effect on cognitive improvement was observed for THA, however, direct comparison of their action is impossible since THA was administered i.p. [105]. Additionally, we are also displaying other beneficial properties of ***S*-K1035**, that are not conveyed to the action of THA, like inhibition of Aβ-self/AChE-induced aggregation and inhibition of nNOS as shown *in vitro*. From a long-term view point of view of AD therapy, ***S*-K1035** may deliver much appreciable effect not only to reduce the symptoms of AD but also to mitigate pathological signs of the disease.

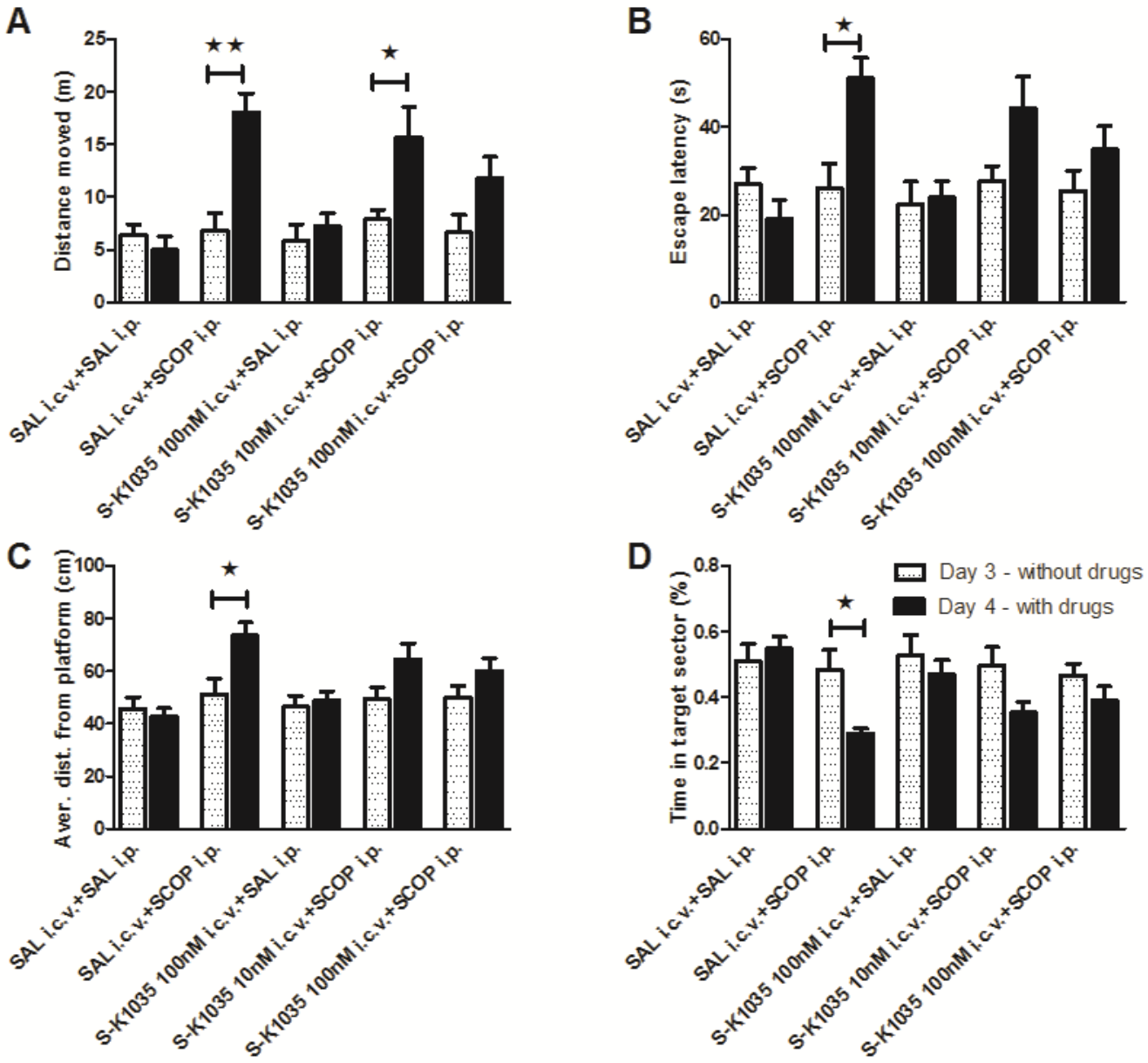

Figure 6. Effects of ***S*-K1035** in the scopolamine-induced model of cognitive deficit in Morris water maze comparing group performance on days 3 and 4. A - distance moved to reach the platform, B – escape latency, C – average distance from the platform, and D – time in the target sector.

The performance of the group on MWM day 3 (group baseline, without drugs) was compared with the performance of the same group on day 4 (with drugs). In scopolamine treated rats (SAL i.c.v. + SCOP i.p.) the distance moved (Figure 6 A) was increased ($p = 0.0043$). In rats treated with scopolamine and 10 nM ***S*-K1035** (***S*-K1035** 10 nM i.c.v. + SCOP i.p.), the distance was also increased ($p = 0.0411$), whereas there was no significant change in the distance moved for rats treated with scopolamine and 100 nM ***S*-K1035** (***S*-K1035** 100 nM i.c.v.+SCOP i.p.). This indicate the therapeutic effect of the higher dose of ***S*-K1035** in this parameter. Scopolamine (SAL i.c.v. + SCOP i.p.) caused a significant impairment of rat performance in parameters of escape latency (Figure 6 B, $p = 0.0194$), average distance from the platform (Figure 6 C, $p = 0.0152$) and time in the target sector (Figure 6 D, $p = 0.0411$). Both the lower (***S*-K1035** 10 nM i.c.v. +

ACCEPTED MANUSCRIPT

SCOP i.p.) and higher (***S*-K1035** 100 nM i.c.v. + SCOP i.p.) doses of ***S*-K1035** were able to alleviate the effect of scopolamine in all considered parameters (significant differences between day 3 and day 4 were not found). Saline (SAL i.c.v.+SAL i.p.) or the higher dose of ***S*-K1035** alone (***S*-K1035** 100 nM i.c.v.+SAL i.p.) did not have any detrimental effect on any parameter of the rat performance in MWM. All values represent mean ± SEM, * $p < 0.05$, ** $p < 0.01$.

Conclusions

This study describes the design, synthesis, *in vitro* and *in vivo* evaluation of new tacrine-tryptophan heterodimers. The synthesis of both enantiomers of ***R*-K1035** and ***rac*-K1035** has allowed to assess differences in potency with respect to the multiple tested biological activities. ***S*-K1035** was found to demonstrate the highest levels of *h*AChE and *h*BChE inhibition if compared to reference standards THA, 7-MEOTA and 6-Cl-THA. Moreover, the crystal structure confirmed the ability of ***S*-K1035** to target both the CAS and PAS of AChE. All the new hybrids also significantly inhibited Aβ_{42} self-aggregation and the *h*AChE-induced Aβ_{40} aggregation. Most of them were predicted to cross BBB via passive diffusion and exhibited moderate inhibitory activity against nNOS. ***S*-K1035** as distinctive *h*AChE/*h*BChE inhibitor was selected in order to determinate its toxic profile. ***S*-K1035** showed higher HepG2 and CHO-K1 cytotoxicity than tacrine-based analogues, however, these data displayed only the direct effect on isolated cell lines omitting the drug metabolism and behavior under *in vivo* conditions. Assessment of the acute toxicity of ***S*-K1035** was performed on rats. In agreement with a more complex fate of a drug in a whole body compared to isolated cells, the safety behavior of ***S*-K1035**, compared to THA, was reversed. Indeed, the MTD of ***S*-K1035** was found to be 70 mg·kg^{-1}, a value which is two times higher than that found for THA, meaning ***S*-K1035** can be considered safer than THA when administered to rats. Based on these results, the therapeutic effect of ***S*-K1035** in a scopolamine-induced cognitive deficit rat model was investigated using Morris water maze that confirmed pro-cognitive potential.

All of these results suggested that the newly developed tacrine-tryptophan derivatives represent a novel promising MTDLs that deserve further investigation for their potential use against AD.

Experimental section

Chemistry. General Methods. All reagents were reagent grade quality and obtained from Sigma-Aldrich (Prague, Czech Republic). Solvents for synthesis of tacrine-tryptophan hybrids were obtained from Penta Chemicals Co. (Czech Republic). All experiments were carried out under nitrogen atmosphere. Thin layer chromatography (TLC) was performed on aluminium sheets precoated with silica gel 60 F254 (Merck, Prague, Czech Republic) and then visualized by UV 254. Column chromatography was performed at normal pressure on silica gel 100 (particle size of 0.063-0.200 mm, 70-230 mesh ASTM, Fluka, Prague, Czech Republic). Mass spectra were recorded using a combination of high performance liquid chromatography and mass spectrometry. The analytical system Dionex Ultimate 3000 LC-MS was connected with a Orbitrap Q

ACCEPTED MANUSCRIPT

Exactive Plus hybrid spectrometer (Thermo Fisher Scientific, Bremen, Germany). ^{1}H-NMR and ^{13}C-NMR spectra were recorded with a Varian Mercury VX BB 300 (operating at 300 MHz for ^{1}H and 75 MHz for ^{13}C) or on a Varian S500 spectrometer (operating at 500 MHz for ^{1}H and 126 MHz for ^{13}C; Varian Comp., Palo Alto, CA). Chemical shifts are reported in parts per million (ppm, δ) relative to tetramethylsilane (TMS). The assignment of chemical shifts is based on standard NMR experiments (^{1}H, ^{13}C, ^{1}H-^{1}H COSY, ^{1}H-^{13}C HSQC, HMBC, DEPT). All of the final compounds showed ≥95% purity by analytical UHPLC (uncalibrated compound purity was determined at the wavelength of 254 nm as a percent ratio between the peak area of the compound and the total area of all peaks in the chromatogram; see Supporting information). Electronic circular dichroism (ECD), a chiroptical method, was used to determine the absolute configuration of the newly prepared hybrids. Our assumption that the hybrids adopt the same configuration corresponding with L-tryptophan has been confirmed. For more information, see Supporting information. Melting points were measured on a microheating stage PHMK 05 (VEB Kombinant Nagema, Radebeul, Germany) and are presented as uncorrected.

Pan assay interference compounds (PAINS) analysis. We have analyzed ***S*-K1024-K1044, *R*-K1035** and ***rac*-K1035** for known classes of assay interference compounds [107]. These compounds were not recognized as PAINS according to the Free ADME-Tox Filtering Tool (FAF-Drugs4) program (http://fafdrugs4.mti.univ-paris-diderot.fr/) or as aggregators according to the software "Aggregator Advisor" (http://advisor.bkslab.org/).

General Procedure for Synthesis of N-[(tert-butoxy)carbonyl]-L-tryptophan (**16**).

The reaction mixture of L-tryptophan (**13**, 4.89 mmol), triethylamine (9.79 mmol) and di-*tert*-butyl dicarbonate (Boc_2O, 6.36 mmol) was stirred in methanol (10 mL) under the nitrogen at room temperature for 24 hours. After the evaporation of methanol under the pressure, the final product was isolated in 87% yield.

General Procedure for Synthesis of N-[(tert-butoxy)carbonyl]-D-tryptophan (**17**).

The reaction mixture of D-tryptophan (**14**, 4.89 mmol), triethylamine (9.79 mmol) and di-*tert*-butyl dicarbonate (Boc_2O, 6.36 mmol) was stirred in methanol (10 mL) under the nitrogen at room temperature for 24 hours. After the evaporation of methanol under the pressure, the final product was isolated in 86% yield.

General Procedure for Synthesis of N-[(tert-butoxy)carbonyl]-DL-tryptophan (**18**).

The reaction mixture of DL-tryptophan (**15**, 4.89 mmol), triethylamine (9.79 mmol) and di-*tert*-butyl dicarbonate (Boc_2O, 6.36 mmol) was stirred in methanol (10 mL) under the nitrogen at room temperature for 24 hours. After the evaporation of methanol under the pressure, the final product was isolated in 88% yield.

General Procedure for Synthesis of N-(7-methoxy-1,2,3,4-tetrahydroacridin-9-yl)alkane-1,ω-diamines (**19-25**), *N*-(6-chloro-1,2,3,4-tetrahydroacridin-9-yl)alkane-1,ω-diamines (**26-32**) and *N*-(1,2,3,4-tetrahydroacridin-9-yl)alkane-1,ω-diamines (**33-39**).

ACCEPTED MANUSCRIPT

The reaction mixture of phenol (18 mmol) and appropriate 9-chlorotacrine (**10-12**, 2.01 mmol) was heated at 90 °C to form a liquid. To this mixture was added appropriate diamine (12 mmol) and refluxed at 130 °C for 4 hours. Then, the mixture was cooled to the room temperature and 20% aqueous solution of sodium hydroxide was added. The solution was extracted with dichloromethane. The organic layer was washed with brine and water and dried with sodium sulphate. The appropriate intermediate was purified by column chromatography using mobile phase ethylacetate/methanol/triethylamine (8:1:0.2). Yield: 70-90%.

General Procedure for Synthesis of Tacrine-Tryptophan Hybrids (***S*-K1024-K1044**).

N-[(*tert*-Butoxy)carbonyl]-L-tryptophan (**16**, 0.89 g, 2.95 mmol) was dissolved in dimethylformamide (10 mL) and stirred with triethylamine (1.22 mL, 8.85 mmol) at room temperature under nitrogen. Benzotriazol-1-yloxytris(dimethylamino)phosphonium hexafluorophosphate (BOP, 1.30 g, 2.95 mmol) was added to the reaction mixture after 30 minutes. Then, appropriate *N*-(1,2,3,4-tetrahydroacridin-9-yl)alkane-1,ω-diamine (**19-39**, 0.8 g, 2.95 mmol) was added to the mixture 1 hour later. This mixture was stirred at room temperature for 24 hours. The solution was extracted with ethylacetate/water (1:1) (3 × 100 mL:100 mL) and organic layer was dried over Na_2SO_4 and then evaporated under the pressure. The crude product was purified by column chromatography using mobile phase chloroform/methanol (50:1). Finally, an intermediate *tert*-butyl 1-(2-(*N*-(1,2,3,4-tetrahydroacridin-9-ylamino)ethylcarbamoyl)-2-(1*H*-indole-3-yl) ethylcarbamate (**40-62**) was dissolved in methanol (20 mL). 4 M HCl (20 mL) was added to the mixture. This reaction mixture was stirred at room temperature for 24 hours. Then, all the solvents were evaporated under the pressure to obtain required dihydrochloride.

Tert-butyl 1-(2-(7-methoxy-1,2,3,4-tetrahydroacridin-9-ylamino)ethylcarbamoyl)-2-(1*H*-indole-3-yl) ethylcarbamate (**40**). Yield 44%. ^{1}H NMR (500 MHz, DMSO-d_6) δ 10.77 (m, 1H), 8.08 (t, *J* = 5.7 Hz, 1H), 7.64 (d, *J* = 9.1 Hz, 1H), 7.53 (d, *J* = 7.9 Hz, 1H), 7.40 (d, *J* = 2.7 Hz, 1H), 7.29 (d, *J* = 8.0 Hz, 1H), 7.22 (dd, *J* = 9.1, 2.7 Hz, 1H), 7.09 (d, *J* = 2.4 Hz, 1H), 6.98 (m, 2H), 6.73 (d, *J* = 8.1 Hz, 1H), 4.13 (m, 1H), 3.88 (s, 3H), 3.29 (m, 2H), 2.98 (m, 1H), 2.87 (m, 3H), 2.71 (m, 2H), 2.49 (m, 2H), 1.98 (m, 2H), 1.80 (m, 2H), 1.28 (s, 9H). ^{13}C NMR (126 MHz, DMSO-d_6) δ 172.82, 170.52, 155.75, 155.34, 155.17, 149.94, 136.20, 129.10, 127.49, 123.75, 120.97, 120.88, 120.55, 118.60, 118.29, 116.73, 111.40, 110.33, 101.83, 78.16, 59.94, 55.62, 55.41, 47.50, 32.89, 29.17, 28.29, 27.95, 25.23, 22.88, 22.49, 20.94. HRMS $[M + H]^+$: 558.3078 (calculated for $[C_{32}H_{40}N_5O_4]^+$: 558.3075).

Tert-butyl 1-(2-(7-methoxy-1,2,3,4-tetrahydroacridin-9-ylamino)propylcarbamoyl)-2-(1*H*-indole-3-yl) ethylcarbamate (**41**). Yield 15%; mp 83.3-87.6 °C. ^{1}H NMR (500 MHz, Methanol-d_4) δ 7.66 (d, *J* = 9.2 Hz, 1H), 7.53 (d, *J* = 7.9 Hz, 1H), 7.47 (m, 1H), 7.30 (m, 1H), 7.26 (d, *J* = 8.1 Hz, 1H), 7.07 (s, 1H), 6.98 (m, 2H), 4.27 (m, 1H), 3.90 (s, 3H), 3.42 (m, 2H), 3.30 (m, 3H), 3.19 (m, 3H), 2.95 (m, 2H), 2.73 (m, 2H), 1.89 (m, 2H), 1.67 (m, 2H), 1.34 (s, 9H). ^{13}C NMR (126 MHz, Methanol-d_4) δ 176.36, 175.37, 158.12, 157.55, 154.47, 154.05, 137.97, 128.76, 126.34, 124.55, 123.41, 122.38, 121.08, 119.73, 119.37, 112.23, 111.38,

110.96, 103.27, 80.64, 61.53, 57.33, 56.35, 45.44, 37.36, 31.75, 29.20, 28.61, 26.22, 23.76, 22.11, 22.07, 20.86. HRMS $[M + H]^+$: 572.3225 (calculated for $[C_{33}H_{42}N_5O_4]^+$: 572.3232).

ACCEPTED MANUSCRIPT

Tert-butyl 1-(2-(7-methoxy-1,2,3,4-tetrahydroacridin-9-ylamino)butylcarbamoyl)-2-(1*H*-indole-3-yl) ethylcarbamate (**42**). Yield 79%. ^{1}H NMR (500 MHz, Methanol-d_4) δ 7.66 (d, *J* = 9.2 Hz, 1H), 7.53 (d, *J* = 7.7 Hz, 1H), 7.34 (d, *J* = 2.7 Hz, 1H), 7.27 (d, *J* = 8.1 Hz, 1H), 7.23 (dd, *J* = 9.2, 2.7 Hz, 1H), 7.05 (s, 1H), 7.02 (m, 1H), 6.96 (m, 1H), 4.25 (t, *J* = 7.1 Hz, 1H), 3.88 (s, 3H), 3.38 (m, 2H), 3.13 (m, 2H), 3.00 (m, 2H), 2.92 (t, *J* = 6.1 Hz, 2H), 2.70 (t, *J* = 6.0 Hz, 2H), 1.93 (s, 9H), 1.87 (m, 4H), 1.45 (m, 2H), 1.18 (m, 2H). ^{13}C NMR (126 MHz, Methanol-d_4) δ 176.34, 174.69, 172.96, 157.68, 156.20, 152.70, 142.54, 137.97, 128.69, 124.55, 123.26, 121.30, 119.57, 117.66, 112.19, 110.98, 102.99, 80.59, 61.51, 57.18, 56.13, 48.48, 39.97, 33.40, 29.37, 28.62, 27.63, 26.17, 24.00, 23.53, 22.06, 20.85. HRMS $[M + H]^+$: 586.3380 (calculated for $[C_{34}H_{44}N_5O_4]^+$: 586.3388).

Tert-butyl 1-(2-(7-methoxy-1,2,3,4-tetrahydroacridin-9-ylamino)pentylcarbamoyl)-2-(1*H*-indole-3-yl) ethylcarbamate (**43**) Yield 28%; 72.7-75.4 °C. ^{1}H NMR (500 MHz, DMSO-d_6) δ 10.77 (m, 1H), 7.83 (t, *J* = 5.7 Hz, 1H), 7.63 (d, *J* = 9.1 Hz, 1H), 7.55 (d, *J* = 7.9 Hz, 1H), 7.40 (d, *J* = 2.7 Hz, 1H), 7.30 (d, *J* = 8.1 Hz, 1H), 7.18 (dd, *J* = 9.1, 2.7 Hz, 1H), 6.99 (m, 2H), 6.66 (d, *J* = 8.4 Hz, 2H), 4.12 (m, 1H), 3.85 (s, 3H), 3.00 (m, 2H), 2.86 (t, *J* = 6.4 Hz, 3H), 2.71 (t, *J* = 6.2 Hz, 2H), 2.50 (m, 3H), 1.80 (m, 2H), 1.75 (m, 4H), 1.49 (m, 2H), 1.40 (m, 2H), 1.28 (s, 9H). ^{13}C NMR (126 MHz, DMSO-d_6) δ 171.68, 170.53, 155.74, 155.60, 149.61, 142.76, 136.21, 129.93, 127.54, 123.75, 121.39, 120.96, 120.10, 118.67, 118.28, 117.22, 111.40, 110.44, 101.72, 78.10, 59.95, 55.58, 55.36, 47.44, 38.35, 33.37, 28.31, 28.14, 26.76, 25.46, 23.00, 22.71, 22.69, 22.28, 20.95. HRMS $[M + H]^+$: 600.3546 (calculated for $[C_{35}H_{46}N_5O_4]^+$: 600.3545).

Tert-butyl 1-(2-(7-methoxy-1,2,3,4-tetrahydroacridin-9-ylamino)hexylcarbamoyl)-2-(1*H*-indole-3-yl) ethylcarbamate (**44**) Yield 74%. ^{1}H NMR (500 MHz, DMSO-d_6) δ 10.79 (m, 1H), 7.78 (t, *J* = 5.7 Hz, 1H), 7.63 (d, *J* = 9.1 Hz, 1H), 7.55 (d, *J* = 7.9 Hz, 1H), 7.41 (d, *J* = 2.8 Hz, 1H), 7.30 (d, *J* = 8.0 Hz, 1H), 7.18 (dd, *J* = 9.1, 2.7 Hz, 1H), 7.10 (d, *J* = 2.0 Hz, 1H), 6.98 (m, 2H), 6.69 (d, *J* = 8.3 Hz, 1H), 4.12 (m, 1H), 3.85 (s, 3H), 3.31 (m, 6H), 3.01 (m, 3H), 2.87 (m, 3H), 2.71 (m, 2H), 2.49 (m, 2H), 1.78 (m, 6H), 1.28 (s, 9H). ^{13}C NMR (126 MHz, DMSO-d_6) δ 171.87, 155.76, 155.56, 149.61, 142.86, 136.19, 130.02, 127.52, 126.11, 124.37, 123.73, 121.47, 120.94, 118.64, 117.27, 111.38, 110.42, 101.68, 78.05, 59.93, 55.53, 47.70, 38.57, 33.42, 32.46, 30.81, 30.78, 29.18, 28.29, 26.36, 25.50, 25.11, 23.00, 22.75, 20.93. HRMS $[M + H]^+$: 614.3692 (calculated for $[C_{36}H_{48}N_5O_4]^+$: 614.3701).

Tert-butyl 1-(2-(7-methoxy-1,2,3,4-tetrahydroacridin-9-ylamino)heptylcarbamoyl)-2-(1*H*-indole-3-yl) ethylcarbamate (**45**) Yield 86%. ^{1}H NMR (500 MHz, DMSO-d_6) δ 10.79 (s, 1H), 7.77 (t, *J* = 5.7 Hz, 1H), 7.63 (dd, *J* = 9.1, 1.6 Hz, 1H), 7.56 (d, *J* = 7.9 Hz, 1H), 7.41 (d, *J* = 2.6 Hz, 1H), 7.30 (d, *J* = 8.0 Hz, 1H), 7.18 (m, 1H), 7.10 (d, *J* = 2.2 Hz, 1H), 6.99 (m, 2H), 6.68 (d, *J* = 8.3 Hz, 1H), 4.13 (m, 1H), 3.85 (s, 3H), 3.31 (m, 8H), 3.00 (m, 4H), 2.87 (m, 2H), 2.71 (m, 2H), 2.49 (m, 2H), 1.79 (m, 6H), 1.29 (s, 9H). ^{13}C NMR (126 MHz, DMSO-d_6) δ 171.83, 170.50, 155.70, 149.69, 142.77, 136.19, 129.94, 127.53, 123.72, 121.40,

ACCEPTED MANUSCRIPT

121.37, 120.93, 120.06, 118.64, 118.26, 117.19, 111.38, 110.42, 101.73, 78.05, 59.93, 55.53, 55.34, 47.73, 38.62, 33.37, 30.81, 29.07, 28.76, 28.30, 28.10, 26.57, 26.42, 25.46, 22.98, 22.73, 20.94. HRMS $[M + H]^+$: 628.3846 (calculated for $[C_{37}H_{50}N_5O_4]^+$: 628.3858).

Tert-butyl 1-(2-(7-methoxy-1,2,3,4-tetrahydroacridin-9-ylamino)octylcarbamoyl)-2-(1*H*-indole-3-yl) ethylcarbamate (**46**) Yield 40%. ^{1}H NMR (500 MHz, Methanol-d_4) δ 7.65 (dd, *J* = 9.2, 1.1 Hz, 1H), 7.60 (d, *J* = 2.5 Hz, 1H), 7.52 (d, *J* = 7.9 Hz, 1H), 7.48 (m, 1H), 7.28 (d, *J* = 8.2 Hz, 1H), 7.04 (s, 1H), 7.01 (d, *J* = 7.7 Hz, 1H), 6.94 (t, *J* = 7.5 Hz, 1H), 4.25 (m, 1H), 3.93 (s, 3H), 3.87 (m, 2H), 3.14 (m, 2H), 2.98 (m, 2H), 2.68 (m, 2H), 1.93 (s, 16H), 1.78 (m, 2H), 1.35 (s, 9H). ^{13}C NMR (126 MHz, Methanol-d_4) δ 176.37, 174.61, 158.47, 157.15, 150.50, 137.94, 134.50, 128.72, 125.38, 124.51, 122.31, 121.70, 119.68, 119.32, 118.51, 112.87, 112.22, 110.94, 104.96, 80.62, 57.16, 56.47, 49.28, 48.74, 40.80, 40.26, 31.80, 30.06, 30.00, 29.39, 29.14, 28.60, 27.55, 27.23, 25.28, 23.04, 22.06, 21.79. HRMS $[M + H]^+$: 642.4010 (calculated for $[C_{38}H_{52}N_5O_4]^+$: 642.4014).

Tert-butyl 1-(2-(6-chloro-1,2,3,4-tetrahydroacridin-9-ylamino)ethylcarbamoyl)-2-(1*H*-indole-3-yl) ethylcarbamate (**47**) Yield 91%. ^{1}H NMR (500 MHz, Methanol-d_4) δ 8.13 (d, *J* = 9.2 Hz, 1H), 7.66 (d, *J* = 2.2 Hz, 1H), 7.47 (dt, *J* = 7.7, 1.1 Hz, 1H), 7.39 (dd, *J* = 9.2, 2.2 Hz, 1H), 7.15 (d, *J* = 8.0 Hz, 1H), 7.07 (s, 1H), 6.84 (m, 2H), 4.29 (t, *J* = 6.9 Hz, 1H), 3.68 (m, 2H), 3.45 (m, 2H), 2.88 (m, 2H), 2.46 (s, 2H), 1.93 (s, 9H), 1.35 (s, 6H). ^{13}C NMR (126 MHz, Methanol-d_4) δ 176.36, 172.99, 157.20, 155.73, 143.20, 138.22, 137.76, 128.71, 127.99, 125.99, 124.56, 122.25, 121.79, 119.67, 119.17, 116.84, 114.67, 112.11, 110.60, 80.73, 61.52, 57.09, 40.62, 31.12, 29.02, 28.61, 25.02, 23.19, 22.34, 22.06, 20.85. HRMS $[M + H]^+$: 562.2573 (calculated for $[C_{31}H_{37}ClN_5O_3]^+$: 562.2580).

Tert-butyl 1-(2-(6-chloro-1,2,3,4-tetrahydroacridin-9-ylamino)propylcarbamoyl)-2-(1*H*-indole-3-yl) ethylcarbamate (**48**) Yield 83%. ^{1}H NMR (300 MHz, Methanol-d_4) δ 8.04 (d, *J* = 9.2 Hz, 1H), 7.68 (d, *J* = 2.2 Hz, 1H), 7.53 (m, 1H), 7.32 (dd, *J* = 9.1, 2.2 Hz, 1H), 7.24 (d, *J* = 7.9 Hz, 1H), 7.06 (s, 1H), 6.97 (m, 2H), 4.26 (t, *J* = 7.0 Hz, 1H), 3.37 (m, 1H), 3.16 (m, 2H), 2.92 (m, 2H), 2.66 (m, 2H), 1.92 (s, 9H), 1.88 (m, 3H), 1.34 (m, 6H). ^{13}C NMR (75 MHz, Methanol-d_4) δ 175.32, 172.96, 157.53, 154.11, 146.30, 137.95, 136.49, 128.74, 126.82, 125.56, 124.82, 124.57, 122.36, 119.73, 119.38, 118.55, 116.23, 112.21, 110.92, 80.62, 61.52, 57.32, 46.01, 37.35, 33.10, 31.49, 29.23, 28.60, 25.78, 23.69, 23.11, 22.06. HRMS $[M + H]^+$: 576.2728 (calculated for $[C_{32}H_{39}ClN_5O_3]^+$: 576.2736).

Tert-butyl 1-(2-(6-chloro-1,2,3,4-tetrahydroacridin-9-ylamino)butylcarbamoyl)-2-(1*H*-indole-3-yl) ethylcarbamate (**49**) Yield 91%. ^{1}H NMR (500 MHz, Methanol-d_4) δ 8.13 (d, *J* = 9.2 Hz, 1H), 7.66 (d, *J* = 2.2 Hz, 1H), 7.47 (dt, *J* = 7.7, 1.1 Hz, 1H), 7.39 (dd, *J* = 9.2, 2.2 Hz, 1H), 7.15 (d, *J* = 8.0 Hz, 1H), 7.07 (s, 1H), 6.84 (m, 2H), 4.29 (t, *J* = 6.9 Hz, 1H), 3.68 (m, 2H), 3.45 (m, 2H), 2.88 (m, 2H), 2.46 (s, 2H), 1.93 (s, 9H), 1.35 (s, 6H). ^{13}C NMR (126 MHz, Methanol-d_4) δ 171.98, 170.49, 157.15, 155.28, 151.59, 136.19, 133.52, 127.51, 126.02, 125.13, 123.93, 123.75, 120.94, 118.63, 118.25, 117.86, 115.23, 111.38, 110.41,

78.07, 59.92, 55.37, 47.66, 38.33, 32.61, 28.29, 28.10, 27.87, 24.94, 22.68, 22.51, 22.04, 20.93. HRMS [M + H]$^+$: 590.2889 (calculated for $[C_{33}H_{41}ClN_5O_3]^+$: 590.2893).

ACCEPTED MANUSCRIPT

Tert-butyl 1-(2-(6-chloro-1,2,3,4-tetrahydroacridin-9-ylamino)pentylcarbamoyl)-2-(1*H*-indole-3-yl) ethylcarbamate (**50**) Yield 46%. ^{1}H NMR (500 MHz, DMSO-d_6) δ 10.76 (d, *J* = 2.3 Hz, 1H), 8.20 (d, *J* = 9.1 Hz, 1H), 7.79 (t, *J* = 5.7 Hz, 1H), 7.71 (dd, *J* = 2.3, 0.9 Hz, 1H), 7.53 (d, *J* = 7.9 Hz, 1H), 7.40 (m, 1H), 7.29 (d, *J* = 8.1 Hz, 1H), 7.09 (d, *J* = 2.3 Hz, 1H), 6.97 (m, 2H), 6.67 (d, *J* = 8.2 Hz, 1H), 4.11 (m, 1H), 3.50 (m, 2H), 3.01 (m, 3H), 2.87 (m, 3H), 2.65 (m, 2H), 1.78 (m, 4H), 1.75 (m, 2H), 1.58 (m, 2H), 1.34 (m, 2H), 1.28 (s, 9H). ^{13}C NMR (126 MHz, DMSO-d_6) δ 171.92, 171.63, 155.28, 152.36, 136.20, 134.19, 127.51, 126.37, 124.18, 124.02, 123.93, 123.75, 120.94, 118.62, 118.26, 117.24, 114.68, 111.39, 110.40, 78.08, 59.93, 55.38, 47.98, 38.50, 30.13, 28.85, 28.30, 28.09, 24.74, 23.65, 22.68, 22.32, 21.77, 20.93. HRMS [M + H]$^+$: 604.3045 (calculated for $[C_{34}H_{43}ClN_5O_3]^+$: 604.3049).

Tert-butyl 1-(2-(6-chloro-1,2,3,4-tetrahydroacridin-9-ylamino)hexylcarbamoyl)-2-(1*H*-indole-3-yl) ethylcarbamate (**51**) Yield 41%; mp 77.5-81.9 °C. ^{1}H NMR (300 MHz, Chloroform-*d*) δ 8.72 (m, 1H), 7.87 (m, 2H), 7.63 (d, *J* = 7.6 Hz, 1H), 7.26 (m, 1H), 7.11 (m, 2H), 7.01 (d, *J* = 2.3 Hz, 1H), 4.38 (m, 1H), 3.44 (t, *J* = 7.2 Hz, 2H), 3.07 (m, 6H), 2.65 (m, 3H), 1.89 (m, 5H), 1.55 (m, 2H), 1.41 (s, 9H), 1.21 (m, 4H). ^{13}C NMR (75 MHz, Chloroform-*d*) δ 171.57, 158.81, 155.41, 151.11, 147.32, 136.21, 134.30, 127.33, 126.65, 124.73, 124.28, 123.16, 122.07, 119.54, 118.81, 117.97, 115.38, 111.19, 110.50, 80.01, 55.28, 49.23, 39.11, 33.47, 31.41, 29.05, 28.53, 28.25, 26.31, 26.21, 24.42, 22.74, 22.41. HRMS [M + H]$^+$: 618.3209 (calculated for $[C_{35}H_{45}ClN_5O_3]^+$: 618.3206).

Tert-butyl 1-(2-(6-chloro-1,2,3,4-tetrahydroacridin-9-ylamino)heptylcarbamoyl)-2-(1*H*-indole-3-yl) ethylcarbamate (**52**) Yield 74%. ^{1}H NMR (500 MHz, Methanol-d_4) δ 8.08 (d, *J* = 9.1 Hz, 1H), 7.69 (d, *J* = 2.2 Hz, 1H), 7.53 (d, *J* = 7.9 Hz, 1H), 7.31 (dd, *J* = 9.2, 2.2 Hz, 1H), 7.27 (d, *J* = 8.1 Hz, 1H), 6.99 (m, 3H), 4.26 (m, 1H), 3.56 (m, 2H), 3.30 (m, 2H), 3.12 (m, 2H), 2.93 (m, 3H), 2.65 (m, 2H), 1.87 (m, 4H), 1.62 (m, 2H), 1.35 (s, 9H), 1.27 (m, 5H), 1.11 (m, 2H). ^{13}C NMR (126 MHz, Methanol-d_4) δ 174.57, 158.82, 157.46, 154.03, 147.18, 137.98, 136.22, 128.78, 126.90, 125.31, 125.24, 124.50, 122.33, 119.70, 119.38, 118.71, 116.06, 112.20, 110.97, 80.59, 61.52, 57.13, 40.23, 33.40, 32.02, 29.95, 29.89, 29.44, 28.63, 27.71, 27.53, 25.70, 23.74, 23.23, 22.05, 20.85. HRMS [M + H]$^+$: 632.3359 (calculated for $[C_{36}H_{47}ClN_5O_3]^+$: 632.3362).

Tert-butyl 1-(2-(6-chloro-1,2,3,4-tetrahydroacridin-9-ylamino)octylcarbamoyl)-2-(1*H*-indole-3-yl) ethylcarbamate (**53**) Yield 43%. ^{1}H NMR (500 MHz, Methanol-d_4) δ 8.14 (d, *J* = 9.1 Hz, 1H), 7.69 (d, *J* = 2.2 Hz, 1H), 7.53 (d, *J* = 7.9 Hz, 1H), 7.35 (dd, *J* = 9.1, 2.2 Hz, 1H), 7.27 (d, *J* = 8.1 Hz, 1H), 7.00 (m, 3H), 4.26 (m, 1H), 3.63 (m, 2H), 3.13 (m, 2H), 2.93 (m, 2H), 2.66 (m, 2H), 1.93 (m, 10H), 1.89 (m, 4H), 1.67 (m, 2H), 1.35 (s, 9H), 1.10 (m, 2H). ^{13}C NMR (126 MHz, Methanol-d_4) δ 174.58, 172.98, 157.66, 154.69, 146.01, 137.98, 136.89, 128.78, 127.21, 125.50, 124.50, 124.23, 122.33, 119.70, 119.37, 118.17, 115.64, 112.21, 110.98, 80.58, 61.52, 57.14, 40.28, 32.69, 31.91, 30.14, 30.09, 29.43, 28.63, 28.32, 27.70, 27.55, 25.53, 23.59, 22.98, 22.06, 20.85. HRMS [M + H]$^+$: 646.3510 (calculated for $[C_{37}H_{49}ClN_5O_3]^+$: 646.3519).

ACCEPTED MANUSCRIPT

Tert-butyl 1-(2-(1,2,3,4-tetrahydroacridin-9-ylamino)ethylcarbamoyl)-2-(1*H*-indole-3-yl) ethylcarbamate (**54**) Yield 28%. ^{1}H NMR (500 MHz, Methanol-d_4) δ 8.04 (d, *J* = 8.6 Hz, 1H), 7.73 (m, 1H), 7.57 (m, 1H), 7.52 (d, *J* = 7.8 Hz, 1H), 7.37 (m, 1H), 7.24 (d, *J* = 8.1 Hz, 1H), 7.05 (s, 1H), 6.95 (m, 2H), 4.28 (m, 1H), 3.51 (m, 2H), 3.30 (m, 2H), 2.93 (t, *J* = 6.1 Hz, 2H), 2.62 (t, *J* = 6.2 Hz, 2H), 1.87 (m, 4H), 1.34 (s, 9H), 1.17 (m, 2H). ^{13}C NMR (126 MHz, Methanol-d_4) δ 176.35, 175.80, 157.82, 157.52, 153.59, 137.95, 130.41, 128.75, 126.57, 125.07, 124.72, 124.54, 122.37, 120.45, 119.75, 119.33, 116.33, 112.21, 110.83, 80.67, 57.20, 49.51, 41.16, 33.35, 29.20, 28.62, 25.85, 23.87, 23.33, 22.06, 20.85. HRMS $[M + H]^+$: 528.2972 (calculated for $[C_{31}H_{38}N_5O_3]^+$: 528.2970).

Tert-butyl 1-(2-(1,2,3,4-tetrahydroacridin-9-ylamino)propylcarbamoyl)-2-(1*H*-indole-3-yl) ethylcarbamate (**55**) Yield 23%; mp 88.3-92.7 °C. ^{1}H NMR (500 MHz, Methanol-d_4) δ 8.05 (d, *J* = 8.5 Hz, 1H), 7.74 (m, 1H), 7.54 (m, 2H), 7.36 (m, 1H), 7.26 (d, *J* = 8.1 Hz, 1H), 7.06 (s, 1H), 6.98 (m, 2H), 4.28 (m, 1H), 3.16 (m, 2H), 2.95 (t, *J* = 6.0 Hz, 2H), 2.69 (t, *J* = 5.9 Hz, 2H), 1.92 (m, 4H), 1.88 (m, 2H), 1.60 (m, 2H), 1.34 (s, 9H), 1.18 (m, 2H). ^{13}C NMR (126 MHz, Methanol-d_4) δ 175.18, 172.95, 158.45, 157.52, 153.39, 147.02, 137.97, 130.11, 128.77, 127.18, 125.02, 124.55, 122.38, 120.96, 119.74, 119.41, 116.74, 112.22, 110.96, 80.62, 61.51, 57.28, 46.10, 37.52, 33.71, 31.62, 28.61, 26.12, 23.97, 23.49, 22.06, 20.85. HRMS $[M + H]^+$: 542.3134 (calculated for $[C_{32}H_{40}N_5O_3]^+$: 542.3126).

Tert-butyl 1-(2-(1,2,3,4-tetrahydroacridin-9-ylamino)butylcarbamoyl)-2-(1*H*-indole-3-yl) ethylcarbamate (**56**) Yield 42%. ^{1}H NMR (500 MHz, Methanol-d_4) δ 8.02 (d, *J* = 8.5 Hz, 1H), 7.74 (dd, *J* = 8.5, 1.2 Hz, 1H), 7.52 (m, 2H), 7.33 (m, 1H), 7.26 (d, *J* = 8.0 Hz, 1H), 7.05 (s, 1H), 6.98 (m, 2H), 4.26 (m, 1H), 3.38 (m, 2H), 3.14 (m, 2H), 2.94 (t, *J* = 6.1 Hz, 2H), 2.67 (t, *J* = 5.8 Hz, 2H), 1.86 (m, 4H), 1.33 (m, 13H), 1.18 (s, 2H). ^{13}C NMR (126 MHz, Methanol-d_4) δ 174.65, 172.94, 159.10, 157.46, 153.03, 147.90, 137.98, 129.70, 128.82, 127.94, 124.73, 124.37, 122.37, 121.27, 119.74, 119.46, 116.80, 112.20, 110.98, 80.58, 61.51, 57.18, 39.95, 34.17, 29.39, 28.63, 28.32, 27.54, 26.10, 24.07, 23.66, 22.06, 20.85. HRMS $[M + H]^+$: 556.3275 (calculated for $[C_{33}H_{42}N_5O_3]^+$: 556.3283).

Tert-butyl 1-(2-(1,2,3,4-tetrahydroacridin-9-ylamino)pentylcarbamoyl)-2-(1*H*-indole-3-yl) ethylcarbamate (**57**) Yield 25%; mp 73.3-76.8 °C. ^{1}H NMR (300 MHz, Methanol-d_4) δ 8.04 (m, 1H), 7.75 (m, 1H), 7.52 (m, 2H), 7.33 (m, 1H), 7.24 (d, *J* = 7.9 Hz, 1H), 6.97 (m, 3H), 4.25 (m, 1H), 3.39 (m, 2H), 3.11 (m, 2H), 2.94 (m, 4H), 2.69 (m, 2H), 1.95 (m, 2H), 1.87 (m, 6H), 1.50 (m, 2H), 1.34 (s, 9H). ^{13}C NMR (75 MHz, Methanol-d_4) δ 174.58, 172.92, 159.07, 157.44, 153.17, 147.91, 137.96, 129.71, 128.79, 127.93, 124.70, 124.42, 122.35, 121.30, 119.71, 119.42, 116.78, 112.18, 110.96, 80.55, 61.50, 57.14, 40.14, 34.16, 31.91, 29.83, 29.42, 28.63, 26.09, 25.01, 24.07, 23.68, 22.06, 20.85. HRMS $[M + H]^+$: 570.3434 (calculated for $[C_{34}H_{44}N_5O_3]^+$: 570.3439).

Tert-butyl 1-(2-(1,2,3,4-tetrahydroacridin-9-ylamino)hexylcarbamoyl)-2-(1*H*-indole-3-yl) ethylcarbamate (**58**) Yield 25%. ^{1}H NMR (500 MHz, DMSO-d_6) δ 10.77 (s, 1H), 8.13 (d, *J* = 8.6 Hz, 1H), 7.75 (m, 1H), 7.70 (dd, *J* = 8.5, 1.2 Hz, 1H), 7.54 (m, 1H), 7.35 (m, 1H), 7.29 (d, *J* = 8.0 Hz, 1H), 7.09 (d, *J* = 2.3 Hz, 1H),

ACCEPTED MANUSCRIPT

6.99 (m, 1H), 6.66 (d, *J* = 5.4 Hz, 6H), 4.11 (m, 1H), 3.43 (m, 2H), 3.00 (m, 2H), 2.89 (t, *J* = 6.2 Hz, 2H), 2.68 (t, *J* = 6.0 Hz, 2H), 2.49 (m, 2H), 1.79 (m, 4H), 1.75 (m, 6H), 1.53 (m, 2H), 1.28 (s, 9H). ^{13}C NMR (126 MHz, DMSO-d_6) δ 171.61, 170.49, 156.68, 155.25, 151.29, 136.19, 128.71, 127.52, 127.09, 123.71, 123.62, 123.50, 120.93, 119.74, 118.62, 118.26, 115.32, 111.37, 110.41, 78.06, 59.92, 55.35, 48.03, 38.56, 32.87, 30.67, 29.10, 28.29, 26.21, 26.16, 25.07, 22.67, 22.32, 20.92. HRMS $[M + H]^+$: 584.3593 (calculated for $[C_{35}H_{46}N_5O_3]^+$: 584.3596).

Tert-butyl 1-(2-(1,2,3,4-tetrahydroacridin-9-ylamino)heptylcarbamoyl)-2-(1*H*-indole-3-yl) ethylcarbamate (**59**) Yield 52%. ^{1}H NMR (500 MHz, Methanol-d_4) δ 8.08 (d, *J* = 8.6 Hz, 1H), 7.75 (m, 1H), 7.54 (m, 2H), 7.35 (m, 1H), 7.28 (d, *J* = 8.0 Hz, 1H), 7.00 (m, 3H), 4.26 (m, 1H), 3.51 (t, *J* = 7.2 Hz, 2H), 3.10 (m, 2H), 2.96 (m, 2H), 2.72 (m, 2H), 1.89 (m, 4H), 1.60 (m, 2H), 1.36 (s, 9H), 1.27 (m, 10H). ^{13}C NMR (126 MHz, Methanol-d_4) δ 174.55, 172.96, 158.90, 157.48, 153.40, 147.71, 138.01, 129.85, 128.82, 127.74, 124.73, 124.47, 122.36, 121.20, 119.73, 119.42, 116.66, 112.21, 111.00, 80.59, 61.52, 57.13, 40.27, 34.05, 33.06, 32.22, 30.74, 29.97, 29.46, 28.64, 27.80, 27.59, 26.10, 24.07, 23.66, 20.85. HRMS $[M + H]^+$: 598.3749 (calculated for $[C_{36}H_{48}N_5O_3]^+$: 598.3752).

Tert-butyl 1-(2-(1,2,3,4-tetrahydroacridin-9-ylamino)octylcarbamoyl)-2-(1*H*-indole-3-yl) ethylcarbamate (**60**) Yield 83%. ^{1}H NMR (500 MHz, DMSO-d_6) δ 10.78 (s, 1H), 8.33 (d, *J* = 8.7 Hz, 1H), 7.78 (m, 2H), 7.53 (m, 2H), 7.43 (d, *J* = 7.1 Hz, 1H), 7.29 (d, *J* = 8.0 Hz, 1H), 7.09 (d, *J* = 2.2 Hz, 1H), 6.98 (m, 1H), 6.68 (d, *J* = 8.3 Hz, 1H), 4.12 (m, 1H), 3.77 (m, 2H), 3.03 (m, 2H), 2.95 (m, 2H), 2.64 (m, 2H), 2.52 (m, 6H), 1.82 (m, 6H), 1.69 (m, 2H), 1.29 (s, 9H), 1.17 (m, 4H). ^{13}C NMR (126 MHz, DMSO-d_6) δ 171.85, 155.26, 151.50, 139.03, 136.19, 132.37, 127.51, 125.00, 124.25, 123.71, 120.92, 120.31, 118.60, 118.24, 116.18, 111.99, 111.87, 111.38, 110.41, 78.06, 55.36, 47.56, 45.92, 38.63, 36.64, 36.61, 30.05, 29.11, 28.75, 28.72, 28.30, 28.09, 26.29, 26.20, 24.16, 21.73, 20.73. HRMS $[M + H]^+$: 612.3901 (calculated for $[C_{37}H_{50}N_5O_3]^+$: 612.3903).

Tert-butyl 1-(2-(6-chloro-1,2,3,4-tetrahydroacridin-9-ylamino)hexylcarbamoyl)-2-(1*H*-indole-3-yl) ethylcarbamate (**61**) Yield 15%. 1H NMR (500 MHz, Methanol-d_4) δ 8.31 (d, J = 9.3 Hz, 1H), 7.82 (d, J = 8.4 Hz, 1H), 7.70 (d, J = 8.3 Hz, 1H), 7.66 (d, J = 2.2 Hz, 1H), 7.50 (m, 2H), 7.45 (m, 1H), 7.27 (d, J = 8.1 Hz, 1H), 7.05 (s, 1H), 6.98 (dt, J = 40.3, 7.4 Hz, 2H), 4.26 (t, J = 7.0 Hz, 1H), 3.86 (t, J = 7.3 Hz, 2H), 3.21 – 3.11 (m, 2H), 3.04 (m, 2H), 2.92 (t, J = 6.0 Hz, 2H), 2.61 (t, J = 5.8 Hz, 2H), 1.94 (m, 4H), 1.76 (m, 2H), 1.36 (s, 11H), 1.22 (m, 4H). 13C NMR (126 MHz, Methanol-d_4) δ 174.64, 157.62, 151.85, 140.40, 139.99, 137.92, 128.69, 127.90, 126.92, 126.69, 124.50, 122.30, 119.68, 119.31, 119.05, 118.57, 115.32, 113.23, 112.19, 111.49, 110.94, 80.61, 79.43, 57.16, 40.02, 39.99, 31.13, 29.91, 29.39, 29.22, 28.61, 27.12, 24.48, 22.76, 21.67. HRMS $[M + H]^+$: 618.3209 (calculated for $[C_{35}H_{45}ClN_5O_3]^+$: 618.3207).

Tert-butyl 1-(2-(6-chloro-1,2,3,4-tetrahydroacridin-9-ylamino)hexylcarbamoyl)-2-(1*H*-indole-3-yl) ethylcarbamate (**62**) Yield 60%. ^{1}H NMR (500 MHz, Methanol-d_4) δ 8.30 (d, *J* = 9.3 Hz, 1H), 7.68 (d, *J* = 8.3 Hz, 1H), 7.66 (d, *J* = 2.2 Hz, 1H), 7.53 (m, 2H), 7.42 (m, 1H), 7.26 (d, *J* = 8.1 Hz, 1H), 7.04 (s, 1H),

ACCEPTED MANUSCRIPT

6.97 (dt, *J* = 40.8, 7.4 Hz, 2H), 4.26 (t, *J* = 7.0 Hz, 1H), 3.85 (t, *J* = 7.3 Hz, 2H), 3.16 (m, 2H), 3.06 (m, 2H), 2.91 (t, *J* = 6.0 Hz, 2H), 2.60 (t, *J* = 5.8 Hz, 2H), 1.92 (m, 4H), 1.76 (m, 2H), 1.36 (s, 11H), 1.24 (m, 4H). 13C NMR (126 MHz, Methanol-d_4) δ 174.63, 157.59, 151.83, 140.39, 139.95, 137.90, 128.69, 127.53, 126.69, 124.49, 122.29, 119.67, 119.04, 118.56, 115.30, 113.22, 112.18, 111.58, 110.93, 80.60, 57.16, 49.84, 40.13, 40.00, 31.12, 29.91, 29.38, 29.21, 28.61, 27.12, 24.46, 22.75, 21.66. HRMS $[M + H]^+$: 618.3209 (calculated for $[C_{35}H_{45}ClN_5O_3]^+$: 618.3205).

N-(2-(7-methoxy-1,2,3,4-tetrahydroacridin-9-ylamino)ethyl-2-amino-3-(1*H*-indole-3-yl)propylamide dihydrochloride (***S*-K1024**) Yield 99%; mp 97.1-99.2 °C. Purity: 98%. ^{1}H NMR (500 MHz, DMSO-d_6) δ 11.05 (d, *J* = 2.4 Hz, 1H), 9.29 (t, *J* = 5.6 Hz, 1H), 8.38 (d, *J* = 5.5 Hz, 3H), 7.96 (d, *J* = 9.2 Hz, 1H), 7.82 (d, *J* = 2.6 Hz, 1H), 7.62 (d, *J* = 7.9 Hz, 1H), 7.49 (dd, *J* = 9.2, 2.4 Hz, 1H), 7.28 (d, *J* = 8.2 Hz, 1H), 7.20 (d, *J* = 2.4 Hz, 1H), 6.94 (m, 2H), 3.93 (s, 3H), 3.37 (m, 2H), 3.11 (m, 2H), 2.99 (m, 2H), 2.71 (m, 2H), 2.49 (m, 2H), 1.77 (m, 5H). ^{13}C NMR (126 MHz, DMSO-d_6) δ 169.39, 156.85, 154.96, 150.05, 136.33, 132.63, 127.22, 124.91, 124.18, 121.16, 118.63, 118.47, 117.77, 111.51, 111.30, 107.09, 103.74, 56.53, 53.07, 45.97, 34.20, 28.08, 27.17, 25.10, 21.98, 20.41, 18.76. HRMS $[M + H]^+$: 458.2549 (calculated for $[C_{27}H_{32}N_5O_2]^+$: 458.2551).

N-(2-(7-methoxy-1,2,3,4-tetrahydroacridin-9-ylamino)propyl-2-amino-3-(1*H*-indole-3-yl)propylamide dihydrochloride (***S*-K1025**) Yield 61%; mp 97.2-101.4 °C. Purity: 99.9%. ^{1}H NMR (500 MHz, DMSO-d_6) δ 11.08 (d, *J* = 2.5 Hz, 1H), 9.06 (m, 1H), 8.35 (d, *J* = 5.2 Hz, 3H), 7.98 (d, *J* = 9.2 Hz, 2H), 7.84 (d, *J* = 2.6 Hz, 1H), 7.66 (d, *J* = 7.9 Hz, 1H), 7.49 (dd, *J* = 9.2, 2.4 Hz, 1H), 7.31 (d, *J* = 8.1 Hz, 1H), 7.23 (d, *J* = 2.4 Hz, 1H), 6.97 (m, 2H), 3.93 (m, 4H), 3.76 (m, 2H), 3.15 (m, 4H), 3.00 (m, 2H), 2.71 (m, 2H), 1.75 (m, 6H). ^{13}C NMR (126 MHz, DMSO-d_6) δ 168.87, 157.11, 155.12, 150.21, 136.62, 132.87, 127.53, 125.19, 124.36, 121.42, 121.25, 119.01, 118.74, 117.95, 111.78, 111.50, 107.50, 103.88, 56.76, 43.77, 36.05, 30.40, 28.32, 27.61, 25.33, 23.06, 22.21, 20.70. HRMS $[M + H]^+$: 472.2702 (calculated for $[C_{28}H_{34}N_5O_2]^+$: 472.2708).

N-(2-(7-methoxy-1,2,3,4-tetrahydroacridin-9-ylamino)butyl-2-amino-3-(1*H*-indole-3-yl)propylamide dihydrochloride (***S*-K1026**) Yield 96%. Purity: 99%. ^{1}H NMR (500 MHz, Methanol-d_4) δ 7.75 (dd, *J* = 9.2, 1.7 Hz, 1H), 7.65 (t, *J* = 2.2 Hz, 1H), 7.60 (dt, *J* = 7.3, 1.2 Hz, 1H), 7.49 (dt, *J* = 4.7, 2.0 Hz, 2H), 7.21 (d, *J* = 1.8 Hz, 1H), 7.00 (m, 2H), 4.08 (m, 1H), 3.95 (s, 3H), 3.81 (t, *J* = 7.2 Hz, 2H), 3.20 (m, 2H), 2.99 (m, 2H), 2.73 (m, 2H), 1.92 (m, 6H), 1.61 (m, 2H), 1.40 (m, 2H).^{13}C NMR (126 MHz, Methanol-d_4) δ 170.01, 158.64, 157.04, 150.75, 138.06, 134.40, 128.41, 125.63, 125.40, 122.67, 121.79, 120.09, 119.34, 118.73, 112.90, 112.46, 108.12, 104.95, 56.78, 55.25, 48.06, 40.01, 29.26, 29.10, 28.81, 27.14, 25.77, 23.18, 21.84. HRMS $[M + H]^+$: 486.2682 (calculated for $[C_{29}H_{36}N_5O_2]^+$: 486.2864).

N-(2-(7-methoxy-1,2,3,4-tetrahydroacridin-9-ylamino)pentyl-2-amino-3-(1*H*-indole-3-yl)propylamide dihydrochloride (***S*-K1027**) Yield 73%; mp 155.0-157.7 °C. Purity: 99.9%. ^{1}H NMR (500 MHz, DMSO-d_6) δ 11.13 (d, *J* = 2.5 Hz, 1H), 8.75 (t, *J* = 5.6 Hz, 1H), 8.32 (d, *J* = 5.5 Hz, 3H), 7.97 (d, *J* = 9.2 Hz, 1H), 7.84 (d, *J* = 2.6 Hz, 1H), 7.64 (d, *J* = 7.9 Hz, 1H), 7.51 (s, 2H), 7.30 (d, *J* = 2.7 Hz, 3H), 7.20 (d, *J* = 2.4 Hz, 1H),

ACCEPTED MANUSCRIPT

6.97 (m, 2H), 3.92 (s, 3H), 3.75 (m, 2H), 3.10 (m, 3H), 2.99 (m, 3H), 2.70 (m, 2H), 2.49 (m, 3H), 1.78 (m, 4H), 1.60 (m, 2H), 1.35 (m, 2H). ^{13}C NMR (126 MHz, DMSO-d_6) δ 169.39, 156.85, 154.96, 150.05, 136.33, 132.63, 127.22, 124.91, 124.18, 121.16, 118.63, 118.47, 117.77, 111.51, 111.30, 107.09, 103.74, 56.53, 56.21, 53.07, 45.97, 40.20, 39.20, 34.20, 28.08, 27.17, 25.10, 21.98, 20.41, 18.76. HRMS $[M + H]^+$: 500.3021 (calculated for $[C_{30}H_{38}N_5O_2]^+$: 500.3021).

N-(2-(7-methoxy-1,2,3,4-tetrahydroacridin-9-ylamino)hexyl-2-amino-3-(1*H*-indole-3-yl)propylamide dihydrochloride (***S*-K1028**) Yield 99%; mp 132.4-135.6 °C. Purity: 96%. ^{1}H NMR (500 MHz, Methanol-d_4) δ 7.73 (d, *J* = 9.2 Hz, 1H), 7.64 (d, *J* = 2.4 Hz, 1H), 7.59 (d, *J* = 7.8 Hz, 1H), 7.47 (dd, *J* = 9.1, 2.3 Hz, 1H), 7.32 (d, *J* = 8.0 Hz, 1H), 7.19 (s, 1H), 7.01 (m, 2H), 4.07 (t, *J* = 7.3 Hz, 1H), 3.95 (s, 3H), 3.87 (t, *J* = 7.2 Hz, 2H), 3.30 (m, 2H), 3.18 (m, 2H), 2.99 (m, 2H), 2.73 (m, 2H), 1.91 (m, 4H), 1.74 (t, *J* = 7.5 Hz, 2H), 1.31 (m, 4H), 1.17 (m, 2H). ^{13}C NMR (126 MHz, Methanol-d_4) δ 169.87, 158.54, 157.06, 150.60, 138.05, 134.41, 128.36, 125.51, 122.67, 121.76, 120.08, 119.23, 118.60, 112.78, 112.48, 108.09, 104.93, 56.68, 55.20, 53.83, 40.44, 31.81, 29.73, 29.23, 28.82, 27.38, 27.31, 25.67, 23.15, 21.85, 21.66. HRMS $[M + H]^+$: 514.3176 (calculated for $[C_{31}H_{40}N_5O_2]^+$: 514.3177).

N-(2-(7-methoxy-1,2,3,4-tetrahydroacridin-9-ylamino)heptyl-2-amino-3-(1*H*-indole-3-yl)propylamide dihydrochloride (***S*-K1029**) Yield 85%; mp 125.1-128.9 °C. Purity: 96%. ^{1}H NMR (500 MHz, DMSO-d_6) δ 11.11 (d, *J* = 2.5 Hz, 1H), 8.61 (s, 1H), 8.30 (d, *J* = 5.3 Hz, 3H), 7.98 (d, *J* = 9.2 Hz, 1H), 7.81 (d, *J* = 2.5 Hz, 1H), 7.63 (d, *J* = 7.9 Hz, 1H), 7.50 (dd, *J* = 9.2, 2.5 Hz, 1H), 7.33 (d, *J* = 8.1 Hz, 1H), 7.20 (d, *J* = 2.4 Hz, 1H), 6.99 (m, 2H), 3.92 (s, 3H), 3.78 (m, 2H), 3.18 (m, 2H), 3.01 (m, 3H), 2.69 (m, 3H), 1.78 (m, 5H), 1.67 (m, 2H), 1.22 (m, 6H), 1.12 (m, 2H). ^{13}C NMR (126 MHz, DMSO-d_6) δ 168.24, 156.66, 154.92, 149.78, 136.35, 132.74, 127.31, 124.85, 123.95, 121.14, 120.98, 118.70, 118.46, 117.46, 111.54, 110.97, 107.25, 103.90, 56.31, 53.05, 46.63, 38.84, 30.50, 28.69, 28.47, 28.01, 27.43, 26.32, 26.17, 24.95, 21.92, 20.47. HRMS $[M + H]^+$: 528.3335 (calculated for $[C_{32}H_{42}N_5O_2]^+$: 528.3334).

N-(2-(7-methoxy-1,2,3,4-tetrahydroacridin-9-ylamino)octyl-2-amino-3-(1*H*-indole-3-yl)propylamide dihydrochloride (***S*-K1030**) Yield 79%; mp 163.5-166.2 °C. Purity: 97%. ^{1}H NMR (500 MHz, Methanol-d_4) δ 7.75 (d, *J* = 9.2 Hz, 1H), 7.65 (d, *J* = 2.4 Hz, 1H), 7.60 (d, *J* = 7.9 Hz, 1H), 7.49 (m, 1H), 7.33 (d, *J* = 8.1 Hz, 1H), 7.19 (s, 1H), 7.03 (m, 2H), 4.06 (t, *J* = 7.5 Hz, 1H), 3.95 (s, 3H), 3.89 (t, *J* = 7.2 Hz, 2H), 3.18 (m, 2H), 3.00 (m, 4H), 2.73 (m, 2H), 1.92 (m, 4H), 1.79 (m, 2H), 1.39 (m, 2H), 1.25 (m, 8H). ^{13}C NMR (126 MHz, Methanol-d_4) δ 169.85, 158.55, 157.14, 150.61, 138.08, 134.47, 128.37, 125.52, 125.37, 122.71, 121.79, 120.14, 119.21, 118.61, 112.83, 112.51, 108.10, 104.98, 58.31, 56.64, 55.23, 40.62, 31.94, 30.14, 30.11, 29.82, 29.24, 28.84, 27.67, 25.62, 23.15, 21.87, 21.35. HRMS $[M + H]^+$: 542.3483 (calculated for $[C_{33}H_{44}N_5O_2]^+$: 542.3490).

N-(2-(6-chloro-1,2,3,4-tetrahydroacridin-9-ylamino)ethyl-2-amino-3-(1*H*-indole-3-yl)propylamide dihydrochloride (***S*-K1031**) Yield 56%; mp 65.1-68.5 °C. Purity: 97%. ^{1}H NMR (300 MHz, D_2O) δ 7.63 (d, *J* = 9.4 Hz, 1H), 7.35 (d, *J* = 2.1 Hz, 1H), 7.14 (m, 3H), 6.72 (d, *J* = 7.9 Hz, 1H), 6.26 (m, 1H), 3.51 (m, 2H),

3.29 (m, 2H), 2.67 (dt, *J* = 7.9, 4.1 Hz, 2H), 2.01 (m, 6H), 1.67 (m, 2H). ^{13}C NMR (75 MHz, D_2O) δ 171.34, 154.92, 150.15, 138.59, 138.43, 135.68, 127.25, 126.83, 125.54, 121.66, 119.30, 117.90, 117.77, 113.93, 111.98, 111.28, 105.97, 53.73, 39.50, 30.83, 30.20, 28.23, 26.55, 23.06, 21.77. HRMS $[M + H]^+$: 462.2052 (calculated for $[C_{26}H_{29}ClN_5O]^+$: 462.2056).

N-(2-(6-chloro-1,2,3,4-tetrahydroacridin-9-ylamino)propyl-2-amino-3-(1*H*-indole-3-yl)propylamide dihydrochloride (***S*-K1032**) Yield 53%; mp 82.2-85.3 °C. Purity: 98%. ^{1}H NMR (500 MHz, D_2O) δ 7.56 (d, *J* = 9.3 Hz, 1H), 7.32 (d, *J* = 2.1 Hz, 1H), 7.18 (m, 3H), 6.83 (d, *J* = 8.0 Hz, 1H), 6.62 (m, 2H), 4.13 (m, 1H), 3.17 (m, 2H), 3.11 (m, 2H), 2.74 (m, 2H), 2.22 (m, 4H), 1.81 (m, 4H), 1.41 (m, 2H). ^{13}C NMR (126 MHz, D_2O) δ 169.05, 154.72, 149.89, 137.89, 135.32, 126.42, 124.95, 124.50, 124.46, 121.18, 121.06, 118.62, 117.57, 117.30, 112.87, 111.51, 110.91, 106.10, 53.90, 44.63, 36.37, 30.23, 28.68, 27.66, 26.53, 22.85, 21.02. HRMS $[M + H]^+$: 476.2210 (calculated for $[C_{27}H_{31}ClN_5O]^+$: 476.2212).

N-(2-(6-chloro-1,2,3,4-tetrahydroacridin-9-ylamino)butyl-2-amino-3-(1*H*-indole-3-yl)propylamide dihydrochloride (***S*-K1033**) Yield 83%; mp 88.5-91.7 °C. Purity: 97%. ^{1}H NMR (500 MHz, DMSO-d_6) δ 11.09 (d, *J* = 2.3 Hz, 1H), 8.75 (t, *J* = 5.6 Hz, 1H), 8.44 (d, *J* = 9.3 Hz, 1H), 8.30 (d, *J* = 5.5 Hz, 3H), 8.11 (d, *J* = 2.2 Hz, 1H), 8.01 (s, 1H), 7.63 (d, *J* = 7.9 Hz, 1H), 7.56 (dd, *J* = 9.3, 2.2 Hz, 1H), 7.30 (m, 1H), 7.21 (d, *J* = 2.3 Hz, 1H), 7.01 (dd, *J* = 8.2, 6.9 Hz, 1H), 6.93 (m, 1H), 3.94 (m, 1H), 3.77 (m, 2H), 3.12 (m, 3H), 3.00 (m, 1H), 2.98 (m, 2H), 2.49 (m, 2H), 1.79 (m, 4H), 1.62 (m, 2H), 1.37 (m, 2H). ^{13}C NMR (126 MHz, DMSO-d_6) δ 168.38, 155.55, 151.21, 138.80, 137.09, 136.33, 127.84, 127.26, 125.38, 124.87, 121.13, 118.69, 118.46, 118.03, 114.30, 111.70, 111.50, 107.23, 53.06, 46.89, 38.32, 34.19, 28.07, 27.43, 25.88, 24.21, 22.67, 21.54. HRMS $[M + H]^+$: 490.2367 (calculated for $[C_{28}H_{33}ClN_5O]^+$: 490.2369).

N-(2-(6-chloro-1,2,3,4-tetrahydroacridin-9-ylamino)pentyl-2-amino-3-(1*H*-indole-3-yl)propylamide dihydrochloride (***S*-K1034**) Yield 74 %; mp 83.4-87.8 °C. Purity: 98%. ^{1}H NMR (500 MHz, DMSO-d_6) δ 11.12 (d, *J* = 2.4 Hz, 1H), 8.69 (t, *J* = 5.6 Hz, 1H), 8.45 (d, *J* = 9.3 Hz, 1H), 8.31 (d, *J* = 5.5 Hz, 3H), 8.12 (d, *J* = 2.2 Hz, 1H), 8.05 (s, 1H), 7.63 (d, *J* = 7.9 Hz, 1H), 7.56 (dd, *J* = 9.2, 2.2 Hz, 1H), 7.44 (m, 1H), 7.30 (m, 2H), 7.20 (d, *J* = 2.4 Hz, 1H), 6.97 (m, 2H), 3.94 (m, 1H), 3.78 (m, 2H), 3.13 (m, 3H), 2.98 (m, 3H), 2.63 (m, 2H), 1.78 (m, 4H), 1.67 (m, 2H), 1.33 (m, 2H), 1.22 (m, 2H). ^{13}C NMR (126 MHz, DMSO-d_6) δ 168.31, 155.53, 151.40, 138.86, 137.10, 136.36, 127.89, 127.30, 125.39, 124.87, 121.15, 118.73, 118.49, 118.05, 114.27, 111.67, 111.55, 107.26, 56.21, 53.06, 47.26, 34.21, 29.54, 28.36, 28.07, 27.46, 23.54, 21.54, 20.35. HRMS $[M + H]^+$: 504.2524 (calculated for $[C_{29}H_{35}ClN_5O]^+$: 504.2525).

N-(2-(6-chloro-1,2,3,4-tetrahydroacridin-9-ylamino)hexyl-2-amino-3-(1*H*-indole-3-yl)propylamide dihydrochloride (***S*-K1035**) Yield 75%; mp 141.1-143.5 °C. Purity: 99.9%. ^{1}H NMR (500 MHz, DMSO-d_6) δ 11.12 (d, *J* = 2.5 Hz, 1H), 8.65 (t, *J* = 5.6 Hz, 1H), 8.46 (d, *J* = 9.2 Hz, 1H), 8.32 (d, *J* = 5.5 Hz, 3H), 8.15 (d, *J* = 2.2 Hz, 1H), 7.62 (d, *J* = 7.9 Hz, 1H), 7.55 (dd, *J* = 9.2, 2.2 Hz, 1H), 7.20 (d, *J* = 2.4 Hz, 1H), 6.97 (m, 2H), 3.95 (m, 1H), 3.80 (m, 2H), 3.17 (t, *J* = 6.3 Hz, 2H), 2.99 (m, 4H), 2.63 (m, 2H), 1.79 (m, 4H), 1.66 (m, 2H), 1.22 (m, 6H). ^{13}C NMR (126 MHz, DMSO-d_6) δ 168.23, 155.49, 151.17, 138.82, 137.04, 136.32,

ACCEPTED MANUSCRIPT

ACCEPTED MANUSCRIPT

127.80, 127.29, 125.33, 124.79, 121.09, 118.68, 118.43, 118.02, 114.29, 111.62, 111.50, 107.24, 56.16, 53.03, 47.16, 29.78, 28.63, 28.05, 27.38, 25.97, 25.87, 24.20, 22.66, 21.53, 20.34. HRMS $[M + H]^+$: 518.2681 (calculated for $[C_{30}H_{37}ClN_5O]^+$: 518.2682).

N-(2-(6-chloro-1,2,3,4-tetrahydroacridin-9-ylamino)heptyl-2-amino-3-(1*H*-indole-3-yl)propylamide dihydrochloride (***S*-K1036**) Yield 84%; mp 121.8-125.9 °C. Purity: 96%. ^{1}H NMR (500 MHz, DMSO-d_6) δ 10.82 (d, *J* = 2.3 Hz, 1H), 8.39 (d, *J* = 9.3 Hz, 1H), 8.01 (d, *J* = 2.2 Hz, 1H), 7.89 (s, 1H), 7.82 (t, *J* = 5.7 Hz, 1H), 7.55 (m, 2H), 7.29 (d, *J* = 8.1 Hz, 1H), 7.08 (d, *J* = 2.3 Hz, 1H), 6.97 (m, 2H), 6.68 (d, *J* = 8.2 Hz, 1H), 4.12 (m, 1H), 3,81 (m, 2H), 3.67 (m, 2H), 3.00 (m, 4H), 2.60 (m, 2H), 1.79 (m, 4H), 1.70 (m, 2H), 1.28 (s, 8H). ^{13}C NMR (126 MHz, DMSO-d_6) δ 171.87, 155.58, 155.25, 151.10, 138.80, 137.18, 136.17, 127.74, 125.34, 123.70, 120.88, 118.58, 118.20, 114.20, 111.66, 111.37, 110.36, 78.04, 55.39, 48.75, 47.43, 29.81, 29.02, 28.44, 26.24, 26.17, 23.97, 22.66, 21.46, 20.34. HRMS $[M + H]^+$: 532.2829 (calculated for $[C_{31}H_{39}ClN_5O]^+$: 532.2838).

N-(2-(6-chloro-1,2,3,4-tetrahydroacridin-9-ylamino)octyl-2-amino-3-(1*H*-indole-3-yl)propylamide dihydrochloride (***S*-K1037**) Yield 76%; mp 151.9-154.3 °C. Purity: 95%. ^{1}H NMR (500 MHz, Methanol-d_4) δ 8.36 (d, *J* = 9.2 Hz, 1H), 7.82 (d, *J* = 2.2 Hz, 1H), 7.59 (d, *J* = 7.9 Hz, 1H), 7.51 (m, 2H), 7.32 (m, 1H), 7.01 (m, 2H), 4.08 (t, *J* = 7.3 Hz, 1H), 3.91 (t, *J* = 7.3 Hz, 2H), 3.18 (m, 2H), 2.99 (m, 3H), 2.66 (m, 3H), 1.93 (m, 4H), 1.81 (m, 2H), 1.40 (m, 2H), 1.27 (m, 6H), 1.13 (m, 2H). 13C NMR (126 MHz, DMSO-d_6) δ 168.28, 155.62, 151.21, 138.89, 137.15, 136.39, 127.84, 127.34, 125.38, 124.89, 121.20, 118.72, 118.51, 118.10, 114.34, 111.71, 111.57, 107.28, 67.19, 53.10, 47.41, 34.36, 31.52, 29.88, 28.76, 28.11, 27.48, 27.06, 24.17, 22.46, 21.57, 20.40. HRMS $[M + H]^+$: 546.2991 (calculated for $[C_{32}H_{41}ClN_5O]^+$: 546.2995).

N-(2-(1,2,3,4-tetrahydroacridin-9-ylamino)ethyl-2-amino-3-(1*H*-indole-3-yl)propylamide dihydrochloride (***S*-K1038**) Yield 87%; mp 192.4-195.3 °C. Purity: 96%. ^{1}H NMR (300 MHz, DMSO-d_6) δ 14.25 (s, 1H), 11.06 (d, *J* = 2.5 Hz, 1H), 9.36 (t, *J* = 5.6 Hz, 1H), 8.44 (d, *J* = 9.2 Hz, 2H), 8.02 (dd, *J* = 8.6, 1.2 Hz, 1H), 7.83 (m, 2H), 7.55 (m, 2H), 7.23 (m, 2H), 6.90 (m, 2H), 4.26 (m, 2H), 3.99 (m, 1H), 3.85 (m, 2H), 3.13 (m, 2H), 2.98 (m, 2H), 2.59 (m, 2H), 1.78 (m, 4H). 13C NMR (75 MHz, DMSO-d_6) δ 169.65, 155.74, 150.68, 138.05, 136.28, 132.65, 127.22, 125.42, 125.20, 124.92, 121.12, 119.26, 118.60, 118.46, 115.64, 111.48, 111.42, 107.05, 56.19, 53.04, 46.96, 34.17, 28.07, 27.14, 24.09, 21.66. HRMS $[M + H]^+$: 428.2442 (calculated for $[C_{26}H_{30}N_5O]^+$: 428.2445).

N-(2-(1,2,3,4-tetrahydroacridin-9-ylamino)propyl-2-amino-3-(1*H*-indole-3-yl)propylamide dihydrochloride (***S*-K1039**) Yield 92%; mp 148.8-152.0 °C. Purity: 99.9%. ^{1}H NMR (500 MHz, Methanol-d_4) δ 8.28 (d, *J* = 8.7 Hz, 1H), 7.81 (d, *J* = 4.0 Hz, 2H), 7.54 (m, 2H), 7.23 (d, *J* = 8.0 Hz, 1H), 7.10 (s, 1H), 6.94 (m, 2H), 4.28 (m, 1H), 3.18 (m, 2H), 3.02 (m, 2H), 2.68 (m, 2H), 1.94 (m, 8H), 1.80 (m, 2H). ^{13}C NMR (126 MHz, Methanol-d_4) δ 175.48, 157.91, 151.69, 139.64, 137.92, 133.98, 128.76, 126.44, 126.36, 124.68, 122.30, 120.12, 119.69, 119.40, 117.05, 112.95, 112.26, 110.85, 57.42, 45.69, 37.07, 31.27, 29.36, 28.64, 25.02, 23.01, 21.83. HRMS $[M + H]^+$: 442.2597 (calculated for $[C_{27}H_{32}N_5O]^+$: 442.2602).

ACCEPTED MANUSCRIPT

N-(2-(1,2,3,4-tetrahydroacridin-9-ylamino)butyl-2-amino-3-(1*H*-indole-3-yl)propylamide dihydrochloride (***S*-K1040**) Yield 53%; mp 76.3-81.0 °C. Purity: 98%. ^{1}H NMR (500 MHz, DMSO-d_6) δ 10.78 (d, *J* = 2.4 Hz, 1H), 8.10 (d, *J* = 8.8 Hz, 1H), 7.83 (t, *J* = 5.7 Hz, 1H), 7.69 (dd, *J* = 8.3, 1.2 Hz, 1H), 7.55 (d, *J* = 7.9 Hz, 1H), 7.50 (ddd, *J* = 8.2, 6.7, 1.2 Hz, 1H), 7.32 (m, 2H), 7.10 (d, *J* = 2.3 Hz, 1H), 6.99 (m, 2H), 6.67 (d, *J* = 8.3 Hz, 1H), 4.12 (m, 1H), 3.02 (m, 2H), 2.88 (m, 2H), 2.70 (m, 2H), 1.79 (m, 4H), 1.50 (m, 2H), 1.38 (m, 2H), 1.29 (m, 4H). ^{13}C NMR (126 MHz, DMSO-d_6) δ 171.92, 157.91, 155.26, 150.51, 146.89, 136.19, 128.25, 127.52, 123.74, 123.40, 123.23, 120.93, 120.31, 118.65, 118.25, 115.87, 111.37, 110.42, 78.05, 55.34, 47.83, 38.43, 33.57, 28.30, 26.64, 25.22, 22.90, 22.57. HRMS $[M + H]^+$: 456.2747 (calculated for $[C_{28}H_{34}N_5O]^+$: 456.2758).

N-(2-(1,2,3,4-tetrahydroacridin-9-ylamino)pentyl-2-amino-3-(1*H*-indole-3-yl)propylamide dihydrochloride (***S*-K1041**) Yield 83%; mp 118.5-121.1 °C. Purity: 95%. ^{1}H NMR (300 MHz, D_2O) δ (ppm) 7.73 (d, *J* = 8.6 Hz, 1H), 7.60 (m, 1H), 7.27 (m, 2H), 7.14 (m, 1H), 7.04 (m, 2H), 6.69 (m, 2H), 4.08 (m, 1H), 3.65 (m, 2H), 3.37 (m, 2H), 3.03 (m, 2H), 2.44 (m, 2H), 2.22 (m, 4H), 1.65 (m, 4H), 1.41 (m, 2H), 0.95 (m, 2H). ^{13}C NMR (75 MHz, D_2O) δ 168.82, 154.52, 148.87, 136.93, 135.46, 132.25, 126.23, 124.58, 124.51, 124.38, 121.14, 118.60, 118.18, 117.53, 114.21, 111.05, 110.34, 105.77, 57.28, 53.42, 46.97, 39.06, 30.10, 29.26, 27.11, 26.77, 22.93, 20.92, 19.80. HRMS $[M + H]^+$: 470.2910 (calculated for $[C_{29}H_{36}N_5O]^+$: 470.2915).

N-(2-(1,2,3,4-tetrahydroacridin-9-ylamino)hexyl-2-amino-3-(1*H*-indole-3-yl)propylamide dihydrochloride (***S*-K1042**) Yield 63%; mp 148.7-150.8 °C. Purity: 97%. ^{1}H NMR (300 MHz, Methanol-d_4) δ 8.36 (d, *J* = 8.7 Hz, 1H), 7.80 (m, 2H), 7.58 (m, 2H), 7.32 (m, 1H), 7.19 (s, 1H), 7.00 (m, 2H), 4.09 (m, 1H), 3.90 (t, *J* = 7.3 Hz, 2H), 3.30 (m, 2H), 2.99 (m, 2H), 2.68 (m, 2H), 2.16 (m, 4H), 1.93 (m, 4H), 1.76 (m, 2H), 1.31 (m, 4H). ^{13}C NMR (75 MHz, Methanol-d_4) δ 169.86, 157.77, 151.51, 139.63, 138.02, 133.97, 128.37, 126.48, 126.30, 125.53, 122.64, 120.09, 120.06, 119.27, 116.94, 112.71, 112.47, 108.08, 58.30, 55.18, 40.40, 31.33, 29.69, 27.28, 27.23, 24.97, 22.95, 21.80, 20.82, 20.79. HRMS $[M + H]^+$: 484.3066 (calculated for $[C_{30}H_{38}N_5O]^+$: 484.3017).

N-(2-(1,2,3,4-tetrahydroacridin-9-ylamino)heptyl-2-amino-3-(1*H*-indole-3-yl)propylamide dihydrochloride (***S*-K1043**) Yield 38%; mp 148.7-150.8 °C. Purity: 98%. ^{1}H NMR (500 MHz, D_2O) δ 7.78 (m, 1H), 7.55 (m, 1H), 7.24 (m, 2H), 7.11 (m, 2H), 6.94 (m, 1H), 6.76 (m, 2H), 3.96 (m, 1H), 3.50 (m, 2H), 2.95 (m, 2H), 2.49 (m, 2H), 2.11 (m, 2H), 1.63 (m, 4H), 1.55 (m, 2H), 1.19 (m, 2H), 1.08 (m, 8H). ^{13}C NMR (126 MHz, D_2O) δ 169.03, 157.77, 155.03, 149.12, 137.35, 135.75, 132.42, 126.25, 124.69, 124.54, 121.57, 118.93, 118.48, 117.55, 114.48, 111.41, 110.68, 105.89, 57.40, 53.55, 47.31, 39.30, 29.45, 27.56, 27.45, 27.04, 25.43, 25.40, 22.79, 21.11, 20.04. HRMS $[M + H]^+$: 498.3225 (calculated for $[C_{31}H_{40}N_5O]^+$: 498.3228).

N-(2-(1,2,3,4-tetrahydroacridin-9-ylamino)octyl-2-amino-3-(1*H*-indole-3-yl)propylamide dihydrochloride (***S*-K1044**) Yield 83%. Purity: 95%. ^{1}H NMR (500 MHz, DMSO-d_6) δ 14.20 (s, 1H), 11.09 (s, 1H), 8.43 (d, *J* = 8.6 Hz, 1H), 8.03 (d, *J* = 8.4 Hz, 1H), 7.83 (m, 1H), 7.58 (m, 2H), 7.32 (d, *J* = 8.1 Hz, 1H), 7.21 (s, 1H), 6.99 (m, 2H), 3.94 (m, 1H), 3.83 (m, 2H), 3.17 (m, 2H), 3.02 (m, 2H), 2.66 (m, 2H), 1.81 (m, 4H), 1.70 (m,

2H), 1.20 (m, 10H). ^{13}C NMR (126 MHz, DMSO-d_6) δ 168.23, 155.80, 150.76, 138.06, 136.35, 132.69, 127.33, 125.25, 125.17, 124.86, 121.14, 119.30, 118.69, 118.47, 115.73, 111.54, 111.21, 107.26, 53.06, 52.57, 47.30, 36.65, 34.22, 29.99, 28.78, 28.72, 28.67, 28.07, 27.42, 26.36, 24.25, 21.67. HRMS $[M + H]^+$: 512.3378 (calculated for $[C_{32}H_{42}N_5O]^+$: 512.3384).

N-(2-(6-chloro-1,2,3,4-tetrahydroacridin-9-ylamino)hexyl-2-amino-3-(1*H*-indole-3-yl)propylamide dihydrochloride (***R*-K1035**) Yield 90%; mp 257.2-260.5 °C. Purity: 95%. ^{1}H NMR (500 MHz, Methanol-d_4) δ 8.37 (d, *J* = 9.2 Hz, 1H), 7.77 (d, *J* = 2.1 Hz, 1H), 7.59 (d, *J* = 7.9 Hz, 1H), 7.54 (dd, *J* = 9.2, 2.1 Hz, 1H), 7.34 (d, *J* = 8.1 Hz, 1H), 7.20 (s, 1H), 7.03 (m, 2H), 4.08 (t, *J* = 7.3 Hz, 1H), 3.91 (t, *J* = 7.3 Hz, 2H), 3.32 (m, 2H), 3.21 (m, 2H), 2.98 (t, *J* = 5.9 Hz, 2H), 2.66 (m, 2H), 1.94 (m, 6H), 1.79 (m, 2H), 1.36 (m, 4H). ^{13}C NMR (126 MHz, Methanol-d_4) δ 169.87, 157.65, 152.00, 140.41, 140.00, 138.08, 128.72, 128.34, 126.75, 125.49, 122.71, 120.11, 119.19, 119.11, 115.36, 113.24, 112.49, 108.09, 58.31, 55.20, 40.43, 31.18, 29.74, 29.30, 28.87, 27.32, 27.25, 24.77, 22.84, 21.73. HRMS $[M + H]^+$: 518.2681 (calculated for $[C_{30}H_{37}ClN_5O]^+$: 518.2683).

N-(2-(6-chloro-1,2,3,4-tetrahydroacridin-9-ylamino)hexyl-2-amino-3-(1*H*-indole-3-yl)propylamide dihydrochloride (**rac-K1035**) Yield 97%; mp 227.3-229.9 °C. Purity: 99%. ^{1}H NMR (500 MHz, Methanol-d_4) δ 8.36 (d, *J* = 9.2 Hz, 1H), 7.77 (d, *J* = 2.0 Hz, 1H), 7.59 (dt, *J* = 7.9, 0.9 Hz, 1H), 7.54 (dd, *J* = 9.2, 2.1 Hz, 1H), 7.34 (dt, *J* = 8.1, 0.8 Hz, 1H), 7.20 (s, 1H), 7.03 (m, 2H), 4.08 (t, *J* = 7.3 Hz, 1H), 3.90 (t, *J* = 7.3 Hz, 2H), 3.32 (m, 2H), 3.21 (ddd, *J* = 17.1, 14.0, 7.1 Hz, 2H), 2.98 (t, *J* = 6.0 Hz, 2H), 2.67 (t, *J* = 5.9 Hz, 3H), 1.95 (m, 6H), 1.79 (m, 2H), 1.36 (m, 4H). ^{13}C NMR (126 MHz, Methanol-d_4) δ 169.86, 157.62, 151.98, 140.38, 139.97, 138.07, 128.71, 128.33, 126.73, 125.49, 122.70, 120.10, 119.19, 119.10, 115.35, 113.23, 112.48, 108.08, 58.30, 55.19, 40.43, 31.18, 29.73, 29.30, 28.86, 27.31, 27.24, 24.77, 22.83, 21.72. HRMS $[M + H]^+$: 518.2681 (calculated for $[C_{30}H_{37}ClN_5O]^+$: 518.2685).

Inhibition of human AChE and BChE

The AChE and BChE inhibitory activities of the tested compounds were determined using modified Ellman´s method [62]. Human recombinant acetylcholinesterase (*h*AChE; EC 3.1.1.7), human plasmatic butyrylcholinesterase (*h*BChE; EC 3.1.1.8), 5,5´-dithiobis(2-nitrobenzoic acid) (Ellman´s reagent, DTNB), phosphate buffer solution (PBS, pH 7.4), acetylthiocholine (ATCh), and butyrylthiocholine (BTCh) were purchased from Sigma-Aldrich (Prague, Czech Republic). For measuring purposes – polystyrene Nunc 96-well microplates with flat bottom shape (ThermoFisher Scientific, USA) were utilized. All of the assays were carried out in 0.1 M KH_2PO_4/K_2HPO_4 buffer, pH 7.4. Enzyme solutions were prepared at an activity 2.0 units·mL^{-1} in 2 mL aliquots. The assay medium (100 µL) consisted of 40 µL of 0.1 M PBS (pH 7.4), 20 µL of 0.01 M DTNB, 10 µL of enzyme, and 20 µL of 001 M substrate (ATCh or BTCh iodide solution). Assayed solutions with inhibitors (10 µL, 10^{-3} – 10^{-9} M) were preincubated with *h*AChE or *h*BChE for 5 min. The reaction was started by addition of 20 µL of substrate. The enzyme activity was determined by measuring the increase in absorbance at 412 nm at 37 °C in 2 min intervals using a Multimode microplate

ACCEPTED MANUSCRIPT

ACCEPTED MANUSCRIPT

reader Synergy 2 (Vermont, USA). Each concentration was assayed in triplicate. The obtained data were used to compute the percentage of inhibition (*I*; Equation 1):

$$I = \left(1 - \frac{\Delta A_i}{\Delta A_0}\right) \times 100 \quad [\%] \qquad \text{(Eq. 1)}$$

ΔA_i indicates absorbance change provided by the cholinesterase exposed to AChE inhibitors. ΔA_0 indicates absorbance change caused by the intact cholinesterase (phosphate buffer was used instead of the AChE inhibitor solution). Inhibition potency of tested compounds was expressed as the IC_{50} value (the concentration of inhibitor, which causes 50% cholinesterase inhibition). All calculations were performed using Microsoft Excel software (Redmont, WA, USA) and GraphPad Prism version 5.02 for Windows (GraphPad Software, San Diego, CA) (www.graphpad.com).

Propidium displacement studies. The affinity of selected inhibitors for the peripheral binding site of *Ee*AChE (type VI-S, Sigma-Aldrich, Milano, Italy) was tested using propidium iodide (P) (Sigma-Aldrich, Milano, Italy), a known specific PAS ligand, following the method proposed by Taylor *et al.* [72,73]. The complexation of propidium iodide and AChE [72] determines a shift in the excitation wavelength [72]. A stock solution (4 mM) of ***S*-K1035** was prepared in methanol. *Ee*AChE (2 μM) was first incubated with 8 μM propidium iodide in 1 mM Tris-HCl, pH 8.0. In the back titration experiments of the propidium-AChE complex by ***S*-K1035**, aliquots of the inhibitor (8-56 μM) were added gradually and fluorescence emission was monitored at 635 nm upon excitation at 535 nm. Blanks containing propidium alone, inhibitor plus propidium and *Ee*AChE alone were prepared and fluorescence emission was determined. Experiments were carried out at room temperature using a Jasco 6200 spectrofluorometer (Cremella, Italy) and a 0.5 mL quartz cuvette. Raw data were processed following the method by Taylor and Lappi [73] to estimate K_D values assuming a dissociation constant value for propidium for *Ee*AChE equals to 0.7 μM [74].

Inhibition of AChE-induced Aβ_{40} aggregation [90]. Aβ_{40}, supplied as trifluoroacetate salt, was purchased from Bachem AG (Bubendorf, Switzerland). Aβ_{40} (2 mg·mL^{-1}) was dissolved in 1,1,1,3,3,3-hexafluoro-2-propanol (HFIP) and lyophilized and redissolved in DMSO to achieve a concentration of 2.3 mM. Stock solutions of tested inhibitors were prepared in methanol (1.5-2 mM) and diluted in the assay buffer. Aliquots of 2 μL Aβ_{40} peptide in DMSO were incubated in 0.215 M sodium phosphate buffer (pH 8.0) at a final concentration of 230 μM for 24 h. For co-incubation experiments aliquots (16 μL) of *h*AChE (final concentration of 2.30 μM, Aβ/AChE molar ratio 100:1) and AChE in the presence of 2 μL of the tested inhibitor (final inhibitor concentration of 100 μM) in 0.215 M sodium phosphate buffer solution (pH 8.0) were added. Blanks containing Aβ_{40} alone, *h*AChE alone, and Aβ_{40} plus tested inhibitors in 0.215 M sodium phosphate buffer (pH 8.0) were prepared. The final volume of each vial was 20 μL. Each assay was run in duplicate. To quantify amyloid fibril formation, the thioflavin T fluorescence method was then applied

[108]. Due to β-sheet conformation, the fluorescence intensities were monitored for 300 s at λ_{em} = 490 nm (λ_{exc} = 446 nm). We calculate the percentage of inhibition of the AChE-induced aggregation due to the presence of tested compound .

ACCEPTED MANUSCRIPT

Inhibition of Aβ_{42} self-aggregation. As reported in a previously published protocol [88], HFIP pretreated Aβ_{42} samples (Bachem AG) were first solubilized with a CH_3CN/0.3 mM Na_2CO_3/250 mM NaOH (48.4:48.4:3.2) mixture to obtain a 500 µM solution. Experiments were performed by incubating the peptide in 10 mM phosphate buffer (pH = 8.0) containing 10 mM NaCl, at 30 °C for 24 h (final Aβ concentration 50 µM) with and without inhibitor (50 µM, Aβ/inhibitor = 1/1). Blanks containing the tested inhibitors were also prepared and measured. To quantify amyloid fibrils formation, the thioflavin T fluorescence method was used [108]. After incubation, samples were diluted to a final volume of 2.0 mL with 50 mM glycine–NaOH buffer (pH 8.5) containing 1.5 µM thioflavin T. A 300-second-time scan of fluorescence intensity was carried out (λ_{exc} = 446 nm; λ_{em} = 490 nm, FP-6200 fluorometer, Jasco Europe), and values at plateau were averaged after subtracting the background fluorescence of 1.5 µM thioflavin T solution. The fluorescence intensities were compared and the percentual inhibition due to the presence of the inhibitor was calculated by the following formula: $100 - (IF_i/IF_o \times 100)$ where IF_i and IF_o are the fluorescence intensities obtained for Aβ_{42} in the presence and absence of inhibitor, respectively.

Determination of *in vitro* blood-brain barrier permeation

The parallel artificial membrane permeation assay (PAMPA) was used based on the reported protocol [95,96]. The filter membrane of the donor plate was coated with polar brain lipid (PBL, Avanti Polar Lipids, Ins., USA) in dodecane (4 µL of 20 mg·mL^{-1} PBL in dodecane) and the acceptor well was filled with 300 µL of the PBS buffer (V_A; pH = 7.4)). Tested compounds were dissolved first in DMSO and the resulting solution was subsequently mixed with PBS (pH = 7.4) to reach the final concentration of 100 µM in the donor well. Concentration of DMSO did not exceed 0.5% (V/V) in the donor solution. A volume of 300 µL of the donor solution was added to the donor wells (V_D) and the donor filter plate was carefully put on the acceptor plate so that coated membrane was "in touch" with both the donor solution and the acceptor buffer. The test compound diffused from the donor well through the lipid membrane (area = 0.28 cm^2) to the acceptor well. The concentration of the drug in both the donor and the acceptor wells was assessed after 3, 4, 5 and 6 hours of incubation in quadruplicate using the UV plate reader Synergy HT (Biotek, Vermont, USA) at the maximum absorption wavelength of each compound. The concentration of the compounds was calculated from the standard curve and expressed as permeability (P_e) according the equation (2) [97,109]:

$$\log P_e = \log\left\{C \times -ln\left(1 - \frac{[drug]_{acceptor}}{[drug]_{equilibrium}}\right)\right\} \; where \; C = \left(\frac{V_D \times V_A}{(V_D + V_A) \times Area \times time}\right) \text{(Eq. 2)}$$

where, $[drug]_{acceptor}$ is the concentration of the drug in the acceptor compartment in the certain time and $[drug]_{equilibrium}$ is the concentration of the drug in theoretical equilibrium i.e. after dilution of the drug between donor and acceptor compartment.

ACCEPTED MANUSCRIPT

In vitro effects of compounds on the activity of nitric oxide synthase

All evaluated compounds were dissolved in redistilled water. Compounds ***S*-K1024**, ***S*-K1040**, ***S*-K1044** were also sonicated. Basic 1 mM stock solutions were stored at 8 °C for no longer than one month. Estimations of the activity of nitric oxide synthase (nNOS) were performed on purified cortical homogenates from a total of 5 male Wistar rats aged 3 – 5 months. A mixture of the cortexes was homogenized (1:10) in homogenisation buffer (1 mM EGTA, 1 mM dithiothreitol, 20 mM HEPES, 0.32 M sucrose, 14.6 µM pepstatin, 21 µM leupeptin, pH = 7.4), centrifuged at 1200 g for 10 min at 4 °C, and the resulting aliquots of supernatants (2 $mg \cdot mL^{-1}$ of proteins) were stored at -20 °C until assayed. Compounds (final concentrations in the incubation mixtures equaled 46 nM – 68 µM) and supernatants were added to the reaction buffer (homogenisation buffer containing also 200 µM *ß*-nicotinamide adenine dinucleotide phosphate, 50 µM tetrahydrobiopterin and 2.3 µM [14C]arginine (PerkinElmer, USA) and incubated for 30 min at 37°C. All samples contained also 1 µM $CaCl_2$ and some of them 1 mM spermidine (Merck, Prague, Czech Republic). The reaction was terminated by adding a stop buffer (30 mM HEPES, 3 mM EDTA, pH = 5.5) and by rapid cooling. DOWEX 50WX8-200 (Sigma-Aldrich) was used to separate citrulline from arginine, in accordance with our previous study [110].

***In vivo* studies**

Animals

Male Wistar rats (10 – 12 week old) were obtained from Velaz (Prague, Czech Republic) and housed in groups of 4 – 6 in an accredited animal facility. Animals were kept in a controlled holding environment with a 12 h day-night cycle, access to standard rodent diet (Cerea Corp., Czech Republic) and water *ad libitum*. The time of acclimatization was at least 14 days prior to all experimental procedures. The use of animals was approved by the Ethics Committee of the Faculty of Military Health Sciences (Hradec Kralove, Czech Republic). All procedures involving animals were in accordance with contemporary legislation.

Assessment of maximum tolerated dose

The acute toxicity of ***S*-K1035** was evaluated by the assessment of MTD ($mg \cdot kg^{-1}$). Male Wistar Rats (body weight 313 – 370 g) were randomly assigned to experimental groups consisting of two males per one applied dose of ***S*-K1035**. Several doses were administered to identify MTD, the starting dose being 50 $mg \cdot kg^{-1}$. ***S*-K1035** was administered *via* i.p. injection in standardized volume of 1 $mL \cdot kg^{-1}$.

ACCEPTED MANUSCRIPT

Treated rats were extensively observed for signs of toxicity during first two hours; then periodically for 48 hours. Clinical signs, such as cardiovascular, respiratory and nervous system disability, weight loss or reduction of food consumption were monitoring according to Laboratory Animal Science Association (UK) guidelines. Severity of symptoms was classified as mild, moderate and substantial [111]. If category of substantial severity was achieved within 48 h, animals were immediately euthanized by CO_2 and a lower dose was selected for the further group. Similarly, if there was a severe adverse effect or death occurring within few minutes after administration to the first animal in the group, the other animal was not treated and lower dose were selected as well. Another lower/higher dose followed previous dose after 48 hours, depending on severity of symptoms. All animals surviving 48 h were euthanized by CO_2 and subjected to basic macroscopic necropsy. Necropsy was also performed in the case of mortality, examining signs of macroscopic organ toxicity.

Behavioral studies

Animals

Thirty adult male Wistar rats (9 –12 weeks old, 370 –500 g), obtained from the Institute of Physiology Czech Academy of Sciences, accredited breeding colony, were used for described experiments. The rats were housed in pairs in transparent plastic cages (20 × 25 × 40 cm) in an air-conditioned animal room (temperature: 22 ± 1 °C, humidity: 50 –60 %, lights on: 06:00 –18:00 h). Water and standard laboratory food were available ad libitum. After an acclimatization period in the animal room at the Institute of Physiology, Czech Academy of Sciences, the rats were habituated to human manipulations by handling (two days, 10 minutes per day). The behavioral experiments were conducted in the light phase of the day. All experiments were conducted in accordance with the guidelines of the European Union directive 2010/63/EU and approved by the Animal Care and Use Committee of the Institute of Physiology Czech Academy of Sciences and by the Central Committee of the Czech Academy of Sciences. The Institute of Physiology Czech Academy of Sciences possesses the National Institutes of Health Statement of Compliance with Standards for Humane Care and Use of Laboratory Animals.

Surgery

Surgical preparation was performed under 2% isoflurane anesthesia (Abbot Laboratories, Chicago, USA). Rats were placed in a stereotaxic frame (TSE Systems), eyes were covered by medical petroleum jelly (Vaseline®, Unilever, Rotterdam, Netherland) and hairs and scalp were removed. Rats were implanted with guide cannulas in both cerebral ventricles at the coordinates relative to Bregma: AP = -0.80 mm; ML = 1.5 mm; DV = 3.5 mm from skull surface [112]. The cannulas were fixed to the skull with two stainless steel screws and dental cement. After surgery animals had free access to food and water containing analgesics. Seven days after the surgery rats started the Morris water maze evaluation.

Drug application

ACCEPTED MANUSCRIPT

***S*-K1035** was prepared according to the described chemical synthesis. The purity of ***S*-K1035** was >99 % (HPLC detected). ***S*-K1035** was dissolved in sterile saline (0.9% NaCl) for a desired concentration of 10 and 100 nM. The freshly prepared solution was sonicated (20 min), fractioned on low volume aliquots (20 µL) and frozen at -20 °C.

Scopolamine hydrobromide (referred to as scopolamine or SCOP in group names, Sigma-Aldrich, 5 $mg \cdot kg^{-1}$) was dissolved in sterile saline one day before the experiment and stored in cold dark environment. As control, sterile saline (SAL) was used.

The drugs were applied on the MWM day 4. Each rat was pseudo-randomly assigned into one of five treatment groups (N = 6): (1) SAL i.c.v. + SAL i.p.; (2) SAL i.c.v. + SCOP i.p.; (3) ***S*-K1035** 100 nM i.c.v. + SAL i.p.; (4) ***S*-K1035** 10 nM i.c.v. + SCOP i.p.; (5) ***S*-K1035** 100 nM i.c.v. + SCOP i.p. Each rat received one bilateral intracerebroventricular (i.c.v., 60 min prior to MWM testing, ***S*-K1035** or saline) and one intraperitoneal (i.p., 20 min prior to MWM testing, scopolamine or saline) injection.

***S*-K1035** or NaCl was applied into the cerebral ventricles by an infusion pump (TSE Systems, Bad Homburg, Germany) with a constant flow rate 0.5 $\mu L \cdot min^{-1}$; and a total volume 1 µL in each injection. The internal cannula was removed 1 min after the end of the infusion. The volume of i.p. injections was 1 $mL \cdot kg^{-1.}$

Morris water maze (MWM):

The MWM apparatus consisted of a blue plastic circular pool (180 cm in diameter) with a circular platform (10 cm in diameter, submerged 1 cm below the water surface, transparent plastic). The pool was filled with water (23-24 °C, 28 cm deep) colored by a small amount of a non-toxic grey color. MWM task designed by Jackons and Soliman was modified and used [105]. The MWM was conducted during four consecutive days. The rats were trained to find the hidden platform, the position of which was constant (in the center of the NW quadrant). Every testing day each rat underwent four swims from different starting points (N, S, W, E; their order was selected randomly and it was different each day). Animals were released into the water facing the wall of the pool. The trial stopped when the rat found the platform. If the rat did not find the platform in 60 s, it was gently guided to the platform by the experimenter. The drugs were applied only on day 4.

Rats were tracked during the experiment with a camera situated above the maze and connected to a digital tracking system (Tracker, Biosignal Group, New York, USA). The acquired data were stored for an off-line analysis using Carousel Maze Manager 0.4.0 (https://github.com/bahniks/CM_Manager_0_4_0).

Measured parameters and statistics

ACCEPTED MANUSCRIPT

Following parameters were analyzed: distance moved (m), escape latency (s), average distance from the platform (cm), and time in the target sector (percentage of time spent swimming in the 90° sector with the platform in the center). These parameters were analyzed for every swim of day 3 and day 4 MWM and mean values were calculated for these days. The mean performance of a group on MWM day 3 (group's baseline, without drugs) and the mean performance of the same group on day 4 (with drugs) were compared using Mann-Whitney nonparametric test (GraphPad Prism 5.02). This analysis was done for all MWM parameters studied. In addition, performances of day 3 of all groups were compared by ANOVA and Tukey post hoc test (GraphPad Prism 5.02) to find out whether there are any differences in group baseline. This was done for all MWM parameters studied.

ASSOCIATED CONTENT

Supporting information

Determination of the absolute configuration of tacrine-tryptophan derivatives ***S*-K1035**, ***R*-K1035** and **rac-K1035**; *in vitro* cell viability assessment; X-ray crystallography of *Tc*AChE in complex with ***S*-K1035**; X-ray crystallography or *h*BChE in complex with ***S*-K1035** and ***R*-K1035**; purity percentages of target compounds.

Accession Codes

Atomic coordinates and structure factor amplitudes of the *Tc*AChE – ***S*-K1035** complex have been deposited in the Brookhaven Protein Data Bank under the PDB ID code 5NUU, *h*BChE – ***S*-K1035** complex under PDB entry 6I0B and *h*BChE – ***R*-K1035** complex under PDB entry 6I0C. Authors will release atomic coordinates and experimental data upon article publication.

AUTHOR INFOMATION

Corresponding Authors

Maria Laura Bolognesi; Phone: +39 0512099717; E-mail: marialaura.bolognesi@unibo.it

Kamil Kuca; Phone: +420 495833447; E-mail: kamil.kuca@fnhk.cz

Notes

The authors declare no competing financial interest.

Author Contributions

‡ Katarina Chalupova and Jan Korabecny contributed equally.

ACKNOWLEDGEMENT

This work was supported by Ministry of Health of the Czech Republic, grant nr. 15-30954A, by the grant of Ministry of Defence of the Czech Republic – "Long-term organization development plan Medical Aspects of Weapon of Mass Destruction of the Faculty of Military Health Sciences, University of Defence", by the Czech Science Foundation. nr. 17-05292S, and by European Regional Development Fund: Project "PharmaBrain" (no. CZ.02.1.01/0.0/0.0/16_025/0007444). Authors are also grateful to the ELETTRA XRD-1 and ESRF ID29 beamline staff in Trieste (Italy) and Grenoble (France) for their assistance during the data collection. X.B., A-J.G. and F.N. were supported by the Direction Générale de l'Armement (DGA) and Service de Santé des Armées (SSA), grant nr. PDH-2-NRBC-3-C-3201. This work is based upon work from COST Action CA15135.

ACCEPTED MANUSCRIPT

ABBREVIATIONS

ACh, acetylcholine; AChE, acetylcholinesterase; AChEIs, acetylcholinesterase inhibitors; ATCh, acetylthiocholine; ALT, alanine aminotransferase; AD, Alzheimer's disease; A*β*, amyloid-*β*; APP, amyloid precursor protein; AST, aspartate aminotransferase; BOP, benzotriazol-1-yloxytris(dimethylamino)phosphonium hexafluorophosphate; BBB, blood-brain barrier; BCh, butyrylcholine; BChE, butyrylcholinesterase; BTCh, butyrylthiocholine; Boc_2O, di-*tert*-butyl dicarbonate; CAS, catalytic anionic site; CNS, central nervous system; COSY, correlation spectroscopy; CHO-K1, chinese hamster ovary; DMSO, dimethylsulfoxide; DEPT, distortionless enhancement by polarization transfer; DTNB, 5,5'-dithiobis(2-nitrobenzoic acid); ECD, electronic circular dischroism; FDA, Food and Drug Administration; HMBC, heteronuclear multiple-bond correlation; HPLC, high-performance liquid chromatography; HSQC, heteronuclear single-quantum correlation; HFIP, 1,1,1,3,3,3-hexafluoro-2-propanol; *h*AChE, human aetylcholinesterase; *h*BChE, human butyrylcholinesterase; HepG2, human liver carcinoma cell line; 5-HT, serotonin; 6-Cl-THA, 6-chlorotacrine; ChE, cholinesterase; ChEIs, cholinesterase inhibitors; IC, inhibitory concentration; i.c.v., intracerebroventricular; i.m., intramuscular; i.p., intraperitoneal; LC-HRMS, liquid-chromatography-high resolution mass spectrometry; MTT, 3-(4,5-dimethylthiazol-2-yl)-2,5-diphenyl tetrazolium bromide; MTD, maximum tolerated dose; 7-MEOTA, 7-methoxytacrine; MTDLs, multi-target directed ligands; MWM, Morris water maze, *L*-NMMA, N^G-monomethyl-L-arginine; NQ, naphthoquinone; nNOS, neuronal nitric oxide synthase; NO, nitric oxide; 7-NI, 7-nitroindozale; NMR, nuclear magnetic resonance; PAMPA, parallel artificial membrane permeation assay; PAINS, pan assay interference compounds; PAS, peripheral anionic site; P_e, permeability; SAL, saline; SCOP, scopolamine; SI, selectivity index; THA, tacrine; ThT, thioflavin T; TLC, thin layer chromatography; *Tc*AChE; *Torpedo californica* acetylcholinesterase; TEA; triethylamine; Trp, tryptophan

References

[1] L. Piazzi, A. Rampa, A. Bisi, S. Gobbi, F. Belluti, A. Cavalli, M. Bartolini, V. Andrisano, P. Valenti, M. Recanatini, 3-(4-[[Benzyl(methyl)amino]methyl]phenyl)-6,7-dimethoxy-2H-2-chromenone (AP2238) inhibits both acetylcholinesterase and acetylcholinesterase-induced beta-amyloid aggregation: a dual function lead for Alzheimer's disease therapy, J. Med. Chem. 46 (2003) 2279–2282. doi:10.1021/jm0340602.

ACCEPTED MANUSCRIPT

[2] P.D. Sloane, S. Zimmerman, C. Suchindran, P. Reed, L. Wang, M. Boustani, S. Sudha, The public health impact of Alzheimer's disease, 2000-2050: potential implication of treatment advances, Annu. Rev. Public Health. 23 (2002) 213–231. doi:10.1146/annurev.publhealth.23.100901.140525.
[3] V. Tumiatti, A. Minarini, M.L. Bolognesi, A. Milelli, M. Rosini, C. Melchiorre, Tacrine derivatives and Alzheimer's disease, Curr. Med. Chem. 17 (2010) 1825–1838.
[4] E. Scarpini, P. Scheltens, H. Feldman, Treatment of Alzheimer's disease: current status and new perspectives, Lancet Neurol. 2 (2003) 539–547.
[5] J.B. Paulson, M. Ramsden, C. Forster, M.A. Sherman, E. McGowan, K.H. Ashe, Amyloid Plaque and Neurofibrillary Tangle Pathology in a Regulatable Mouse Model of Alzheimer's Disease, Am. J. Pathol. 173 (2008) 762–772. doi:10.2353/ajpath.2008.080175.
[6] H.W. Querfurth, F.M. LaFerla, Alzheimer's disease, N. Engl. J. Med. 362 (2010) 329–344. doi:10.1056/NEJMra0909142.
[7] D.J. Selkoe, Alzheimer's disease: genes, proteins, and therapy, Physiol. Rev. 81 (2001) 741–766.
[8] R.T. Bartus, R.L. Dean, B. Beer, A.S. Lippa, The cholinergic hypothesis of geriatric memory dysfunction, Science. 217 (1982) 408–414.
[9] D. Muñoz-Torrero, Acetylcholinesterase inhibitors as disease-modifying therapies for Alzheimer's disease, Curr. Med. Chem. 15 (2008) 2433–2455.
[10] J. Birks, Cholinesterase inhibitors for Alzheimer's disease, Cochrane Database Syst. Rev. (2006) CD005593. doi:10.1002/14651858.CD005593.
[11] N.C. Inestrosa, A. Alvarez, C.A. Pérez, R.D. Moreno, M. Vicente, C. Linker, O.I. Casanueva, C. Soto, J. Garrido, Acetylcholinesterase accelerates assembly of amyloid-beta-peptides into Alzheimer's fibrils: possible role of the peripheral site of the enzyme, Neuron. 16 (1996) 881–891.
[12] A. Alvarez, C. Opazo, R. Alarcón, J. Garrido, N.C. Inestrosa, Acetylcholinesterase promotes the aggregation of amyloid-beta-peptide fragments by forming a complex with the growing fibrils, J. Mol. Biol. 272 (1997) 348–361. doi:10.1006/jmbi.1997.1245.
[13] F.J. Muñoz, N.C. Inestrosa, Neurotoxicity of acetylcholinesterase amyloid beta-peptide aggregates is dependent on the type of Abeta peptide and the AChE concentration present in the complexes, FEBS Lett. 450 (1999) 205–209.
[14] J.L. Sussman, M. Harel, F. Frolow, C. Oefner, A. Goldman, L. Toker, I. Silman, Atomic structure of acetylcholinesterase from Torpedo californica: a prototypic acetylcholine-binding protein, Science. 253 (1991) 872–879.
[15] X. Chen, L. Fang, J. Liu, C.-G. Zhan, Reaction pathway and free energy profiles for butyrylcholinesterase-catalyzed hydrolysis of acetylthiocholine, Biochemistry (Mosc.). 51 (2012) 1297–1305. doi:10.1021/bi201786s.
[16] C. Geula, M.M. Mesulam, Cholinesterases and the pathology of Alzheimer disease, Alzheimer Dis. Assoc. Disord. 9 Suppl 2 (1995) 23–28.
[17] D.J. Selkoe, J. Hardy, The amyloid hypothesis of Alzheimer's disease at 25 years, EMBO Mol. Med. 8 (2016) 595–608. doi:10.15252/emmm.201606210.
[18] M.S. Wolfe, J. De Los Angeles, D.D. Miller, W. Xia, D.J. Selkoe, Are presenilins intramembrane-cleaving proteases? Implications for the molecular mechanism of Alzheimer's disease, Biochemistry (Mosc.). 38 (1999) 11223–11230. doi:10.1021/bi991080q.
[19] S. Paul, S. Planque, Y. Nishiyama, Beneficial catalytic immunity to abeta peptide, Rejuvenation Res. 13 (2010) 179–187. doi:10.1089/rej.2009.0958.
[20] J. Hardy, D.J. Selkoe, The amyloid hypothesis of Alzheimer's disease: progress and problems on the road to therapeutics, Science. 297 (2002) 353–356. doi:10.1126/science.1072994.
[21] S.H. Barage, K.D. Sonawane, Amyloid cascade hypothesis: Pathogenesis and therapeutic strategies in Alzheimer's disease, Neuropeptides. 52 (2015) 1–18. doi:10.1016/j.npep.2015.06.008.
[22] F. Zemek, L. Drtinova, E. Nepovimova, V. Sepsova, J. Korabecny, J. Klimes, K. Kuca, Outcomes of Alzheimer's disease therapy with acetylcholinesterase inhibitors and memantine, Expert Opin. Drug Saf. 13 (2014) 759–774. doi:10.1517/14740338.2014.914168.
[23] A.V. Terry, J.J. Buccafusco, The cholinergic hypothesis of age and Alzheimer's disease-related cognitive deficits: recent challenges and their implications for novel drug development, J. Pharmacol. Exp. Ther. 306 (2003) 821–827. doi:10.1124/jpet.102.041616.
[24] W.K. Summers, A.L. Koehler, G.M. Marsh, K. Tachiki, A. Kling, Long-term hepatotoxicity of tacrine, Lancet Lond. Engl. 1 (1989) 729.
[25] W.K. Summers, Tacrine (THA, Cognex(R)), J. Alzheimers Dis. JAD. 2 (2000) 85–93.

ACCEPTED MANUSCRIPT

[26] O. Soukup, D. Jun, J. Zdarova-Karasova, J. Patocka, K. Musilek, J. Korabecny, J. Krusek, M. Kaniakova, V. Sepsova, J. Mandikova, F. Trejtnar, M. Pohanka, L. Drtinova, M. Pavlik, G. Tobin, K. Kuca, A resurrection of 7-MEOTA: a comparison with tacrine, Curr. Alzheimer Res. 10 (2013) 893–906.

[27] M. Recanatini, A. Cavalli, F. Belluti, L. Piazzi, A. Rampa, A. Bisi, S. Gobbi, P. Valenti, V. Andrisano, M. Bartolini, V. Cavrini, SAR of 9-amino-1,2,3,4-tetrahydroacridine-based acetylcholinesterase inhibitors: synthesis, enzyme inhibitory activity, QSAR, and structure-based CoMFA of tacrine analogues, J. Med. Chem. 43 (2000) 2007–2018.

[28] J. Misik, E. Nepovimova, J. Pejchal, J. Kassa, J. Korabecny, O. Soukup, Cholinesterase Inhibitor 6-Chlorotacrine - In Vivo Toxicological Profile and Behavioural Effects, Curr. Alzheimer Res. 15 (2018) 552–560. doi:10.2174/1567205015666171212105412.

[29] K. Spilovska, J. Korabecny, E. Nepovimova, R. Dolezal, E. Mezeiova, O. Soukup, K. Kuca, Multitarget tacrine hybrids with neuroprotective properties to confront Alzheimer's disease, Curr. Top. Med. Chem. (2016).

[30] M.C. Carreiras, E. Mendes, M.J. Perry, A.P. Francisco, J. Marco-Contelles, The multifactorial nature of Alzheimer's disease for developing potential therapeutics, Curr. Top. Med. Chem. 13 (2013) 1745–1770.

[31] K. Spilovska, J. Korabecny, E. Nepovimova, R. Dolezal, E. Mezeiova, O. Soukup, K. Kuca, Multitarget Tacrine Hybrids with Neuroprotective Properties to Confront Alzheimer's Disease, Curr. Top. Med. Chem. 17 (2017) 1006–1026. doi:10.2174/1568026605666160927152728.

[32] E. Simoni, M. Bartolini, I.F. Abu, A. Blockley, C. Gotti, G. Bottegoni, R. Caporaso, C. Bergamini, V. Andrisano, A. Cavalli, I.R. Mellor, A. Minarini, M. Rosini, Multitarget drug design strategy in Alzheimer's disease: focus on cholinergic transmission and amyloid-β aggregation, Future Med. Chem. 9 (2017) 953–963. doi:10.4155/fmc-2017-0039.

[33] R.R. Ramsay, M.R. Popovic-Nikolic, K. Nikolic, E. Uliassi, M.L. Bolognesi, A perspective on multi-target drug discovery and design for complex diseases, Clin. Transl. Med. 7 (2018) 3. doi:10.1186/s40169-017-0181-2.

[34] J. Li, Z. Lu, L. Xu, Q. Wang, Z. Zhang, J. Fang, Neuroprotective effects of bis(7)-tacrine in a rat model of pressure-induced retinal ischemia, Cell Biochem. Biophys. 68 (2014) 275–282. doi:10.1007/s12013-013-9707-4.

[35] Y.P. Pang, P. Quiram, T. Jelacic, F. Hong, S. Brimijoin, Highly potent, selective, and low cost bis-tetrahydroaminacrine inhibitors of acetylcholinesterase. Steps toward novel drugs for treating Alzheimer's disease, J. Biol. Chem. 271 (1996) 23646–23649.

[36] W. Li, J. Xue, C. Niu, H. Fu, C.S.C. Lam, J. Luo, H.H.N. Chan, H. Xue, K.K.W. Kan, N.T.K. Lee, C. Li, Y. Pang, M. Li, K.W.K. Tsim, H. Jiang, K. Chen, X. Li, Y. Han, Synergistic neuroprotection by bis(7)-tacrine via concurrent blockade of N-methyl-D-aspartate receptors and neuronal nitric-oxide synthase, Mol. Pharmacol. 71 (2007) 1258–1267. doi:10.1124/mol.106.029108.

[37] S.A. Lipton, Paradigm shift in NMDA receptor antagonist drug development: molecular mechanism of uncompetitive inhibition by memantine in the treatment of Alzheimer's disease and other neurologic disorders, J. Alzheimers Dis. JAD. 6 (2004) S61-74.

[38] M. Rosini, E. Simoni, R. Caporaso, A. Minarini, Multitarget strategies in Alzheimer's disease: benefits and challenges on the road to therapeutics, Future Med. Chem. 8 (2016) 697–711. doi:10.4155/fmc-2016-0003.

[39] N. Guzior, A. Wieckowska, D. Panek, B. Malawska, Recent development of multifunctional agents as potential drug candidates for the treatment of Alzheimer's disease, Curr. Med. Chem. 22 (2015) 373–404.

[40] F. Prati, A. De Simone, P. Bisignano, A. Armirotti, M. Summa, D. Pizzirani, R. Scarpelli, D.I. Perez, V. Andrisano, A. Perez-Castillo, B. Monti, F. Massenzio, L. Polito, M. Racchi, A.D. Favia, G. Bottegoni, A. Martinez, M.L. Bolognesi, A. Cavalli, Multitarget drug discovery for Alzheimer's disease: triazinones as BACE-1 and GSK-3β inhibitors, Angew. Chem. Int. Ed Engl. 54 (2015) 1578–1582. doi:10.1002/anie.201410456.

[41] J. Korabecny, R. Dolezal, P. Cabelova, A. Horova, E. Hruba, J. Ricny, L. Sedlacek, E. Nepovimova, K. Spilovska, M. Andrs, K. Musilek, V. Opletalova, V. Sepsova, D. Ripova, K. Kuca, 7-MEOTA-donepezil like compounds as cholinesterase inhibitors: Synthesis, pharmacological evaluation, molecular modeling and QSAR studies, Eur. J. Med. Chem. 82 (2014) 426–438. doi:10.1016/j.ejmech.2014.05.066.

[42] S. Hamulakova, L. Janovec, M. Hrabinova, K. Spilovska, J. Korabecny, P. Kristian, K. Kuca, J. Imrich, Synthesis and biological evaluation of novel tacrine derivatives and tacrine-coumarin hybrids as cholinesterase inhibitors, J. Med. Chem. 57 (2014) 7073–7084. doi:10.1021/jm5008648.

[43] J.-S. Lan, S.-S. Xie, S.-Y. Li, L.-F. Pan, X.-B. Wang, L.-Y. Kong, Design, synthesis and evaluation of novel tacrine-(β-carboline) hybrids as multifunctional agents for the treatment of Alzheimer's disease, Bioorg. Med. Chem. 22 (2014) 6089–6104. doi:10.1016/j.bmc.2014.08.035.

[44] P. Muñoz-Ruiz, L. Rubio, E. García-Palomero, I. Dorronsoro, M. del Monte-Millán, R. Valenzuela, P. Usán, C. de Austria, M. Bartolini, V. Andrisano, A. Bidon-Chanal, M. Orozco, F.J. Luque, M. Medina, A. Martínez, Design,

synthesis, and biological evaluation of dual binding site acetylcholinesterase inhibitors: new disease-modifying agents for Alzheimer's disease, J. Med. Chem. 48 (2005) 7223–7233. doi:10.1021/jm0503289.
[45] V. Hepnarova, J. Korabecny, L. Matouskova, P. Jost, L. Muckova, M. Hrabinova, N. Vykoukalova, M. Kerhartova, T. Kucera, R. Dolezal, E. Nepovimova, K. Spilovska, E. Mezeiova, N.L. Pham, D. Jun, F. Staud, D. Kaping, K. Kuca, O. Soukup, The concept of hybrid molecules of tacrine and benzyl quinolone carboxylic acid (BQCA) as multifunctional agents for Alzheimer's disease, Eur. J. Med. Chem. 150 (2018) 292–306. doi:10.1016/j.ejmech.2018.02.083.
[46] M.I. Rodríguez-Franco, M.I. Fernández-Bachiller, C. Pérez, B. Hernández-Ledesma, B. Bartolomé, Novel tacrine-melatonin hybrids as dual-acting drugs for Alzheimer disease, with improved acetylcholinesterase inhibitory and antioxidant properties, J. Med. Chem. 49 (2006) 459–462. doi:10.1021/jm050746d.
[47] M.I. Fernández-Bachiller, C. Pérez, N.E. Campillo, J.A. Páez, G.C. González-Muñoz, P. Usán, E. García-Palomero, M.G. López, M. Villarroya, A.G. García, A. Martínez, M.I. Rodríguez-Franco, Tacrine-melatonin hybrids as multifunctional agents for Alzheimer's disease, with cholinergic, antioxidant, and neuroprotective properties, ChemMedChem. 4 (2009) 828–841. doi:10.1002/cmdc.200800414.
[48] R. Scherzer-Attali, R. Shaltiel-Karyo, Y.H. Adalist, D. Segal, E. Gazit, Generic inhibition of amyloidogenic proteins by two naphthoquinone-tryptophan hybrid molecules, Proteins. 80 (2012) 1962–1973. doi:10.1002/prot.24080.
[49] M. Frenkel-Pinter, S. Tal, R. Scherzer-Attali, M. Abu-Hussien, I. Alyagor, T. Eisenbaum, E. Gazit, D. Segal, Cl-NQTrp Alleviates Tauopathy Symptoms in a Model Organism through the Inhibition of Tau Aggregation-Engendered Toxicity, Neurodegener. Dis. 17 (2016) 73–82. doi:10.1159/000448518.
[50] S. Butini, E. Guarino, G. Campiani, M. Brindisi, S.S. Coccone, I. Fiorini, E. Novellino, T. Belinskaya, A. Saxena, S. Gemma, Tacrine based human cholinesterase inhibitors: Synthesis of peptidic-tethered derivatives and their effect on potency and selectivity, Bioorg. Med. Chem. Lett. 18 (2008) 5213–5216. doi:10.1016/j.bmcl.2008.08.076.
[51] E. Nepovimova, E. Uliassi, J. Korabecny, L.E. Peña-Altamira, S. Samez, A. Pesaresi, G.E. Garcia, M. Bartolini, V. Andrisano, C. Bergamini, R. Fato, D. Lamba, M. Roberti, K. Kuca, B. Monti, M.L. Bolognesi, Multitarget drug design strategy: quinone-tacrine hybrids designed to block amyloid-β aggregation and to exert anticholinesterase and antioxidant effects, J. Med. Chem. 57 (2014) 8576–8589. doi:10.1021/jm5010804.
[52] H.M. van der Stelt, L.M. Broersen, B. Olivier, H.G.M. Westenberg, Effects of dietary tryptophan variations on extracellular serotonin in the dorsal hippocampus of rats, Psychopharmacology (Berl.). 172 (2004) 137–144. doi:10.1007/s00213-003-1632-6.
[53] R.J. Porter, B.S. Lunn, L.L. Walker, J.M. Gray, C.G. Ballard, J.T. O'Brien, Cognitive deficit induced by acute tryptophan depletion in patients with Alzheimer's disease, Am. J. Psychiatry. 157 (2000) 638–640. doi:10.1176/appi.ajp.157.4.638.
[54] T.A. Jenkins, J.J. Elliott, T.C. Ardis, M. Cahir, G.P. Reynolds, R. Bell, S.J. Cooper, Tryptophan depletion impairs object-recognition memory in the rat: reversal by risperidone, Behav. Brain Res. 208 (2010) 479–483. doi:10.1016/j.bbr.2009.12.030.
[55] A.P. Pawar, K.F. Dubay, J. Zurdo, F. Chiti, M. Vendruscolo, C.M. Dobson, Prediction of "aggregation-prone" and "aggregation-susceptible" regions in proteins associated with neurodegenerative diseases, J. Mol. Biol. 350 (2005) 379–392. doi:10.1016/j.jmb.2005.04.016.
[56] R. Scherzer-Attali, R. Pellarin, M. Convertino, A. Frydman-Marom, N. Egoz-Matia, S. Peled, M. Levy-Sakin, D.E. Shalev, A. Caflisch, E. Gazit, D. Segal, Complete phenotypic recovery of an Alzheimer's disease model by a quinone-tryptophan hybrid aggregation inhibitor, PloS One. 5 (2010) e11101. doi:10.1371/journal.pone.0011101.
[57] T. Zhang, W. Xu, Y. Mu, P. Derreumaux, Atomic and dynamic insights into the beneficial effect of the 1,4-naphthoquinon-2-yl-L-tryptophan inhibitor on Alzheimer's Aβ1-42 dimer in terms of aggregation and toxicity, ACS Chem. Neurosci. 5 (2014) 148–159. doi:10.1021/cn400197x.
[58] M.-K. Hu, L.-J. Wu, G. Hsiao, M.-H. Yen, Homodimeric tacrine congeners as acetylcholinesterase inhibitors, J. Med. Chem. 45 (2002) 2277–2282.
[59] K. Spilovska, J. Korabecny, J. Kral, A. Horova, K. Musilek, O. Soukup, L. Drtinova, Z. Gazova, K. Siposova, K. Kuca, 7-Methoxytacrine-Adamantylamine Heterodimers as Cholinesterase Inhibitors in Alzheimer's Disease Treatment — Synthesis, Biological Evaluation and Molecular Modeling Studies, Molecules. 18 (2013) 2397–2418. doi:10.3390/molecules18022397.
[60] J. Korabecny, M. Andrs, E. Nepovimova, R. Dolezal, K. Babkova, A. Horova, D. Malinak, E. Mezeiova, L. Gorecki, V. Sepsova, M. Hrabinova, O. Soukup, D. Jun, K. Kuca, 7-Methoxytacrine-p-Anisidine Hybrids as Novel Dual Binding Site Acetylcholinesterase Inhibitors for Alzheimer's Disease Treatment, Mol. Basel Switz. 20 (2015) 22084–22101. doi:10.3390/molecules201219836.

[61] H. Franzén, L. Grehn, U. Ragnarsson, Synthesis, properties, and use of Nin-Boc-tryptophan derivatives, J. Chem. Soc., Chem. Commun. (1984) 1699–1700. doi:10.1039/C39840001699.
[62] G.L. Ellman, K.D. Courtney, V. Andres, R.M. Feather-Stone, A new and rapid colorimetric determination of acetylcholinesterase activity, Biochem. Pharmacol. 7 (1961) 88–95.
[63] M. Pohanka, D. Jun, K. Kuca, Improvement of acetylcholinesterase-based assay for organophosphates in way of identification by reactivators, Talanta. 77 (2008) 451–454. doi:10.1016/j.talanta.2008.06.007.
[64] K. Spilovska, J. Korabecny, A. Horova, K. Musilek, E. Nepovimova, L. Drtinova, Z. Gazova, K. Siposova, R. Dolezal, D. Jun, K. Kuca, Design, synthesis and in vitro testing of 7-methoxytacrine-amantadine analogues: a novel cholinesterase inhibitors for the treatment of Alzheimer's disease, Med. Chem. Res. 24 (2015) 2645–2655. doi:10.1007/s00044-015-1316-x.
[65] E. Nepovimova, J. Korabecny, R. Dolezal, K. Babkova, A. Ondrejicek, D. Jun, V. Sepsova, A. Horova, M. Hrabinova, O. Soukup, N. Bukum, P. Jost, L. Muckova, J. Kassa, D. Malinak, M. Andrs, K. Kuca, Tacrine-Trolox Hybrids: A Novel Class of Centrally Active, Nonhepatotoxic Multi-Target-Directed Ligands Exerting Anticholinesterase and Antioxidant Activities with Low In Vivo Toxicity, J. Med. Chem. 58 (2015) 8985–9003. doi:10.1021/acs.jmedchem.5b01325.
[66] J. Jeřábek, E. Uliassi, L. Guidotti, J. Korábečný, O. Soukup, V. Sepsova, M. Hrabinova, K. Kuča, M. Bartolini, L.E. Peña-Altamira, S. Petralla, B. Monti, M. Roberti, M.L. Bolognesi, Tacrine-resveratrol fused hybrids as multi-target-directed ligands against Alzheimer's disease, Eur. J. Med. Chem. 127 (2017) 250–262. doi:10.1016/j.ejmech.2016.12.048.
[67] M. Harel, J.L. Sussman, E. Krejci, S. Bon, P. Chanal, J. Massoulié, I. Silman, Conversion of acetylcholinesterase to butyrylcholinesterase: modeling and mutagenesis, Proc. Natl. Acad. Sci. U. S. A. 89 (1992) 10827–10831.
[68] C.-G. Zhan, F. Zheng, D.W. Landry, Fundamental reaction mechanism for cocaine hydrolysis in human butyrylcholinesterase, J. Am. Chem. Soc. 125 (2003) 2462–2474. doi:10.1021/ja020850+.
[69] X. Barril, S.G. Kalko, M. Orozco, F.J. Luque, Rational design of reversible acetylcholinesterase inhibitors, Mini Rev. Med. Chem. 2 (2002) 27–36.
[70] S. Darvesh, D.A. Hopkins, C. Geula, Neurobiology of butyrylcholinesterase, Nat. Rev. Neurosci. 4 (2003) 131–138. doi:10.1038/nrn1035.
[71] N.H. Greig, T. Utsuki, D.K. Ingram, Y. Wang, G. Pepeu, C. Scali, Q.-S. Yu, J. Mamczarz, H.W. Holloway, T. Giordano, D. Chen, K. Furukawa, K. Sambamurti, A. Brossi, D.K. Lahiri, Selective butyrylcholinesterase inhibition elevates brain acetylcholine, augments learning and lowers Alzheimer beta-amyloid peptide in rodent, Proc. Natl. Acad. Sci. U. S. A. 102 (2005) 17213–17218. doi:10.1073/pnas.0508575102.
[72] P. Taylor, J. Lwebuga-Mukasa, S. Lappi, J. Rademacher, Propidium—a Fluorescence Probe for a Peripheral Anionic Site on Acetylcholinesterase, Mol. Pharmacol. 10 (1974) 703–708.
[73] P. Taylor, S. Lappi, Interaction of fluorescence probes with acetylcholinesterase. The site and specificity of propidium binding, Biochemistry (Mosc.). 14 (1975) 1989–1997.
[74] N. Nunes-Tavares, A. Nery da Matta, C.M. Batista e Silva, G.M.N. Araújo, S.R.W. Louro, A. Hassón-Voloch, Inhibition of acetylcholinesterase from Electrophorus electricus (L.) by tricyclic antidepressants, Int. J. Biochem. Cell Biol. 34 (2002) 1071–1079.
[75] H. Dvir, D.M. Wong, M. Harel, X. Barril, M. Orozco, F.J. Luque, D. Muñoz-Torrero, P. Camps, T.L. Rosenberry, I. Silman, J.L. Sussman, 3D structure of Torpedo californica acetylcholinesterase complexed with huprine X at 2.1 A resolution: kinetic and molecular dynamic correlates, Biochemistry (Mosc.). 41 (2002) 2970–2981.
[76] X. Zha, D. Lamba, L. Zhang, Y. Lou, C. Xu, D. Kang, L. Chen, Y. Xu, L. Zhang, A. De Simone, S. Samez, A. Pesaresi, J. Stojan, M.G. Lopez, J. Egea, V. Andrisano, M. Bartolini, Novel Tacrine-Benzofuran Hybrids as Potent Multitarget-Directed Ligands for the Treatment of Alzheimer's Disease: Design, Synthesis, Biological Evaluation, and X-ray Crystallography, J. Med. Chem. 59 (2016) 114–131. doi:10.1021/acs.jmedchem.5b01119.
[77] J.P. Colletier, B. Sanson, F. Nachon, E. Gabellieri, C. Fattorusso, G. Campiani, M. Weik, Conformational flexibility in the peripheral site of Torpedo californica acetylcholinesterase revealed by the complex structure with a bifunctional inhibitor, J. Am. Chem. Soc. 128 (2006) 4526–4527. doi:10.1021/ja058683b.
[78] M. Harel, I. Schalk, L. Ehret-Sabatier, F. Bouet, M. Goeldner, C. Hirth, P.H. Axelsen, I. Silman, J.L. Sussman, Quaternary ligand binding to aromatic residues in the active-site gorge of acetylcholinesterase, Proc. Natl. Acad. Sci. U. S. A. 90 (1993) 9031–9035.
[79] E.H. Rydberg, B. Brumshtein, H.M. Greenblatt, D.M. Wong, D. Shaya, L.D. Williams, P.R. Carlier, Y.-P. Pang, I. Silman, J.L. Sussman, Complexes of alkylene-linked tacrine dimers with Torpedo californica acetylcholinesterase: Binding of Bis5-tacrine produces a dramatic rearrangement in the active-site gorge, J. Med. Chem. 49 (2006) 5491–5500. doi:10.1021/jm060164b.

ACCEPTED MANUSCRIPT

ACCEPTED MANUSCRIPT

[80] M.C. Desai, P.F. Thadeio, C.A. Lipinski, D.R. Liston, R.W. Spencer, I.H. Williams, Physical parameters for brian uptake: optimizing log P, log D and pKa of T H A, Bioorg. Med. Chem. Lett. 1 (1991) 411–414. doi:10.1016/S0960-894X(00)80267-X.

[81] W.D. Mallender, T. Szegletes, T.L. Rosenberry, Acetylthiocholine binds to asp74 at the peripheral site of human acetylcholinesterase as the first step in the catalytic pathway, Biochemistry (Mosc.). 39 (2000) 7753–7763.

[82] L. Gremer, D. Schölzel, C. Schenk, E. Reinartz, J. Labahn, R.B.G. Ravelli, M. Tusche, C. Lopez-Iglesias, W. Hoyer, H. Heise, D. Willbold, G.F. Schröder, Fibril structure of amyloid-β(1-42) by cryo-electron microscopy, Science. 358 (2017) 116–119. doi:10.1126/science.aao2825.

[83] A.P. Pawar, K.F. Dubay, J. Zurdo, F. Chiti, M. Vendruscolo, C.M. Dobson, Prediction of "aggregation-prone" and "aggregation-susceptible" regions in proteins associated with neurodegenerative diseases, J. Mol. Biol. 350 (2005) 379–392. doi:10.1016/j.jmb.2005.04.016.

[84] R. Azriel, E. Gazit, Analysis of the minimal amyloid-forming fragment of the islet amyloid polypeptide. An experimental support for the key role of the phenylalanine residue in amyloid formation, J. Biol. Chem. 276 (2001) 34156–34161. doi:10.1074/jbc.M102883200.

[85] E. Gazit, A possible role for pi-stacking in the self-assembly of amyloid fibrils, FASEB J. Off. Publ. Fed. Am. Soc. Exp. Biol. 16 (2002) 77–83. doi:10.1096/fj.01-0442hyp.

[86] O.S. Makin, E. Atkins, P. Sikorski, J. Johansson, L.C. Serpell, Molecular basis for amyloid fibril formation and stability, Proc. Natl. Acad. Sci. U. S. A. 102 (2005) 315–320. doi:10.1073/pnas.0406847102.

[87] A. Frydman-Marom, M. Rechter, I. Shefler, Y. Bram, D.E. Shalev, E. Gazit, Cognitive-performance recovery of Alzheimer's disease model mice by modulation of early soluble amyloidal assemblies, Angew. Chem. Int. Ed Engl. 48 (2009) 1981–1986. doi:10.1002/anie.200802123.

[88] M. Bartolini, C. Bertucci, M.L. Bolognesi, A. Cavalli, C. Melchiorre, V. Andrisano, Insight into the kinetic of amyloid beta (1-42) peptide self-aggregation: elucidation of inhibitors' mechanism of action, Chembiochem Eur. J. Chem. Biol. 8 (2007) 2152–2161. doi:10.1002/cbic.200700427.

[89] M. Bartolini, M. Naldi, J. Fiori, F. Valle, F. Biscarini, D.V. Nicolau, V. Andrisano, Kinetic characterization of amyloid-beta 1-42 aggregation with a multimethodological approach, Anal. Biochem. 414 (2011) 215–225. doi:10.1016/j.ab.2011.03.020.

[90] M. Bartolini, C. Bertucci, V. Cavrini, V. Andrisano, beta-Amyloid aggregation induced by human acetylcholinesterase: inhibition studies, Biochem. Pharmacol. 65 (2003) 407–416.

[91] A.E. Reyes, M.A. Chacón, M.C. Dinamarca, W. Cerpa, C. Morgan, N.C. Inestrosa, Acetylcholinesterase-Abeta complexes are more toxic than Abeta fibrils in rat hippocampus: effect on rat beta-amyloid aggregation, laminin expression, reactive astrocytosis, and neuronal cell loss, Am. J. Pathol. 164 (2004) 2163–2174.

[92] A.E. Reyes, D.R. Perez, A. Alvarez, J. Garrido, M.K. Gentry, B.P. Doctor, N.C. Inestrosa, A monoclonal antibody against acetylcholinesterase inhibits the formation of amyloid fibrils induced by the enzyme, Biochem. Biophys. Res. Commun. 232 (1997) 652–655. doi:10.1006/bbrc.1997.6357.

[93] M.L. Bolognesi, R. Banzi, M. Bartolini, A. Cavalli, A. Tarozzi, V. Andrisano, A. Minarini, M. Rosini, V. Tumiatti, C. Bergamini, R. Fato, G. Lenaz, P. Hrelia, A. Cattaneo, M. Recanatini, C. Melchiorre, Novel class of quinone-bearing polyamines as multi-target-directed ligands to combat Alzheimer's disease, J. Med. Chem. 50 (2007) 4882–4897. doi:10.1021/jm070559a.

[94] M.L. Bolognesi, M. Bartolini, F. Mancini, G. Chiriano, L. Ceccarini, M. Rosini, A. Milelli, V. Tumiatti, V. Andrisano, C. Melchiorre, Bis(7)-tacrine derivatives as multitarget-directed ligands: Focus on anticholinesterase and antiamyloid activities, ChemMedChem. 5 (2010) 1215–1220. doi:10.1002/cmdc.201000086.

[95] L. Di, E.H. Kerns, K. Fan, O.J. McConnell, G.T. Carter, High throughput artificial membrane permeability assay for blood-brain barrier, Eur. J. Med. Chem. 38 (2003) 223–232.

[96] L.F.N. Lemes, G. de Andrade Ramos, A.S. de Oliveira, F.M.R. da Silva, G. de Castro Couto, M. da Silva Boni, M.J.R. Guimarães, I.N.O. Souza, M. Bartolini, V. Andrisano, P.C. do Nascimento Nogueira, E.R. Silveira, G.D. Brand, O. Soukup, J. Korábečný, N.C. Romeiro, N.G. Castro, M.L. Bolognesi, L.A.S. Romeiro, Cardanol-derived AChE inhibitors: Towards the development of dual binding derivatives for Alzheimer's disease, Eur. J. Med. Chem. 108 (2016) 687–700. doi:10.1016/j.ejmech.2015.12.024.

[97] F. Wohnsland, B. Faller, High-throughput permeability pH profile and high-throughput alkane/water log P with artificial membranes, J. Med. Chem. 44 (2001) 923–930.

[98] T.L. Riss, R.A. Moravec, A.L. Niles, S. Duellman, H.A. Benink, T.J. Worzella, L. Minor, Cell Viability Assays, in: G.S. Sittampalam, N.P. Coussens, K. Brimacombe, A. Grossman, M. Arkin, D. Auld, C. Austin, J. Baell, B. Bejcek, J.M.M. Caaveiro, T.D.Y. Chung, J.L. Dahlin, V. Devanaryan, T.L. Foley, M. Glicksman, M.D. Hall, J.V. Haas, J. Inglese, P.W. Iversen, S.D. Kahl, S.C. Kales, M. Lal-Nag, Z. Li, J. McGee, O. McManus, T. Riss, O.J. Trask, J.R.

Weidner, M.J. Wildey, M. Xia, X. Xu (Eds.), Assay Guid. Man., Eli Lilly & Company and the National Center for Advancing Translational Sciences, Bethesda (MD), 2004. http://www.ncbi.nlm.nih.gov/books/NBK144065/ (accessed September 17, 2018).

[99] J. Patocka, D. Jun, K. Kuca, Possible role of hydroxylated metabolites of tacrine in drug toxicity and therapy of Alzheimer's disease, Curr. Drug Metab. 9 (2008) 332–335.

[100] F.J. Jiménez-Jiménez, H. Alonso-Navarro, M.T. Herrero, E. García-Martín, J.A.G. Agúndez, An Update on the Role of Nitric Oxide in the Neurodegenerative Processes of Parkinson's Disease, Curr. Med. Chem. 23 (2016) 2666–2679.

[101] C. Volbracht, J. van Beek, C. Zhu, K. Blomgren, M. Leist, Neuroprotective properties of memantine in different in vitro and in vivo models of excitotoxicity, Eur. J. Neurosci. 23 (2006) 2611–2622. doi:10.1111/j.1460-9568.2006.04787.x.

[102] W. Li, J. Xue, C. Niu, H. Fu, C.S.C. Lam, J. Luo, H.H.N. Chan, H. Xue, K.K.W. Kan, N.T.K. Lee, C. Li, Y. Pang, M. Li, K.W.K. Tsim, H. Jiang, K. Chen, X. Li, Y. Han, Synergistic neuroprotection by bis(7)-tacrine via concurrent blockade of N-methyl-D-aspartate receptors and neuronal nitric-oxide synthase, Mol. Pharmacol. 71 (2007) 1258–1267. doi:10.1124/mol.106.029108.

[103] Dejmek, L., 7-MEOTA, 1990 (n.d.) 126–129.

[104] R.A. Lenz, J.D. Baker, C. Locke, L.E. Rueter, E.G. Mohler, K. Wesnes, W. Abi-Saab, M.D. Saltarelli, The scopolamine model as a pharmacodynamic marker in early drug development, Psychopharmacology (Berl.). 220 (2012) 97–107. doi:10.1007/s00213-011-2456-4.

[105] J.J. Jackson, M.R. Soliman, Effects of tacrine (THA) on spatial reference memory and cholinergic enzymes in specific rat brain regions, Life Sci. 58 (1996) 47–54.

[106] A.M. Janas, S.C. Cunningham, K.B. Duffy, B.D. Devan, N.H. Greig, H.W. Holloway, Q.-S. Yu, A.L. Markowska, D.K. Ingram, E.L. Spangler, The cholinesterase inhibitor, phenserine, improves Morris water maze performance of scopolamine-treated rats, Life Sci. 76 (2005) 1073–1081. doi:10.1016/j.lfs.2004.06.028.

[107] J.B. Baell, G.A. Holloway, New Substructure Filters for Removal of Pan Assay Interference Compounds (PAINS) from Screening Libraries and for Their Exclusion in Bioassays, J. Med. Chem. 53 (2010) 2719–2740. doi:10.1021/jm901137j.

[108] H. Naiki, K. Higuchi, K. Nakakuki, T. Takeda, Kinetic analysis of amyloid fibril polymerization in vitro, Lab. Investig. J. Tech. Methods Pathol. 65 (1991) 104–110.

[109] K. Sugano, H. Hamada, M. Machida, H. Ushio, High throughput prediction of oral absorption: improvement of the composition of the lipid solution used in parallel artificial membrane permeation assay, J. Biomol. Screen. 6 (2001) 189–196. doi:10.1089/108705701300362728.

[110] J. Fang, R.B. Silverman, A Cellular Model for Screening Neuronal Nitric Oxide Synthase Inhibitors, Anal. Biochem. 390 (2009) 74–78. doi:10.1016/j.ab.2009.04.004.

[111] Guidance on dose level selection for regulatory general toxicology studies for pharmaceuticals, (n.d.). https://www.norecopa.no/3r-guide/guidance-on-dose-level-selection-for-regulatory-general-toxicology-studies-for-pharmaceuticals (accessed June 22, 2018).

[112] B. Seyer, V. Pham, A.L. Albiston, S.Y. Chai, Cannula implantation into the lateral ventricle does not adversely affect recognition or spatial working memory, Neurosci. Lett. 628 (2016) 171–178. doi:10.1016/j.neulet.2016.06.034.

ACCEPTED MANUSCRIPT

ACCEPTED MANUSCRIPT

Highlights:

- Tacrine-tryptophan hybrids inhibited both cholinesterases in nanomolar concentrations
- Highlighted compound ***S*-K1035** displayed Aβ_{42} self-aggregation as well as *h*AChE-induced Aβ_{40} aggregation
- Complex of *Tc*AChE and ***S*-K1035** was elucidated by X-ray crystallography
- Difference in activity between **K1035** enantiomers was explored by conducting X-ray crystallography with *h*BChE
- *In vivo* pro-cognitive effect of ***S*-K1035** was confirmed in scopolamine-induced amnesia model in rats

ACCEPTED MANUSCRIPT